arXiv:1611.07961v1 [astro-ph.CO] 23 Nov 2016

Bose-Einstein-condensed scalar field dark matter and the gravitational wave background from inflation: new cosmological constraints and its detectability by LIGO

Bohua Li* and Paul R. Shapiro†
Department of Astronomy and Texas Cosmology Center, The University of Texas at Austin, 2515 Speedway C1400, Austin, TX 78712, USA

Tanja Rindler-Daller‡
Institut für Astrophysik, Universitätssternwarte Wien, University of Vienna, A-1180 Vienna, Austria
Department of Physics and Michigan Center for Theoretical Physics, University of Michigan, Ann Arbor, MI 48109, USA

(Dated: November 24, 2016)

We consider an alternative dark matter candidate to WIMP cold dark matter (CDM), ultralight bosonic dark matter ($m \gtrsim 10^{-22}\mathrm{eV}/c^2$) described by a complex scalar field (SFDM) with a global $U(1)$ symmetry, for which the comoving particle number density, or charge density, is conserved after particle production during standard reheating ($w = 0$). We allow for a repulsive self-interaction. In a ΛSFDM universe, SFDM starts relativistic, evolving from stiff ($w = 1$) to radiation-like ($w = 1/3$), before becoming nonrelativistic at late times ($w = 0$). Thus, before the familiar radiation-dominated era, there is an earlier era of stiff-SFDM-domination. During both the stiff-SFDM-dominated and radiation-dominated eras, the expansion rate is *higher* than in ΛCDM, since SFDM contributes to the relativistic degrees of freedom of the ΛSFDM universe when it is either stiff or radiationlike. Transitions between these eras, determined by SFDM particle mass m and the quartic self-interaction coupling strength λ, are therefore constrained by cosmological observables, particularly N_{eff}, the effective number of neutrino species during BBN, and z_{eq}, the redshift of matter-radiation equality. Furthermore, since the homogeneous energy density contributed by the stochastic gravitational wave background (SGWB) from inflation is amplified during the stiff-SFDM-dominated era, it can contribute a radiationlike component large enough to affect these cosmological observables, by further boosting the expansion rate after the stiff era ends. Remarkably, this same amplification makes possible the detection of the SGWB at high frequencies by current laser interferometer experiments, e.g., aLIGO/Virgo and eLISA. For SFDM particle parameters that satisfy these cosmological constraints, the amplified SGWB is detectable by LIGO for a broad range of reheat temperatures T_{reheat}, for values of the tensor-to-scalar ratio r currently allowed by CMB polarization measurements. For a given r, if SFDM parameters are chosen which marginally satisfy the cosmological constraints (which maximizes the total energy density of the SGWB), then the SGWB is maximally detectable for values of T_{reheat} which correspond to the epoch of horizon reentry for modes whose frequencies lie within the $10-50$ Hz LIGO sensitive frequency band today. For example, if $r = 0.01$, the maximally detectable model for $(\lambda/(mc^2)^2,\ m) = (10^{-18}\ \mathrm{eV}^{-1}\mathrm{cm}^3,\ 8\times10^{-20}\ \mathrm{eV}/c^2)$ corresponds to $T_{\mathrm{reheat}} \simeq 10^4$ GeV, for which we predict an aLIGO O1 run detection with signal-to-noise ratio of ~ 10. A nondetection by aLIGO O1 would provide a new kind of cosmological constraint on SFDM, therefore. A wider range of SFDM parameters and reheat temperatures should be accessible to the aLIGO/Virgo O5 run, with the potential to detect this unique signature of the SFDM model. For $r = 0.01$ and $\lambda/(mc^2)^2 = 10^{-18}\ \mathrm{eV}^{-1}\mathrm{cm}^3$, for example, a 3σ detection is predicted for $600 \lesssim T_{\mathrm{reheat}}(\mathrm{GeV}) \lesssim 10^7$.

PACS numbers: 98.80.-k, 95.35.+d, 98.80.Cq, 98.80.Ft, 04.30.-w

I. INTRODUCTION

A. Cold dark matter: WIMPs or something else?

The nature of the dark matter (DM) remains one of the most profound open problems in cosmology. Observations of the large-scale structure (LSS) of

* bohuali@astro.as.utexas.edu
† shapiro@astro.as.utexas.edu
‡ tanja.rindler-daller@univie.ac.at

the universe and the cosmic microwave background (CMB) are consistent with dark matter which forms structure as if it was created "cold", i.e., it can be modeled as collisionless particles with nonrelativistic random microscopic motions. The cold dark matter (CDM) model has been very successful in describing structure formation on large scales as hierarchical, with the smallest objects forming first and merging over time to form ever-larger objects — "halos" in virial equilibrium — connected by filaments surrounding largely empty voids in a "cosmic web of structure" [1], [2, 3], [4], [5, 6], [7]. Candidate particles for DM can be found in many extensions to the Standard Model (SM) of particle physics. Traditionally, the most studied candidate particles for the standard, collisionless CDM are WIMPs (weakly interacting massive particles), the lightest supersymmetric partner particles predicted by models of supersymmetry ("SUSY"), thermal relics whose mass range allows gravitational clustering to form objects down to Earth-mass.

Despite its success on large scales, the standard, collisionless CDM model has been challenged by observations of galactic and sub-galactic scales. First, N-body simulations of collisionless CDM predict a universal cuspy density profile for DM halos. However, measurements of the density profiles of various dark-matter-dominated systems, e.g., dwarf spheroidal galaxies, low-surface-brightness galaxies, even some galaxy clusters, have suggested shallower profiles, or even cores at their centers (the "cusp/core problem") [8–12]. Such N-body simulations also predict a large-overabundance of subhalos in the Local Group compared with the observed number of satellite galaxies (the "missing satellites problem") [13, 14]. In addition, it has been pointed out that, after abundance matching, the most massive subhalos of a Milky-Way-like galaxy predicted by standard CDM simulations are too dense to host the brightest satellites of the Milky Way (the "too big to fail" problem) [15, 16].

Meanwhile, attempts to detect WIMP DM particles either directly or indirectly (i.e., as astronomical sources following their decay or annihilation into radiation or other particles) have thus far been unsuccessful [17–20]. The range of particle models and parameters which remain viable for WIMP DM has, in fact, been substantially reduced by these nondetections.

These nondetections of WIMPs and the structure formation discrepancies described above, between theory and observations, for the standard model of CDM as cold, collisionless particles suggest that an alternative at the particle level to WIMPs as CDM may be required. Such an alternative must retain the successes of CDM with regard to LSS formation and the CMB, as well as the thermodynamic evolution of the background universe in the standard Big Bang cosmology.

One such variant of CDM which we have considered before is that of complex scalar field dark matter (SFDM), involving ultra-light bosons [21, 22] (where it is referred to as Bose-Einstein condensate CDM, or BEC-CDM); [23] (hereafter "Paper I"). For additional description of this model and the related literature, we refer the reader to these papers. With regard to LSS, SFDM provides a natural length scale, below which structure formation is suppressed, leading to fewer subhalos and generally, to a lower density of DM in the central regions of galaxies. On larger scales, however, structure formation in SFDM is the same as for cold, collisionless particles. In Paper I, we considered the cosmological evolution of the homogeneous Big-Bang background universe in the presence of SFDM and showed that the SFDM behaved like a perfect fluid with an equation-of-state (EOS) parameter $w \equiv p/\rho$ which evolved from stiff ($w = 1$) to radiationlike ($w = 1/3$) to nonrelativistic CDM-like ($w = 0$). At early times the stiff EOS made the SFDM dominate the total energy density of the universe, with consequences for the expansion history. This made it possible for us to use observational constraints to derive the allowed range of SFDM particle parameters. Here we will revisit this problem by making two significant advances, as described in the sections below. First, we will embed the SFDM model more fully in the standard inflationary paradigm, to create a more holistic ΛSFDM cosmology. Second, we will take account of the gravitational-wave (GW) background from inflation and its amplification in the presence of SFDM, leading to the possibility of its detection at high frequencies by laser interferometer experiments like the Advanced LIGO/Virgo experiment (shortened as "aLIGO/Virgo"). A preliminary summary of some of this new work was presented in [24].

B. Complex SFDM: Bose-Einstein-condensed ultralight particles as cold dark matter

The SFDM model considered in Paper I and in [21, 22] is one type in a family of cold dark matter candidates involving bosonic particles associated with a scalar field. The best-known example of bosonic dark matter is the QCD axion, a real (pseudo-)scalar field proposed to resolve the strong CP problem. Its attractive self-interaction is so weak that it is usually neglected, leaving only the

quadratic mass term in the potential. The mass of the QCD axion currently allowed by astronomical observational constraints is $\sim 10^{-5}$ eV/c^2. Structure formation in QCD axion DM is like that for cold, collisionless particles on all scales of astrophysical interest, so the small-scale structure problems of CDM described above in §I A remain for the QCD axion DM, as well. As a generalization, ultralight axions or axion-like particles (ALPs) are also predicted by extensions to the Standard Model, which could serve as dark matter as long as their mass is $> 10^{-33}$ eV/$c^2 \sim H_0 \cdot \hbar/c^2$ (H_0 is the Hubble constant at the present). The self-interaction of these ultralight ALPs, too, is generally assumed to be so weak that it can be neglected when comparing model predictions to astrophysical data. However, we caution against this neglect, since our SFDM results for the case which includes a *repulsive* self-interaction, show that even a tiny self-interaction can be dynamically important; it is not clear why the same should not be true for attractive cases. When the mass of the non-interacting axion is above 10^{-18} eV/c^2, dark matter comprised of ALPs is dynamically indistinguishable from collisionless CDM on large scales [25]. For particle masses smaller than this, however, their de Broglie wavelength inside galactic halos, which sets a scale below which structure formation is suppressed, can be large enough to affect the small scales identified in §I A above as problematic for standard CDM.

In fact, other ultra-light scalar field particles have been proposed as DM candidates by various authors, which all mimic standard CDM above some length scale but deviate on sufficiently small scales, motivated by the small-scale problems of standard CDM. While the genesis of ultra-light bosonic DM is *a priori* model-dependent, many of those models share the property of axion DM that the DM bosons are considered to be born cold with high occupation number, such that they can be described by a classical scalar field. The choice of potentials and particle masses does vary, however. Non-interacting DM has been considered by, e.g., [26], [27], [28–30] ("fuzzy dark matter"), [31] ("quantum wave dark matter"), [32, 33] ("ultralight axions"), [34, 35] ("scalar field dark matter"), [36]. On the other hand, self-interacting DM has been studied in, e.g., [37] ("fluid dark matter"), [38, 39] ("repulsive dark matter"), and [40–45]. In the self-interacting[1] DM case (including our SFDM model with a quartic potential [21, 22], referred to there as BEC-CDM), the suppression of small-scale structure can also result from the pressure force associated with its repulsive potential, rather than solely from the "quantum pressure" associated with large de Broglie wavelength as in the non-interacting case. When the minimum length scale for structure associated with the repulsive self-interaction is greater than that due to quantum pressure, this is referred to as the Thomas-Fermi regime.

Amongst the models mentioned above, there are many which propose that DM bosons are initially in a Bose-Einstein condensate (BEC), or will form a BEC at some stage in cosmic history. In our previous work [21, 22], we studied the nonlinear behavior of the BEC wave function (or, the order parameter), in the context of DM halo structure. We applied the Gross-Pitaevskii equation coupled to the Poisson equation to study the equilibrium structure of BEC-CDM halos, including the effects of angular momentum and the possible formation of quantum vortices.

The formation of a BEC in QCD axion DM has also been studied. A detailed analysis of the condensation process for the QCD axion has been made by [49, 50]. However, controversies remain about the formation of a BEC and whether it depends on the sign of the self-interaction or whether the classical field description is sufficient in general [51, 52]. This debate is partly due to the difficulty of forming a BEC for bosons described by a *real* scalar field (the axion case), while the condensation process occurs naturally, even in the early universe, for bosons described by a *complex* scalar field (the case for our SFDM model) with a global $U(1)$ symmetry, associated with a (conserved) Noether charge [53–55], as described below.

In the *complex* SFDM model presented here, DM appears in the wake of reheating, following inflation. An example of such a microphysical implementation can be found in [55]. The idea is that, upon inflaton decay, DM bosons and antibosons are created, as are the SM particles. We assume that the complex scalar field was born with a large charge, or comoving charge density, Q, which is the difference between the number density of bosons and antibosons. Owing to the global $U(1)$ symmetry of the complex scalar field, Q is a conserved quantity.

[1] The self-interaction term used here should not be confused with the kind of self-interacting, CDM particles referred to elsewhere in the literature as SIDM, suggested by [46], which we have studied in [47] and [48]. In SIDM, particle self-interaction manifests itself as two-body elastic scattering which adds "collisionality" to the otherwise collisionless CDM gas, but does not make a BEC or exhibit any form of macroscopic quantum coherence.

In thermal equilibrium, while DM bosons and antibosons are annihilated away (leaving no antibosons behind), the majority of DM particles will find themselves rapidly occupying their ground state (the zero-momentum state). In Paper I, following [53] and [54], we pointed out that Bose-Einstein condensation for DM particles of mass m occurs as long as $k_{\rm B}Q/S \gg 1$ initially, where $k_{\rm B}$ is the Boltzmann constant and S is the comoving entropy density. In a cosmological setting, both Q and S are conserved. Now, that ground state which remains is a BEC with charge approximately equal to Q. As a result, the DM can thereafter be described as a classical field, hence complex scalar field dark matter – SFDM. In this sense, complex SFDM belongs to the wider family of asymmetric DM, in which the DM anti-particles have disappeared, leaving a fixed amount of DM particles behind. The charge density Q is related to the present-day SFDM energy density $\rho_{\rm SFDM,0}$, by $\rho_{\rm SFDM,0}/mc^2Q \simeq 1$, as one will naturally expect for CDM at the present. We note that the relation above is described in [56] as the "spintessence" limit (see also [57], [58]), while they also showed another limit which mimics the behavior of a real scalar field when $\rho_{\rm SFDM,0}/mc^2Q \gg 1$, i.e., negligible charge density. We emphasize that SFDM shall, hereafter, refer only to *complex* scalar field dark matter in this paper.

C. Cosmic Evolution of ΛSFDM

We studied the (background) evolution of complex SFDM in detail in Paper I, by solving numerically the equation of motion of SFDM in an expanding universe, adopting a spatially flat Friedmann-Lemaître-Robertson-Walker (FLRW) background metric. We called it ΛSFDM, since all the cosmic components of the ΛCDM model are adopted, except for collisionless CDM which is replaced by SFDM. We assumed that the present cosmic DM abundance is entirely given by the current $\rho_{\rm SFDM}$, which also determines the (conserved) charge density of SFDM, Q, as described in the section above. The evolution of SFDM is determined by the form of the potential in its Langrangian, as for any other cosmological scalar field. Let ψ be the complex scalar field describing the condensate of DM bosons, we adopt the following Lagrangian density (in units of energy density)

$$\mathcal{L} = \frac{\hbar^2}{2m} g^{\mu\nu}\partial_\mu\psi^*\partial_\nu\psi - \frac{1}{2}mc^2|\psi|^2 - \frac{\lambda}{2}|\psi|^4, \quad (1)$$

with signature $(+,-,-,-)$. $|\psi|$ denotes the modulus of ψ. m is the DM boson mass and we choose the energy-independent 2-boson self-interaction strength to be repulsive or zero, $\lambda \geq 0$. We will elaborate more about this Lagrangian density in §II A 1.

The SFDM parameters of interest are motivated by the small-scale CDM structure problems mentioned above. In its CDM-like phase—when the quadratic term in Eq. (1) dominates—, SFDM can provide two characteristic (Jeans) length scales below which structure formation is suppressed. Regardless of self-interaction, the quantum nature of SFDM particles always smoothes fluctuations below their de-Broglie wavelength. For example, DM particles with mass $m \simeq 10^{-22}$ eV$/c^2$ would have a corresponding de-Broglie wave length $\lambda_{\rm deB}$ of order kpc (i.e., typical scale of CDM small-scale structure problems). Moreover, there arises another length scale, $l_{\rm SI}$, from the (repulsive) self-interaction, should it be significant, given by $\lambda/(mc^2)^2$. In fact, in the Thomas-Fermi regime, $l_{\rm SI}$ is the only length scale that is responsible for suppressing structure growth, as long as $l_{\rm SI} \gg \lambda_{\rm deB}$. For instance, $l_{\rm SI} \simeq 1$ kpc if $\lambda/(mc^2)^2 = 2\times10^{-18}$ eV^{-1} cm^3. Hence, m can be larger than the value of interest suggested by the noninteracting case, if λ is higher as well, and yet the model retains its characteristic length scale, as long as the ratio $\lambda/(mc^2)^2$ stays constant (see [21] for details). We note that fiducial dimensional couplings of order $\lambda \approx 10^{-62}$ eV cm^3 correspond to dimensionless couplings of order[2] $\lambda m^2c/\hbar^3 \approx 10^{-92}$ for $m = 10^{-22}$ eV$/c^2$. While couplings even this small are enough to resolve the small-scale problems for higher mass DM particles, they also render these models qualitatively different[3] from those with $\lambda \equiv 0$.

In Paper I we found that, in the early universe, self-interacting SFDM starts relativistic, with an equation of state (EOS) evolving from stiff ($w \equiv p/\rho \simeq 1$) to radiationlike ($w \simeq 1/3$), before becoming nonrelativistic at late times ($w \simeq 0$). In the limit of a vanishing self-interaction ($\lambda \to 0$), the intermediate radiationlike phase of SFDM simply vanishes as well. In either case, it is the kinetic term in Eq. (1) that dominates the energy density of SFDM at early times, and the EOS of SFDM approaches that

[2] This number is roughly 40 orders of magnitudes below the coupling for a $m \sim 10^{-5}$ eV QCD axion. The self-interaction is attractive for the latter, however.

[3] This qualitative change in models, when a small coupling is added (i.e. a quartic term), has been found already earlier in the literature on boson stars, which are also described as self-gravitating scalar fields, see [59]. So, it is not too surprising to re-discover similar consequences for scalar fields as the dark matter.

of maximal "stiff" matter, $w_{\rm SFDM} \simeq 1$. This evolutionary phase of a scalar field has sometimes been referred to as "fast-roll". When the fast-rolling scalar field is the dominant component of the universe, this period of the expansion history is also referred to as "kination" [60–62]. It is important to note that this earliest stiff phase of SFDM appears in all models, and is a generic feature of scalar field dynamics [63]. At later times, the quartic term in (1) can dominate the SFDM energy density, for large enough $\lambda/(mc^2)^2$. Then, the EOS of SFDM is that of radiation, namely $w_{\rm SFDM} \simeq 1/3$. The early universe thus experiences a boost in its expansion rate due to this extra relativistic species in both, the stiff and radiationlike phases of SFDM. Finally, the (quadratic) mass term in Eq. (1) guarantees that SFDM behaves like CDM in the late universe, with or without self-interaction. More precisely, this term must dominate after the time of matter-radiation equality at a scale factor of $a_{\rm eq} \simeq 3 \times 10^{-4}$, in order to reproduce a period of "CDM-like" matter domination with $w_{\rm SFDM} \simeq 0$, the same as that in ΛCDM during which structure forms. The transitions between these phases, determined by SFDM particle mass and self-interaction coupling strength, are therefore constrained by cosmological observables, particularly $N_{\rm eff}$, the effective number of neutrino species during Big Bang nucleosynthesis (BBN), and $z_{\rm eq}$, the redshift of matter-radiation equality. Unlike other models that yield a higher value of $N_{\rm eff}$ than the standard value $N_{\rm eff,standard} = 3.046$ [64] accounting for the three Standard Model neutrinos, for which the elevated $N_{\rm eff}$ is the same at all times including BBN and $z_{\rm eq}$, SFDM allows $N_{\rm eff}$ to be higher at BBN than at $z_{\rm eq}$. In Paper I, we found that $m \geq 2.4 \times 10^{-21}$ eV$/c^2$ and 9.5×10^{-19} eV^{-1} cm$^3 \leq \lambda/(mc^2)^2 \leq 4 \times 10^{-17}$ eV^{-1} cm^3, due to cosmological constraints on $N_{\rm eff}$ and $z_{\rm eq}$.

To reiterate, before the familiar radiation-dominated era, there is an earlier era of stiff-SFDM-domination, and the expansion rate in the early ΛSFDM universe is increased compared with that in ΛCDM. Interestingly, in our model, dark matter dominates twice in the history of the universe: first in its stiff phase before BBN, and later in its dust-like phase, giving rise to a standard CDM-like matter era.

In this paper, we will expand our previous analysis by embedding ΛSFDM in the standard inflation paradigm and studying the impact of SFDM on primordial gravitational waves (GWs) produced during inflation, which contribute to $N_{\rm eff}$ as well.

D. SFDM within the standard inflationary cosmology

In Paper I, we showed that by setting the conserved charge of the complex scalar field so as to match the abundance of the DM in the observed universe at the present, and evolving the field and background universe together over time, the field was compelled to dominate the total energy density at early times. We stopped short, however, of asking how this SFDM-dominated phase was consistent with standard inflationary cosmology in which the energy density was dominated initially by the inflaton field. Here we merge these two pictures self-consistently by postulating that the end of inflation was followed by reheating, in which the inflaton decayed primarily into SFDM, while also producing the other particles of the SM.

More precisely, we envisage the early cosmic evolution as follows. Standard slow-roll single-field inflation produces nearly scale-invariant fluctuations of the metric of the universe, which can be decomposed into scalar, vector and tensor fluctuations. The energy scale during inflation is related to the ratio of the amplitude of tensor perturbations to the scalar amplitude, also called the tensor-to-scalar ratio, r. This quantity is pursued by CMB polarization experiments [65, 66], because primordial tensor perturbations induce quadrupole anisotropies in the CMB temperature, which leaves an imprint on the B-mode of CMB polarization (the "recombination bump" in the BB power spectrum) [66, 67]. The spectrum of (nearly) scale-invariant tensor perturbations can be parametrized by a power law, determined by the tensor amplitude A_t (the product of the scalar amplitude A_s and r) and the tensor spectral index n_t. These tensor perturbations will become gravitational waves (GWs) once they reenter the horizon. We further assume that inflation is followed by an epoch of reheating with matter-like EOS, $w = 0$. This is a reasonable choice for a prolonged period of reheating (see, e.g. [68]). As already described in §I B, we are interested in scenarios in which the DM bosons are born at the end of reheating with a high charge density and low entropy density, thus they find themselves rapidly occupying their ground state (the zero-momentum state). As soon as SFDM arises, its energy density obeys a stiff EOS. Again, this is because for a scalar field, the kinetic term in the Lagrangian, Eq. (1), goes as a^{-6}. As a result, SFDM dominates the cosmic energy budget at early times, compared to other cosmic components. In summary, it is reasonable to assume that the transition between the end of reheating and the onset of the stiff phase of SFDM is

short. For simplicity, we adopt an instant transition, i.e. the reheating temperature $T_{\rm reheat}$ at the end of reheating also corresponds to the point after which there is the "stiff" era.

We note that in this work the only source of primordial GWs that we consider are those predicted by the "vanilla" single-field slow-roll inflation model, for which the consistency relation, $n_t = -r/8$, holds. Tensor fluctuations from inflation are isotropic and stochastic in nature. Therefore, they contribute to the stochastic gravitational wave background (SGWB), giving rise to an effective homogeneous energy density of primordial GWs, which we will elaborate in more detail in §II A 2. Such a SGWB is described by its energy density spectrum, $\Omega_{\rm GW}(k,a)$, i.e. the fractional energy density carried by GWs per logarithmic wavenumber interval at any comoving wavenumber k and scale factor a. The dispersion relation of GWs today is simply given by $f = kc/2\pi$, in which f is the (comoving) frequency. The differential GW energy density at any frequency f generically decays like radiation $\sim a^{-4}$ once that mode reenters the horizon.

As we will show in this paper, it is the stiff era caused by SFDM that will amplify the GWs produced during inflation. It was first considered by Grishchuk in his seminal paper [69] that cosmological GWs can be amplified in a universe whose EOS is stiffer than that of radiation, i.e., $w > 1/3$, implying that the corresponding $\Omega_{\rm GW}(k,a)$, which indicates their contribution to the total energy density of the universe, will increase over time. While the goal of Grishchuk's paper was to find the conditions in which gravitons can be massively produced in the early universe, from primordial tensor-type quantum fluctuations (see [70] and references therein for a review), we study the post-inflationary evolution of existing GWs produced during inflation, within the modern-day inflationary paradigm. We will point out in this paper that, for any mode k, $\Omega_{\rm GW}(k,a)$ evaluated at a time much later than the horizon reentry of this mode, depends on the critical energy density of the universe when this mode crossed the horizon, and, the duration of its subhorizon radiationlike decay since horizon crossing. We will show that, for any mode k which reenters prior to the end of the stiff phase, it is the shortening of the radiationlike decay due to the stiff phase, compared to the ΛCDM expansion history, that is responsible for the amplification of $\Omega_{\rm GW}(k,a)$. The expansion history of ΛSFDM with its stiff era will, therefore, predict a characteristic GW energy density spectrum $\Omega_{\rm GW}(k,a)$ at a late time, in which the spectrum shows a blue-tilt, $\Omega_{\rm GW}(k,a) \propto k$, for any mode k reentering during the stiff era ($w = 1$), peaks at $k_{\rm reheat}$ for the mode that reenters at the end of reheating ($w = 0$), and declines for higher k as $\Omega_{\rm GW}(k,a) \propto k^{-2}$ (red-tilt). We calculate the present-day GW energy density spectrum, $\Omega_{\rm GW}(f) \equiv \Omega_{\rm GW}(k = 2\pi f/c, a = 1)$, as probed by current and future laser interferometer experiments [71, 72]. These experiments are sensitive to the tensor deformation of space, or the strain, induced by incoming GWs, to a high accuracy. We predict a detectable signal from SGWB generated by *standard* inflation, within reach of the sensitivity of the ongoing Advanced LIGO/Virgo experiments, for a broad range of $T_{\rm reheat}$ and SFDM parameters. This provides a novel science target, given that the expected signal from the standard cosmological model lies many orders of magnitudes below the sensitivity limit of those experiments. Meanwhile, pulsar timing array (PTA) experiments [73–75] also detect strain signals, but at lower frequency ranges. We remark that the predicted SGWB signal in the ΛSFDM model, however, lies well below the upper bounds reported by current PTA experiments in those frequency ranges.

The SGWB also affects the expansion history as an extra relativistic degree of freedom by boosting the expansion rate of the background universe, thereby contributing to $N_{\rm eff}$. In contrast to ΛCDM with standard inflation, in which the contribution to the background energy density of the universe from primordial GWs is negligible (and thus uninteresting), ΛSFDM, however, amplifies those primordial GWs so that they need to be taken into account in the budget of $N_{\rm eff}$. Therefore, the SGWB from inflation actually needs to be included in the Friedmann equation for the average universe in a self-consistent manner. In other words, we must study the backreaction of the inflationary SGWB on the expansion rate of the average universe, which in turn affects the evolution of the SGWB, itself, an effect which has been neglected in previous literature. In light of this effect, $N_{\rm eff}$ thus has two additional sources: the direct contribution from SFDM, and a new one from the *enhanced* $\Omega_{\rm GW}$. This puts additional constraints on the SFDM parameters, m and $\lambda/(mc^2)^2$. In what follows, we will update the $N_{\rm eff}$ and $z_{\rm eq}$ constraints on the SFDM parameters studied in our Paper I, incorporating the new effect from primordial SGWB.

The impact on the primordial SGWB of an early era whose EOS is stiffer than radiation (with $1 \geq w \geq 1/3$) has been considered in different contexts in previous literature, in which such an era was postulated to arise before BBN, without specifying what the agent might be which gives rise to such a phase. The requirement that the amplification of the SGWB relative to the standard radiation com-

ponents not violate observational constraints on the early universe was discussed by [76] (based on [77]). They expressed this by defining an effective EOS parameter $\hat{w}$, which is a weighted mean of w over cosmic time, for which they calculated an upper limit. They also pointed out that the high-frequency extrapolation of the same SGWB which contributed to the expansion rate at early times might be detected or constrained by future GW laser interferometer experiments. Unlike the present work described, this work did not take account of the back-reaction of the GWs on the expansion rate, however. The possibility that inflation ended with the onset of a brief stiff era was considered by [78], who calculated its effect on the SGWB energy density assuming the EOS switched from a constant value of w for the stiff era to $w = 1/3$ for the radiation-dominated era. Unlike the present work, there was no allowance for a standard reheating epoch between the end of inflation and the stiff era. In fact, [78] speculated that amplification of the SGWB during the stiff era might, instead, lead to a reheating *driven* by GWs which reentered the horizon during the stiff era. Finally, we note that the context in which the stiff era appears in the present work as an inevitable consequence of the SFDM evolution has no precedent in earlier work.

This paper is organized as follows. In §II, we present the basic equations concerning the composition and expansion history of the ΛSFDM model, and the homogeneous evolution of each component, especially SFDM and the SGWB from inflation. In §III, we discuss the solutions to these equations, providing both analytical insights and numerical treatment, especially with regard to the SGWB, and show the holistic expansion history of ΛSFDM from inflation through the present. We also describe our numerical method for a self-consistent account of the SGWB, and show the evolution of several example ΛSFDM models from our numerical calculations, which delineate the evolutionary phases in ΛSFDM and demonstrate a nontrivial contribution from the amplified SGWB from inflation. In §IV, we then derive the new constraints on the SFDM particle parameters required to satisfy the cosmological observables $z_{\rm eq}$ and $N_{\rm eff}$, and discuss the impact of the SGWB on these constraints, which is dependent on the values of r and $T_{\rm reheat}$. In §V, we present one of our most remarkable results: the present-day inflationary SGWB energy density spectrum in the ΛSFDM model is so highly amplified relative to its amplitude in ΛCDM that it may be detectable by the ongoing Advanced LIGO/Virgo (aLIGO/Virgo) experiment. We will show that the expected signal-to-noise ratio (SNR) of this unique SGWB signal can be significant for a wide range of SFDM parameters and reheat temperatures, for currently allowed values of r. The SFDM model may thus be tested for parameters in this range, and the accessible range will grow over time as aLIGO/Virgo completes its planned observing runs. Hence, our results provide an additional motivation for LIGO to search for SGWB signals, since this has the potential to probe the nature of dark matter, reheating physics and inflation parameters. In §VI, we briefly discuss several aspects in which our results in this paper can be extended in anticipation of future developments of measurements of BBN light-element abundances, and of the space laser interferometer mission eLISA (the "Evolved LISA"). We summarize our conclusions in §VII. Appendices A–C contain some additional materials which we defer from the main text for better readability.

II. BASIC EQUATIONS

A. The Background universe

As in Paper I, we will consider the background universe which is homogeneous and isotropic on large scales. In this work, its metric tensor $g_{\mu\nu}$ is dominated by the spatially-flat Friedmann-Lemaître-Robertson-Walker (FLRW) metric, yet allowing *tensor* perturbations as well (scalar and vector perturbations are set to zero). In the cosmological "comoving frame" [4], it can be written as

$$\begin{aligned} \mathrm{d}s^2 &\equiv g_{\mu\nu}\mathrm{d}x^\mu \mathrm{d}x^\nu = (\bar{g}_{\mu\nu} + \delta g_{\mu\nu})\mathrm{d}x^\mu \mathrm{d}x^\nu \\ &= c^2\mathrm{d}t^2 - a^2(t)(\delta_{ij} + h_{ij})\mathrm{d}x^i \mathrm{d}x^j, \end{aligned} \tag{2}$$

where $a(t)$ is the scale factor, $\bar{g}_{\mu\nu}$ is the unperturbed FLRW metric, and h_{ij} is a symmetric tensor which characterizes tensor perturbations to the metric, $|h_{ij}| \ll 1$ (weak-field limit). The gauge-invariant h_{ij} satisfies the transverse and traceless conditions (see, e.g., [79]), [5]

$$\partial_i h^{ij} = 0, \quad h_i{}^i = 0, \tag{3}$$

where indices of h_{ij} are raised and lowered by the spatial background metric δ_{ij}; $h^{ij} = \delta^{ik}\delta^{jl}h_{kl}$. In

[4] Rigorously speaking, this reference frame is exactly comoving with cosmic flows only if the universe is perfectly homogeneous and isotropic, i.e., no fluctuations.

[5] If h_{ij} is instead a generic 3-tensor that describes spatial metric perturbations, the conditions in Eq. (3) would be regarded as coordinate conditions, known as the transverse-traceless (TT) gauge [80].

this paper, we follow the Einstein summation convention. While we only consider the homogeneous average universe here, it is understood that there may be generic small perturbations as well, the growth of which we do not study in this paper. The metric perturbations associated with the tensor modes are special, however, in that they also contribute an effective stress-energy tensor $T_{\mu\nu,\,\mathrm{GW}}$ as gravitational waves, as we show in §II A 2 and Appendix A 1.

The evolution of the metric of the background universe is governed by the Einstein field equations,

$$R^{\mu}_{\ \nu} - \frac{1}{2}R = \frac{8\pi G}{c^4}T^{\mu}_{\ \nu}, \tag{4}$$

where $R^{\mu}_{\ \nu}$ is the Ricci tensor which can be calculated from the metric in Eq. (2). The time-time component of the stress-energy tensor, $T^0_{\ 0}$, defines the energy density. For the background universe, it is sufficient to solve only the time-time component of the Einstein field equations, which amounts to the Friedmann equation, plus the energy conservation equations of each component that constitutes the total $T_{\mu\nu}$ of the universe (see [81]). In many cases, the latter can be derived from the equation of motion of the component. Therefore, we will evaluate both sides of the time-time component of Eq. (4) and also find the contribution to the total energy density of the universe from each component.

The expansion of the homogeneous FLRW universe is governed by the Friedmann equation, which is derived from the time-time component of the Einstein equations (4). For our model,

$$H^2(t) \equiv \left(\frac{\mathrm{d}a/\mathrm{d}t}{a}\right)^2 = \begin{cases} H^2_{\mathrm{inf}}, & a < a_{\mathrm{inf}}, \quad (5) \\ H^2_{\mathrm{inf}}\left(\dfrac{a_{\mathrm{inf}}}{a(t)}\right)^3, & a_{\mathrm{inf}} < a < a_{\mathrm{reheat}}, \quad (6) \\ \dfrac{8\pi G}{3c^2}\left[\rho_r(t) + \rho_b(t) + \rho_\Lambda(t) + \rho_{\mathrm{SFDM}}(t) + \rho_{\mathrm{GW}}(t)\right], & a > a_{\mathrm{reheat}}, \quad (7) \end{cases}$$

where a_{inf} is the scale factor at the end of inflation when $H(t) = H_{\mathrm{inf}}$, a_{reheat} is the scale factor when reheating ends at $T = T_{\mathrm{reheat}}$, and we have assumed that $w = 0$ during reheating. In our model, SFDM accounts for all of the cosmological dark matter. Apart from SFDM and gravitational waves, all the other cosmic components are the same than in ΛCDM, i.e. a radiation component ρ_r, baryons ρ_b, and a cosmological constant ρ_Λ (see Eq. [7]). The evolution of each component is described in §III.

1. *Energy density contribution from SFDM*

Let us write down the Lagrangian density of the SFDM again,

$$\mathcal{L} = \frac{\hbar^2}{2m}g^{\mu\nu}\partial_\mu\psi^*\partial_\nu\psi - \frac{1}{2}mc^2|\psi|^2 - \frac{\lambda}{2}|\psi|^4,$$

where the metric $g_{\mu\nu}$ is described in Eq. (2) and the definition of the particle mass m and self-interaction coupling strength λ have been explained in §I C. The field ψ can be written as

$$\psi = |\psi|e^{\mathrm{i}\theta}, \tag{8}$$

where $|\psi|$ is its modulus and θ is its phase.

In general, the stress-energy tensor of a field with Lagrangian density $\mathcal{L}$ is given by

$$T_{\mu\nu} = 2\frac{\delta\mathcal{L}}{\delta g^{\mu\nu}} - g_{\mu\nu}\mathcal{L}. \tag{9}$$

Hence, the stress-energy tensor of SFDM can be evaluated as

$$\begin{aligned} T_{\mu\nu,\,\mathrm{SFDM}} = {} & \frac{\hbar^2}{2m}(\partial_\mu\psi^*\partial_\nu\psi + \partial_\nu\psi^*\partial_\mu\psi) - \\ & - g_{\mu\nu}\left(\frac{\hbar^2}{2m}g^{\rho\sigma}\partial_\rho\psi^*\partial_\sigma\psi - \right. \\ & \left. - \frac{1}{2}mc^2|\psi|^2 - \frac{\lambda}{2}|\psi|^4\right). \end{aligned} \tag{10}$$

In linear theory with the perturbed FLRW metric (2), we have verified that, to the first order, the complex SFDM behaves as a perfect fluid, because $T_{\mu\nu,\,\mathrm{SFDM}}$ can be written in the following form as for a perfect fluid, characterized by its energy density ρ_{SFDM}, isotropic pressure p_{SFDM} and 4-velocity $u^\mu \equiv c(\mathrm{d}x^\mu/\mathrm{d}s)$, with no anisotropic stress,

$$T_{\mu\nu,\,\mathrm{SFDM}} = (\rho_{\mathrm{SFDM}} + p_{\mathrm{SFDM}})u_\mu u_\nu/c^2 - g_{\mu\nu}p_{\mathrm{SFDM}}. \tag{11}$$

For the homogeneous and isotropic background universe, $u^0 = c$ and $u^i = 0$, and thus, $T_{\mu\nu,\ \mathrm{SFDM}}$ becomes diagonal. Its time-time component is recognized as the spatially-averaged energy density of SFDM,

$$\begin{aligned}\rho_{\mathrm{SFDM}} \equiv T^0_{0,\ \mathrm{SFDM}} &= \frac{\hbar^2}{2mc^2}|\partial_t\psi|^2 + \\ &+\frac{1}{2}mc^2|\psi|^2 + \frac{1}{2}\lambda|\psi|^4 \\ &= \frac{\hbar^2}{2mc^2}\left[|\dot{\psi}|^2 + |\psi|^2\dot{\theta}^2\right] \\ &+\frac{1}{2}mc^2|\psi|^2 + \frac{1}{2}\lambda|\psi|^4, \end{aligned} \tag{12}$$

where an "overdot" ($\dot{}$) indicates the derivative with respect to the cosmic time $\mathrm{d}/\mathrm{d}t$, throughout this paper. In the equation above and thereafter, we assume that the complex function ψ always means the spatially-averaged value of the BEC wave function, which adequately accounts for the SFDM contribution to the background universe. The space-space component of $T_{\mu\nu,\ \mathrm{SFDM}}$ is recognized as the spatially-averaged pressure,

$$\begin{aligned}p_{\mathrm{SFDM}} \equiv -T^i_{i,\ \mathrm{SFDM}} &= \frac{\hbar^2}{2mc^2}\left[|\dot{\psi}|^2 + |\psi|^2\dot{\theta}^2\right] \\ &-\frac{1}{2}mc^2|\psi|^2 - \frac{1}{2}\lambda|\psi|^4. \end{aligned} \tag{13}$$

Hereafter in this paper, ρ_{SFDM} and p_{SFDM} will always refer to the homogeneous part of the energy density and pressure of SFDM, which are only functions of time.

Eqs. (12) and (13) can also be rearranged into a useful form, in which ρ_{SFDM} and p_{SFDM} are related to $|\psi|^2$,

$$\begin{aligned}\rho_{\mathrm{SFDM}} &= \frac{\hbar^2}{2mc^2}\left(\frac{(\mathrm{d}|\psi|^2/\mathrm{d}t)^2}{4|\psi|^2} + \frac{(a^3|\psi|^2\dot{\theta})^2}{a^6|\psi|^2}\right) \\ &+\frac{1}{2}mc^2|\psi|^2 + \frac{1}{2}\lambda|\psi|^4, \end{aligned} \tag{14}$$

$$\begin{aligned}p_{\mathrm{SFDM}} &= \frac{\hbar^2}{2mc^2}\left(\frac{(\mathrm{d}|\psi|^2/\mathrm{d}t)^2}{4|\psi|^2} + \frac{(a^3|\psi|^2\dot{\theta})^2}{a^6|\psi|^2}\right) \\ &-\frac{1}{2}mc^2|\psi|^2 - \frac{1}{2}\lambda|\psi|^4. \end{aligned} \tag{15}$$

We note that in the numerator of the 2nd term above, $a^3|\psi|^2\dot{\theta}$ is a conserved quantity as it is proportional to the comoving charge density (see Appendix B in Paper I). In fact,

$$a^3|\psi|^2\dot{\theta} \equiv \frac{mc^2}{\hbar}Q = \rho_{\mathrm{SFDM},0}/\hbar, \tag{16}$$

where $\rho_{\mathrm{SFDM},0}$ is the present-day dark matter energy density. The last equality in the equation above expresses the fact that our SFDM today can be treated as nonrelativistic particles (the spintessence limit, see §I B). On the other hand, it is shown in Paper I that $\dot{\theta} \cong mc^2/\hbar$ when SFDM is nonrelativistic as "dust-like". Therefore, the number density of SFDM at present, equivalent to the comoving charge density, is given by

$$|\psi|^2\Big|_{a=1} = Q = \rho_{\mathrm{SFDM},0}/mc^2. \tag{17}$$

2. Energy density contribution from gravitational waves

As pointed out in [80], gravitational waves, squeezing and stretching the local metric perpendicular to their direction of propagation through space-time, must carry energy. In fact, an (effective) stress-energy tensor of GWs, $T_{\mu\nu,\ \mathrm{GW}}$, can be defined for small tensor perturbations to the background metric, which is slowly-varying on scales larger than the wavelength, as shown in Appendix A 1.

The effective energy density associated with tensor perturbations h_{ij} can be written as follows:

$$\rho_{\mathrm{GW}} \equiv T^0_{0,\ \mathrm{GW}} = \frac{c^2}{64\pi G}\langle\partial_t h_{ij}\partial_t h^{ij} + \frac{c^2}{a^2}\nabla h_{ij}\cdot\nabla h^{ij}\rangle, \tag{18}$$

[77] where the brackets $\langle\cdot\rangle$ denote the spatial average over several wavelengths. In particular, this will describe the effect of the SGWB from inflation of interest here. Since primordial fluctuations (including the tensor sector) produced by most inflation models are predicted to be Gaussian, the SGWB can therefore be fully characterized by its power spectrum. As a result, the spatial average $\langle\cdot\rangle$ defined above is equal to the ensemble average. Furthermore, we assume that this ensemble average of tensor fluctuations is unpolarized and isotropic on large scales, according to the standard paradigm of inflation and reheating, as mentioned in §I D. This guarantees that the SGWB produced by inflation is homogeneous on large scales. Hence, applying the Fourier decomposition to h_{ij} (see Appendix A 2, Eq. [A6]), we can write down the (dimensionless) power spectrum of the SGWB, $\Delta^2_h(k,t)$, or the tensor power spectrum, in terms of its mode functions $h^P_{\mathbf{k}}$, as follows:

$$k^3\langle h^P_{\mathbf{k}}(t)(h^{P'}_{\mathbf{k}'}(t))^*\rangle \equiv 2\pi^2\Delta^2_h(k,t)\delta^{(3)}_D(\mathbf{k}-\mathbf{k}')\frac{\delta_{PP'}}{4}, \tag{19}$$

where $k = |\mathbf{k}|$ is the comoving wavenumber, $P = +, \times$ stands for the two linear polarization states of h_{ij}, $\delta^{(3)}_D$ is the Dirac delta function and $\delta_{PP'}$ denotes the Kronecker delta. As required, $\Delta^2_h(k,t)$ does not

depend on the direction of the comoving wave vector $\mathbf{k}$ nor the polarization state P, only on the magnitude $k = |\mathbf{k}|$, capturing all statistical properties of the stochastic metric perturbation h_{ij}.[6] Inserting Eq. (19) and Eq. (A6) into Eq. (18) yields

$$\rho_{\rm GW}(t) = \frac{c^2}{64\pi G}\int_0^\infty {\rm d}\ln k \left(\left|\frac{\dot{h}^P_{\mathbf{k}}(t)}{h^P_{\mathbf{k}}(t)}\right|^2 \Delta^2_h(k,t) + \frac{k^2c^2}{a^2(t)}\Delta^2_h(k,t)\right), \tag{20}$$

where the term $|\dot{h}^P_{\mathbf{k}}(t)/h^P_{\mathbf{k}}(t)|^2$ has been extracted out of the ensemble average $\langle\cdot\rangle$, because it is deterministic, governed by the equation of motion of $h^P_{\mathbf{k}}(t)$, which we will show in §II C. There we will also explain why $|\dot{h}^P_{\mathbf{k}}(t)/h^P_{\mathbf{k}}(t)|^2$ does not depend on P, i.e., P can be either + or ×. As expected, Eq. (20) shows that $\rho_{\rm GW}(t)$ is homogeneous in space, since it does not depend on position $\mathbf{x}$.

It is useful to define the differential SGWB energy density per logarithmic k as

$$\frac{{\rm d}\rho_{\rm GW}}{{\rm d}\ln k}(k,t) = \frac{c^2}{64\pi G}\left(\left|\frac{\dot{h}^P_{\mathbf{k}}(t)}{h^P_{\mathbf{k}}(t)}\right|^2 + \frac{k^2c^2}{a^2(t)}\right)\Delta^2_h(k,t). \tag{21}$$

B. Equation of motion: scalar field dark matter

The equation of motion for SFDM is the Klein-Gordon equation. For a homogeneous scalar field, it is written as

$$\frac{\hbar^2}{2mc^2}\ddot{\psi} + 3\frac{\hbar^2}{2mc^2}\frac{\dot{a}}{a}\dot{\psi} + \frac{1}{2}mc^2\psi + \lambda|\psi|^2\psi = 0, \tag{22}$$

in terms of the BEC wave function $\psi(t)$. It can be transformed into an equivalent form, namely, the energy conservation equation, in terms of the energy density $\rho_{\rm SFDM}$ and the corresponding pressure, $p_{\rm SFDM}$, as follows:

$$\dot{\rho}_{\rm SFDM} + 3\frac{\dot{a}}{a}(\rho_{\rm SFDM} + p_{\rm SFDM}) = 0. \tag{23}$$

The Klein-Gordon equation (22) can be rearranged into the following form,

$$\frac{\hbar^2}{2mc^2}\left(\frac{{\rm d}^2|\psi|^2}{{\rm d}t^2} - \frac{({\rm d}|\psi|^2/{\rm d}t)^2}{2|\psi|^2}\right) + \frac{\hbar^2}{2mc^2}\frac{3\dot{a}}{a}\frac{{\rm d}|\psi|^2}{{\rm d}t} - \frac{\hbar^2}{mc^2}\frac{(\rho_{\rm SFDM,0}/\hbar)^2}{a^6|\psi|^2} + mc^2|\psi|^2 + 2\lambda|\psi|^4 = 0, \tag{24}$$

where we have made use of Eq. (16), replacing $a^3|\psi|^2\dot{\theta}$ by $\rho_{\rm SFDM,0}/\hbar$. In Eq. (24), the dependent variable is essentially $|\psi|^2$, rather than ψ. We will see later in §III D 1 that it is this equation that we solve numerically to obtain the early phase of the evolution of SFDM.

C. Equation of motion: tensor perturbations

In the absence of anisotropic stresses,[7] the Einstein equation for tensor perturbations h_{ij} in a spatially flat FLRW universe with scale factor a reads

$$\partial_t^2 h_{ij}(\mathbf{x},t) + 3\frac{\dot{a}(t)}{a(t)}\partial_t h_{ij}(\mathbf{x},t) - \frac{c^2}{a^2(t)}\nabla^2 h_{ij}(\mathbf{x},t) = 0. \tag{25}$$

[6] Strictly speaking, to ensure that the tensor power spectrum is only a function of the wavenumber k at any time t, we also need to investigate the evolution of h_{ij} via its equation of motion, which is explained in §II C.

[7] Actually, the presence of free-streaming relativistic neutrinos has been shown by [82] to contribute anisotropic stress which modifies Eq. (25). The correction which results can be treated by a post-facto multiplicative factor which does not depend on wavenumber k, as described in [83].

The above equation is essentially a cosmological wave equation, its corresponding solutions are thus gravitational waves. In fact, the wave nature can be more directly manifested by rewriting the above equation of motion (25) in terms of Fourier mode functions $h^P_{\mathbf{k}}(t)$ (and their conjugate $(h^P_{\mathbf{k}}(t))^*$, see Eq. [A6] for their definition),

$$\ddot{h}^P_{\mathbf{k}}(t) + 3\frac{\dot{a}(t)}{a(t)}\dot{h}^P_{\mathbf{k}}(t) + \frac{k^2c^2}{a^2(t)}h^P_{\mathbf{k}}(t) = 0. \tag{26}$$

The above equation manifestly shows that the equation of motion for tensor perturbations only involves the magnitude $k = |\mathbf{k}|$ of the wave vector, not its direction nor the polarization state $P = +$ or $\times$. Therefore, as long as the initial condition for tensor perturbations is isotropic and unpolarized, so will they always be at any time throughout their evolution. This completes our justification to treat $\Delta^2_h(k,t)$ only as a function of k at any time t. With no loss of generality, we can thereby assume $h^+_{\mathbf{k}}(t) = h^\times_{\mathbf{k}}(t) \equiv h_k(t)$ and henceforth treat $h_k(t)$ only.

In Eq. (26), if we set $a = 1$, its solutions are simply plane waves with the dispersion relation $\omega_k = kc$. Therefore, on time scales much less than a Hubble time, GWs are plane waves propagating at the speed of light, as those detected by the Advanced LIGO experiment, of which sources are binary black hole merger events [84]. For this reason, GWs are also known as gravitational radiation, or radiative degrees of freedom [85].

It is convenient to express Eq. (26) with respect to the conformal time (length), $\tau = c\int dt/a(t)$, leading to an equation for $h_k(\tau)$,

$$h_k''(\tau) + 2\frac{a'(\tau)}{a(\tau)}h_k'(\tau) + k^2h_k(\tau) = 0, \tag{27}$$

where the prime denotes the derivative with respect to conformal time $' \equiv d/d\tau$. We will discuss the evolution of gravitational waves, and some analytical solutions, in §III B.

III. EVOLUTION IN THE ΛSFDM UNIVERSE

In Paper I, we considered a universe with the same cosmic inventory as the basic ΛCDM model except that CDM is replaced by SFDM, the ΛSFDM model. We used the set of cosmological parameters from the Planck 2013 data release [86]. In this work, we will add to ΛSFDM the contribution due to $\rho_{\rm GW}$, as it is currently constrained by upper bounds. Also, we use the updated 2015 Planck data to solve for the evolution of this homogeneous background universe [1]. A summary of the parameters we use can be found in Table I. The fractional energy densities are defined via $\Omega_i(t) \equiv \rho_i(t)/\rho_{\rm crit}(t)$ with the critical energy density of the universe at time t,

$$\rho_{\rm crit}(t) = \frac{3H^2(t)c^2}{8\pi G}. \tag{28}$$

Hereafter in this paper, unless otherwise noted as fluctuations, all physical quantities in space will refer to their spatially homogeneous, isotropic part, i.e., only functions of time.

First, we discuss the evolution of each of the cosmic components separately in §III A–§III C, highlighting certain heuristic aspects. We then put them altogether in §III D to derive the expansion history of the entire background ΛSFDM universe. In our analysis, we adopt the philosophy to start with the (present-day) cosmological parameters, as we know them from CMB measurements, rather than to start with (unknown) initial conditions in the very early universe and propagating them forward in time, in efforts to ending up at the right present-day values. Instead, we will (at first) calculate the evolution backwards in time (similar to Paper I), using cosmological parameters in Table I as initial conditions, up to the end of inflation, whose energy scale is set by our choices of r. The effects of $\Omega_{\rm GW}$, however, will require us to implement a more elaborate scheme than in Paper I. We present the details of the numerical method in §III D 1 below.

h	0.6781	$\Omega_m h^2$	0.141
$\Omega_b h^2$	0.02226	$\Omega_r h^2$	4.184×10^{-5}
$\Omega_c h^2$	0.1186	$z_{\rm eq}$	3365
$T_{\rm CMB}$/K	2.7255	Ω_Λ	0.694
$10^9 A_s$	2.139	$r_{0.05}$	< 0.07 (95%)

TABLE I: Cosmological parameters. All values except $r_{0.05}$ are quoted from the Planck 2015 results: central values of the 68% confidence intervals for the base ΛCDM model with TT+LowP+Lensing data, see Table 4 in [1]. The upper bound of $r_{0.05}$ at the pivot scale $k_* = 0.05$ Mpc^{-1} at 95% confidence is quoted from the latest result of the BICEP2/Keck Array CMB polarization experiment [66].

A. Evolution of SFDM

In our model, DM is entirely made up of SFDM, i.e. $\Omega_c h^2$ in Table I will be taken to refer to the

present-day SFDM energy density, instead of CDM. The discussion in this subsection follows largely the one in Paper I, but since it is of central importance to our model, we want to repeat some of it here for the sake of the reader.

One basic behavior of a scalar field is that it oscillates over time, characterized by its changes in phase θ. The oscillation angular frequency is defined as $\omega \equiv \dot{\theta}$. SFDM behaves differently, depending on whether ω predominates over the expansion rate H or not (oscillation vs. roll). As a result, SFDM passes through certain limit cases as it evolves, in which its EOS is simply barotropic, as we have shown in Paper I.

1. *Scalar field oscillation faster than Hubble expansion ($\omega/H \gg 1$)*

In this regime, the oscillation angular frequency can be derived as (see Paper I)

$$\omega = \frac{mc^2}{\hbar}\sqrt{1+\frac{2\lambda}{mc^2}|\psi|^2}. \tag{29}$$

If ω is much larger than the Hubble parameter H, the exact calculation of the cosmological time evolution of the scalar field is numerically prohibitive, since the necessary time step is too small ($\propto 1/\omega$). Instead, it has been customary in the literature to follow the evolution of the time-averaged values of ρ and p over several oscillation cycles of the field. In this subsection §III A, we omit the subscript "SFDM" in ρ and p for brevity. Multiplying the field equation (22) by ψ^* and then averaging over a time interval that is much longer than the field oscillation period, but much shorter than the Hubble time, results in (see also [27, 87])

$$\frac{\hbar^2}{2mc^2}\langle|\mathrm{d}\psi/\mathrm{d}t|^2\rangle \cong \frac{1}{2}mc^2\langle|\psi|^2\rangle + \lambda\langle|\psi|^4\rangle. \tag{30}$$

Combining this relation with the expressions for energy density (12) and pressure (13) yields,

$$\begin{aligned}\langle\rho\rangle &= mc^2\langle|\psi|^2\rangle + \frac{3}{2}\lambda\langle|\psi|^4\rangle \\ &\approx mc^2\langle|\psi|^2\rangle + \frac{3}{2}\lambda\langle|\psi|^2\rangle^2, \qquad (31)\\ \langle p\rangle &= \frac{1}{2}\lambda\langle|\psi|^4\rangle \approx \frac{1}{2}\lambda\langle|\psi|^2\rangle^2. \qquad (32)\end{aligned}$$

In this regime, we take $\rho = \langle\rho\rangle$ and $p = \langle p\rangle$. The equation of state is then approximately

$$p = \frac{m^2c^4}{18\lambda}\left(\sqrt{1+\frac{6\lambda\rho}{m^2c^4}}-1\right)^2, \tag{33}$$

or equivalently,

$$w \equiv \frac{p}{\rho} = \frac{1}{3}\left[\frac{1}{1+\frac{2mc^2}{3\lambda\langle|\psi|^2\rangle}}\right] \tag{34}$$

(see also [41, 59]). This is referred to as the fast-oscillation approximation in Paper I. We call this regime the *fast-oscillation regime*, and, henceforth, drop the $\langle\rangle$'s around ρ and p in what follows. It encompasses two evolutionary phases of SFDM, as follows:

(1) CDM-like (or "dust"-like) phase: non-relativistic ($w = 0$)

As the universe expands, the dark matter energy density will continuously decrease to the point when the rest-mass energy density dominates the total SFDM energy density, i.e., $\frac{3}{2}\lambda\langle|\psi|^2\rangle^2 \ll mc^2\langle|\psi|^2\rangle$. In this limit, equation (33) reduces to

$$p \approx \frac{\lambda}{2m^2c^4}\rho^2 \approx 0, \tag{35}$$

thus SFDM behaves like non-relativistic dust. Its self-interaction is weak, so that on large scales SFDM is virtually collisionless. Therefore, it evolves like CDM, following the familiar relation,

$$\rho \propto a^{-3}. \tag{36}$$

Then, the field amplitude decays as $|\psi| \propto a^{-3/2}$ and the scale factor goes as $a \sim t^{2/3}$.

(2) Radiationlike phase: relativistic ($w = 1/3$)

At some point early enough, the SFDM will be so dense that the quartic term in the energy density (31), the self-interaction energy, dominates, i.e., $\frac{3}{2}\lambda\langle|\psi|^2\rangle^2 \gg mc^2\langle|\psi|^2\rangle$. In this limit, equation (33) reduces to

$$p \approx \frac{1}{3}\rho \approx \frac{1}{2}\lambda\langle|\psi|^2\rangle^2, \tag{37}$$

and SFDM behaves like radiation. The time evolution is accordingly

$$\rho \propto a^{-4}, \tag{38}$$

while the field amplitude decays as $|\psi| \propto a^{-2}$ with the scale factor $a \sim t^{1/2}$.

It is important to note that SFDM without self-interaction, i.e., when $\lambda = 0$, does *not* undergo this radiationlike phase.

2. Scalar field oscillation slower than Hubble expansion ($\omega/H \ll 1$)

The Hubble parameter increases as one goes back in time, and will eventually exceed the oscillation frequency. This is when the fast oscillation approximation will break down with no closed-form expression for the EOS. In this case, one has to solve the rearranged Klein-Gordon equation (24) exactly, coupled with the Friedmann equations (7). Nonetheless, one can still find a heuristic qualitative description, as follows:

(1) Stiff phase: relativistic limit ($w = 1$)

At sufficiently early times, the expansion rate is much greater than the oscillation frequency, $\omega/H \ll 1$. The energy density and pressure are both dominated by the kinetic term of (12) and (13), $\frac{\hbar^2}{2mc^2}|\partial_t\psi|^2 \propto H^2$. Therefore,

$$p \approx \rho \approx \frac{\hbar^2}{2mc^2}|\partial_t\psi|^2. \tag{39}$$

This stiff EOS implies that the sound speed almost reaches the speed of light, the maximal possible value (this is formally analoguous to the incompressible fluid in Newtonian gas dynamics, where the sound speed is infinity). In this case,

$$\rho \propto a^{-6}, \tag{40}$$

and it can be shown that $\partial_t\psi \propto a^{-3}$, and hence $\psi \propto \log a$, where $a \sim t^{1/3}$. The physical picture of the stiff phase is that, at such an early epoch, the Hubble time is much smaller than the oscillation period so that the complex scalar field cannot even complete one cycle of spin within one Hubble time. Instead, it rolls down the potential well (the "fast-roll" regime). An important implication immediately follows the relation (40) that, as we go back in time approaching the Big Bang ($a \to 0$), the energy density of SFDM should dominate the total energy density of the universe, because it increases faster than that of radiation and of any other component. Therefore, we predict an early era of stiff-SFDM-domination in a ΛSFDM universe, which will be demonstrated in §III D.

B. Tensor fluctuations from inflation and the SGWB

In this subsection, we describe the evolution and implementation of our calculation of the SGWB. To anticipate our full numerical treatment presented in §III D, in which we solve the coupled equations for the SGWB, the SFDM, the standard cosmic components and the expansion rate of the background universe, it will be instructive to show some analytical results first, for the simpler case of constant w (the EOS parameter of the universe). For this purpose, we must derive the energy density contributed by the SGWB, for which we will first need to derive the evolution of the tensor metric perturbations, by solving their equation of motion presented in §II C along with the initial condition posed in §III B 1 below. As we shall see, there are two limits in which this evolution is simplified for a given mode of comoving wavenumber k, in terms of its wavelength ($\propto k^{-1}$) relative to the horizon. It will be sufficient to represent the evolution at all times by stitching these two limits together, in what is known as the *thin-horizon approximation*. With this solution, we will have both the spectrum of the primordial tensor perturbations and of their associated energy density as a function of time.

1. Primordial amplitude

The equation of motion for the tensor modes $h_k(\tau)$ in Eq. (27) requires an initial condition. For our purpose, the initial amplitude of $h_k(\tau)$ is given by the primordial tensor amplitude produced by inflation. During slow-roll inflation, in which the Hubble constant $H(a)$ is slowly varing, fluctuations are exponentially stretched in space, so that for many modes, their proper wavelengths, $2\pi a/k$, will become larger than the Hubble radius $c/H(a)$ (or the horizon). In other words, these modes exit the horizon during inflation. Once a mode is far outside the horizon, the amplitude (of its growing mode) is conserved ("frozen") throughout its superhorizon evolution [81], even after inflation ends. Therefore, we will begin our integration of Eq. (27) for a given mode k when it is far outside the horizon (i.e., $kc \ll aH(a)$) and its initial amplitude, $h_{k,\,\mathrm{init}}$, is given by this superhorizon value. Modes of interest are all far outside the horizon by the end of inflation at $a = a_{\mathrm{inf}}$, so $h_k(a_{\mathrm{inf}}) = h_{k,\,\mathrm{init}}$ for these modes.

These modes will later reenter the horizon at different cosmic times according to their wavelength, while the EOS of the background universe evolves through different cosmic eras. On the other hand, modes reentering during different eras do not know of each other, which means that each mode inherits the memory of its own superhorizon amplitude $h_{k,\,\mathrm{init}}$ with which it started out, at its respective

reentry point a_k.[8] Hereafter in this paper, unless otherwise noted, we will use a_k and $H_k \equiv H(a_k)$ to indicate those quantities at the horizon reentry for mode k, $kc = a_k H_k$.

Note that this initial amplitude $h_{k,\ \rm init}$ is not unique, because of the stochastic nature of the primordial tensor fluctuations produced by inflation. However, this does not prevent us from evaluating $\rho_{\rm GW}(\tau)$, the mean energy density of the inflationary SGWB, in Eq. (20), because the stochasticity in h_k is fully accounted for by the tensor power spectrum $\Delta_h^2(k,\tau)$ defined in Eq. (19). In fact, we only need to know the primordial tensor power spectrum, $\Delta^2_{h,\ \rm init}(k) \equiv \Delta_h^2(k, a_{\rm inf})$, evaluated at $a_{\rm inf}$ for all modes of interest. The evolution of $\Delta_h^2(k,\tau)$, or equivalently, $h_k(\tau)$, at any time later is deterministic, separable from its stochastic initial condition. We can define the tensor transfer function $T_h(k,\tau)$, which encodes this deterministic evolution, as

$$T_h(k,\tau) \equiv \left|\frac{h_k(\tau)}{h_{k,\ \rm init}}\right|^2 = \frac{\Delta_h^2(k,\tau)}{\Delta^2_{h,\ \rm init}(k)}, \qquad (41)$$

the solution of which we will show in §III B 2.

The primordial power spectrum of tensor fluctuations generated during inflation, $\Delta^2_{h,\ \rm init}(k)$, is predicted to be nearly scale-invariant, if inflation is driven by a single slow-rolling scalar field. It can be parametrized by a power law,

$$\Delta^2_{h,\ \rm init}(k) = A_t (k/k_*)^{n_t} \equiv r A_s (k/k_*)^{n_t}, \qquad (42)$$

where A_t (A_s) is the tensor (scalar) amplitude, and the pivot scale $k_* = 0.05\ {\rm Mpc}^{-1}$, following the 2015 Planck data convention [1]. The value of A_s and the latest upper bound of $r = r_{0.05}$ is given in Table I. The tensor spectral index n_t is related to the tensor-to-scalar ratio r by

$$n_t = -r/8, \qquad (43)$$

which is known as the consistency relation. In this paper, we will presume that this relation is valid.

2. *Analytical solutions for tensor metric perturbations in the subhorizon limit*

Closed-form solutions of Eq. (27) for $h_k(\tau)$ exist, if a and the conformal time τ are related via a powerlaw,

$$\frac{a}{a_0} = \left(\frac{\tau}{\tau_0}\right)^\alpha, \qquad (44)$$

where the exponent α depends on the EOS parameter w of the universe, according to

$$\alpha = \frac{2}{1+3w}. \qquad (45)$$

In our case, however, w changes with time, so we cannot adopt Eq. (44) in general. Fortunately, when a mode is well outside the horizon, h_k is independent of time and of the change in w. Furthermore, as long as there are eras of the background expansion history in which w is relatively constant, i.e., in each of these eras Eq. (44) can be applied with a respective constant α over a range of τ, we can insert this relation into Eq. (27), to obtain an analytical solution for the evolution of $h_k(\tau)$ during these eras.

Particularly, if a mode k reenters the horizon in such an era with a constant α, and later becomes deep within the horizon (i.e., $k \gg aH/c$, or $k\tau \gg \alpha$) while still in the same era, one can show that in this subhorizon limit the solution for $h_k(\tau)$, in the eras of interest to us, respectively reads as

- reheating and matter-dominated era: $w = 0, \alpha = 2$

$$h_{k,\ \rm m}(\tau) \simeq h_{k,\ \rm init}\Gamma\left(\frac{5}{2}\right)\frac{4}{\sqrt{\pi}}\frac{\cos(k\tau-\pi)}{(k\tau)^2} \quad \text{for } k\tau \gg 2, \qquad (46)$$

- stiff-SFDM-dominated era: $w = 1, \alpha = \frac{1}{2}$

$$h_{k,\ \rm stiff}(\tau) \simeq h_{k,\ \rm init}\sqrt{\frac{2}{\pi}}\frac{\cos(k\tau-\pi/4)}{(k\tau)^{1/2}} \quad \text{for } k\tau \gg \frac{1}{2}, \qquad (47)$$

[8] There are also modes at the low-k end, whose comoving wavelengths are even larger than the present-day horizon size. Hence, they will never reenter the horizon as the universe has already been in the Λ-dominated era. We do not study these modes in this paper.

- radiation-dominated era: $w = \frac{1}{3}, \alpha = 1$

$$h_{k,\ \mathrm{rad}}(\tau) \simeq h_{k,\ \mathrm{init}} \Gamma \left(\frac{3}{2}\right) \frac{4}{\sqrt{\pi}} \frac{\cos(k\tau - \pi/2)}{k\tau} \quad \text{for } k\tau \gg 1. \tag{48}$$

Thus, the initial (superhorizon) amplitude from inflation, $h_{k,\ \mathrm{init}}$, suffers decay upon horizon reentry, according to those expressions. In terms of the tensor transfer function $T_h(k,\tau)$ defined in Eq. (41), we can see that, in the respective eras considered above,

$$T_h^{\mathrm{m}}(k,\tau) = \Gamma^2 \left(\frac{5}{2}\right) \frac{16}{\pi} \frac{\cos^2(k\tau - \pi)}{(k\tau)^4}, \tag{49}$$

$$T_h^{\mathrm{stiff}}(k,\tau) = \frac{2}{\pi} \frac{\cos^2(k\tau - \pi/4)}{k\tau}, \tag{50}$$

and

$$T_h^{\mathrm{rad}}(k,\tau) = \Gamma^2 \left(\frac{3}{2}\right) \frac{16}{\pi} \frac{\cos^2(k\tau - \pi/2)}{(k\tau)^2}. \tag{51}$$

Indeed, it can be shown that the tensor transfer function in the subhorizon limit for general α reads as

$$T_h(k,\tau) = \frac{\Gamma^2(\alpha_k + \frac{1}{2})}{\pi} \left(\frac{2}{k\tau}\right)^{2\alpha_k} \cos^2(k\tau - \alpha_k \pi/2)$$

$$\simeq \frac{1}{2} \left(\frac{a_k}{a}\right)^2 \frac{\Gamma^2(\alpha_k + \frac{1}{2})}{\pi} \left(\frac{2}{\alpha_k}\right)^{2\alpha_k} \tag{52}$$

(compare also to [77]), where a_k is the scale factor at which the mode k reenters the horizon, $a_k = kc/H_k$, and we averaged over $\cos^2(..)$ to arrive at the second line. The era-dependent parameter $\alpha_k = 2/(1 + 3w(a_k))$ should be evaluated at horizon reentry for each mode k as well. We note that in the second line of Eq. (52), the explicit time variable is a rather than τ. Therefore, this expression for the tensor transfer function $T_h(k,a)$ as a function of a, can be applied at any later time in the subhorizon limit for a given k, regardless of any later change in the EOS parameter w of the background universe.

The factor $\frac{1}{2}(a_k/a)^2$ in Eq. (52) will simply lead to the well-known behavior that for a given k, $\mathrm{d}\rho_{\mathrm{GW}}/\mathrm{d}\ln k$ (see Eq. [21]) decays like radiation ($\propto a^{-4}$) upon horizon reentry (called "redshift-suppression" factor C_1 in [77]), while the remaining factors make sure that the correct subhorizon limit is retrieved when matching the solution at horizon crossing to the superhorizon limit (called "horizon-crossing" factor C_2 in [77]).

There is an additional multiplicative factor which takes account of the effects of anisotropy due to neutrino free streaming (as described in [82, 83]). When relativistic neutrinos are important during the radiation-dominated era, they can damp the tensor fluctuations $h_k(\tau)$ by a multiplicative factor $A \sim 0.8$. This multiplicative factor is *not* included in the analytical solutions above (e.g., Eq. [52] for the tensor transfer function), but will be included later in our numerical solutions (this effect was called "anisotropy factor" C_3 in [77]).

3. *Evaluating* Ω_{GW}

The energy density fraction of the SGWB, $\Omega_{\mathrm{GW}}(a) \equiv 8\pi G \rho_{\mathrm{GW}}(a)/3H^2(a)c^2$, is calculated by integrating Eq. (21) over all modes of interest, divided by $\rho_{\mathrm{crit}}(a)$,

$$\Omega_{\mathrm{GW}}(k,a) \equiv \frac{\mathrm{d}\Omega_{\mathrm{GW}}(a)}{\mathrm{d}\ln k} = \frac{1}{\rho_{\mathrm{crit}}(a)} \frac{\mathrm{d}\rho_{\mathrm{GW}}(a)}{\mathrm{d}\ln k}$$
$$= \frac{\Delta_h^2(k,a)c^2}{24a^2H^2(a)} \left(\left| \frac{h_k'(a(\tau))}{h_k(a(\tau))} \right|^2 + k^2 \right). \tag{53}$$

This form is written in a way that makes apparent the contribution from superhorizon evolution, i.e., the second term in Eq. (53). In the subhorizon limit, the two terms are equal, as $|h_k'(a(\tau))|^2 \cong k^2 |h_k(a(\tau))|^2$. This can be shown by neglecting the Hubble friction term ($\propto a'/a$) in the wave equation (27). In the superhorizon limit, on the other hand, only the second term remains, since $h_k'(a(\tau)) \cong 0$. There remains uncertainty in whether superhorizon modes physically contribute an average stress-energy that can affect the background metric of the universe. However, this contribution, should it exist, is negligible compared to subhorizon modes anyway, as we have confirmed in this work.

1. **Subhorizon limit:**
 In the subhorizon limit $k \ll aH/c$, the energy density spectrum of GWs, $\Omega_{\mathrm{GW}}(k,a)$, can be calculated by solving the linear evolution equation (27). For modes which reenter the horizon when the universe has a fixed EOS, $\Omega_{\mathrm{GW}}(k,a)$, defined above in Eq. (53), is related to the

tensor transfer function defined in Eq. (41), as follows:

$$\Omega_{\rm GW}(k,a) = \frac{\Delta^2_h(k,a)}{12}\left(\frac{kc}{aH}\right)^2 = \frac{\Delta^2_{h,\ \rm init}(k)}{12}\left(\frac{kc}{aH}\right)^2 T_h(k,a). \quad (54)$$

The expressions for $\Omega_{\rm GW}(k,a(\tau))$ which correspond to the above analytical solutions in Eqs. (49-51), after averaging over $\cos^2(..)$, are given by

$$\Omega^{\rm m}_{\rm GW}(k,\tau) \simeq \frac{\Delta^2_{h,\ \rm init}(k)}{24}\cdot\frac{9}{4}\frac{1}{(k\tau)^2}, \quad (55)$$

$$\Omega^{\rm stiff}_{\rm GW}(k,\tau) \simeq \frac{\Delta^2_{h,\ \rm init}(k)}{24}\cdot\frac{8}{\pi}k\tau, \quad (56)$$

$$\Omega^{\rm rad}_{\rm GW}(k,\tau) \simeq \frac{\Delta^2_{h,\ \rm init}(k)}{24}. \quad (57)$$

We note the known k-dependence of $\Omega_{\rm GW}(k,\tau)$ for τ in the different eras, i.e. $\Omega^{\rm m}_{\rm GW}(k,\tau) \propto k^{-2}$, $\Omega^{\rm stiff}_{\rm GW}(k,\tau) \propto k$, and $\Omega^{\rm rad}_{\rm GW}(k,\tau) \propto k^0$, respectively. This dependence on k will be reflected in our prediction of the SGWB energy density spectrum at the present in §V.

We can now illustrate the effect of the amplification of the (differential) GW energy density of a certain mode with wavenumber k which reenters the horizon during the stiff phase, compared to that if the mode reenters the horizon during the radiation-dominated era, as in a standard ΛCDM universe. In fact, combining Eq. (42), Eq. (52) and Eq. (54) yields

$$\Omega_{\rm GW}(k,a) \simeq \frac{rA_s}{24}\left(\frac{ck}{aH}\right)^2\left(\frac{a_k}{a}\right)^2, \quad (58)$$

where we have, for simplicity, neglected the dependence on n_t in Eq. (42) and ignored the factor $\frac{\Gamma^2(\alpha+\frac{1}{2})}{\pi}\left(\frac{2}{\alpha}\right)^{2\alpha}$ in Eq. (52). In this equation above, the scale factor a is at a late time when the expansion histories of the two scenarios, ΛSFDM vs. ΛCDM, converge, so that the Hubble constant $H = H(a)$ is the same for both. Therefore, the only uncommon factor in Eq. (58) is a_k for the two scenarios. In a ΛSFDM universe, suppose now that the stiff era ends and the universe becomes radiation-dominated at $a_{\rm rad}$. The Hubble constant $H_{\rm rad}$ at that time must be approximately the same as that in the ΛCDM scenario, since the evolution of the two universes from that point on up to the present must be the same. From the evolution of the homogenous background universe we have

$$\left(\frac{H_{k,\rm stiff}}{H_{\rm rad}}\right)^2 = \left(\frac{a_{k,\rm stiff}}{a_{\rm rad}}\right)^{-6}, \quad (59)$$

and

$$\left(\frac{H_{k,\rm rad}}{H_{\rm rad}}\right)^2 = \left(\frac{a_{k,\rm rad}}{a_{\rm rad}}\right)^{-4}, \quad (60)$$

where $a_{k,i}$ ($i = \rm stiff, rad$) is the scale factor at which the mode k reenters the horizon, for each scenario, and $H_{k,i}$ is the corresponding Hubble constant. Therefore,

$$\frac{H_{k,\rm stiff}}{H_{k,\rm rad}} = \frac{a^{-3}_{k,\rm stiff}a_{\rm rad}}{a^{-2}_{k,\rm rad}}. \quad (61)$$

Taking into account the fact that $ck = a_{k,\rm stiff}H_{k,\rm stiff} = a_{k,\rm rad}H_{k,\rm rad}$, we rearrange the equation above and obtain

$$a_{k,\rm rad} = \left(\frac{a_{k,\rm stiff}}{a_{\rm rad}}\right)a_{k,\rm stiff}. \quad (62)$$

Since $a_{k,\rm stiff}/a_{\rm rad} < 1$, from the equation above $a_{k,\rm stiff} > a_{k,\rm rad}$. The mode reenters the horizon later (i.e. at a larger scale factor) during the stiff phase than it would during a radiation-dominated universe. Thus, according to Eq. (58) we conclude that a mode that reenters the horizon during the stiff era will contribute a higher GW energy density at late times than it would in the standard scenario, when that mode reenters in the radiation-dominated era.

To view this effect from another perspective, there are two competing factors which combine to make the contribution of a given mode to the GW energy density of the universe bigger in the presence of the stiff phase, as follows. Whatever the initial GW energy density upon horizon reentry at a_k is, thereafter it dilutes like radiation, in proportion to $(a_k/a)^4$. Since $a_{k,\rm stiff} > a_{k,\rm rad}$, there is less dilution to a given late time for the ΛSFDM case with a stiff phase. On the other hand, the super-horizon tensor amplitude is the same in both cases, since we consider the same inflationary model. Therefore, the GW contribution of a mode expressed as a fraction of the critical density at horizon reentry (see Eq. [58]) is

also the same. Since this critical density is proportional to $H_k^2 = c^2k^2/a_k^2$, it is, however, smaller in ΛSFDM than in ΛCDM. This effect makes the contribution to $\rho_{\rm GW}$ at horizon reentry smaller for ΛSFDM than for ΛCDM. To elucidate both of the effects, we can rewrite Eq. (58) in the following way:

$$\Omega_{\rm GW}(k,a) = \frac{rA_s}{24}\frac{H_k^2}{H^2}\left(\frac{a_k}{a}\right)^4 = \left.\frac{{\rm d}\rho_{\rm GW}}{{\rm d}\ln k}\right|_{a=a_k}\left(\frac{a_k}{a}\right)^4\frac{1}{\rho_{\rm crit}(a)}. \quad (63)$$

While a tensor mode reenters the horizon with a lower energy density when it reenters during the stiff phase of a ΛSFDM universe, since $H_{k,\rm stiff} < H_{k,\rm rad}$, however, according to Eq.(63), it reenters at a later scale factor. Hence, its radiationlike energy density does not thereafter dilute so much as in ΛCDM, since $(a_{k,\rm stiff}/a)^4 > (a_{k,\rm rad}/a)^4$. Overall, the latter effect wins, and, therefore, there is a boost in the GW energy density for a mode that reenters the horizon during the stiff-SFDM-dominated era (predicted in §III A 2), relative to what it would have been in ΛCDM.

As we will see in §III D, due to this amplification effect, at a later time, the total $\rho_{\rm GW}(a)$, integrated over all k but dominated by high-frequency modes which have reentered the horizon by the end of the stiff-SFDM-dominated era, will evolve nearly as radiation ($\propto a^{-4}$). Consequently, $\rho_{\rm GW}(a)$ will emerge as a significant contribution to the critical energy density of the ΛSFDM universe, as soon as the radiation-dominated era begins.

2. **Superhorizon limit:**
According to Eq. (53), the superhorizon ($k \gg aH/c$) GW energy density spectrum can be written as

$$\Omega_{\rm GW}(k,a) = \frac{\Delta^2_{h,\ \rm init}(k)}{24}\left(\frac{kc}{aH}\right)^2. \quad (64)$$

Eq. (64) can be applied at all times during the superhorizon evolution of each mode k. Since $kc = a_kH_k$, this equation tells us that every mode reenters the horizon with almost the same fractional energy density ($\approx \Delta^2_{h,\ \rm init}(k)/24$).

3. **Thin-horizon approximation:**
In the *thin-horizon approximation*, the horizon crossing of mode k is assumed to occur suddenly at $a = a_k$, and immediately follows the asymptotic behavior of the subhorizon evolution. We confirm that the assumption of thin-horizon crossing is a very good approximation for all eras of interest to us in the expansion history. As an example, we show in Appendix B the exact solution for $h_k(\tau)$ and $\Omega_{\rm GW}(k,\tau)$, along with the asymptotic solutions for the latter in the sub- and superhorizon regime, for modes which reenter the horizon during reheating with a matter-like EOS ($w = 0$). One can see that the asymptotic solutions of $\Omega_{\rm GW}(k,\tau)$ not only perfectly trace the exact solution, in their regime of validity, but also that the range in $k\tau$ around horizon crossing is rather narrow, validating the thin-horizon approximation.

4. **Total GW energy density:**
We apply the *thin-horizon approximation*, so that for each mode k, the superhorizon evolution of $\Omega_{\rm GW}(k,a)$ is given by Eq. (64) for all $a < a_k$, and the subhorizon evolution is given by Eq. (54) combined with Eq. (52) for all $a > a_k$ (or equivalently, $\tau > \tau_k = \alpha/k$). We can then integrate the fraction of total SGWB energy density over all wavenumbers at any given time,

$$\begin{aligned}\Omega_{\rm GW}(a) &= \int_0^{k_{\rm hor}}\Omega_{\rm GW}(k,a){\rm d}\ln k + \int_{k_{\rm hor}}^{k_{\rm inf}}\Omega_{\rm GW}(k,a){\rm d}\ln k \\ &= \frac{rA_s}{24a^2H^2}\int_0^{k_{\rm hor}}c^2k^2\left(\frac{k}{k_*}\right)^{n_t}{\rm d}\ln k + \frac{rA_s}{12a^2H^2}\int_{k_{\rm hor}}^{k_{\rm inf}}c^2k^2\left(\frac{k}{k_*}\right)^{n_t}T_h(k,a){\rm d}\ln k \\ &= \frac{rA_s}{24(2+n_t)}\left(\frac{k_{\rm hor}}{k_*}\right)^{n_t} + \frac{rA_s}{12a^2H^2}\int_{k_{\rm hor}}^{k_{\rm inf}}a_k^2H_k^2\left(\frac{k}{k_*}\right)^{n_t}T_h(k,a){\rm d}\ln k, \end{aligned} \quad (65)$$

where $k_{\rm inf}$ is the wavenumber of the mode that just exits the horizon and then immediately

reenters, when inflation ends at $a_{\rm inf}$, and we have used the relation $k_{\rm hor} = aH/c$ for the mode that fills the horizon at scale factor a, i.e., $a_{k_{\rm hor}} = a$. The integral in the above equation can be divided into two parts by $k_{\rm reheat}$, the wavenumber of the mode that fills the horizon at the end of reheating, when $T = T_{\rm reheat}$ and $a = a_{\rm reheat}$,

$$\int_{k_{\rm hor}}^{k_{\rm inf}} a_k^2 H_k^2 \left(\frac{k}{k_*}\right)^{n_t} T_h(k,a) {\rm d}\ln k = \int_{k_{\rm reheat}}^{k_{\rm inf}} a_k^2 H_k^2 \left(\frac{k}{k_*}\right)^{n_t} T_h(k,a) {\rm d}\ln k + \int_{k_{\rm hor}}^{k_{\rm reheat}} a_k^2 H_k^2 \left(\frac{k}{k_*}\right)^{n_t} T_h(k,a) {\rm d}\ln k. \tag{66}$$

In the equation above, the contribution from reheating, assuming an EOS with $w = 0$, can be integrated analytically. The result is

$$\int_{k_{\rm reheat}}^{k_{\rm inf}} a_k^2 H_k^2 \left(\frac{k}{k_*}\right)^{n_t} T_h(k,a) {\rm d}\ln k = \frac{1}{2(2-n_t)} \frac{a_{\rm inf}^4 H_{\rm inf}^2}{a^2} \left(\frac{a_{\rm reheat}}{a_{\rm inf}} \left(\frac{k_{\rm reheat}}{k_*}\right)^{n_t} - \left(\frac{k_{\rm inf}}{k_*}\right)^{n_t} \right). \tag{67}$$

C. Other cosmic components

Apart from SFDM and GWs, the other components are the same than in ΛCDM. In Table I, $\Omega_r h^2$, calculated from the CMB temperature today $T_{\rm CMB}$, accounts for the ordinary radiation component, i.e. photons and neutrinos. For simplicity, the neutrinos are considered as *massless* (i.e. SM neutrinos), such that the total matter density fraction today is $\Omega_m = \Omega_b + \Omega_c$, where Ω_b stands for the baryon density fraction at the present. The energy density of baryons (the "ordinary matter") always decays like non-relativistic "dust", $\rho_b(a) \propto a^{-3}$. While the radiation component decays asymptotically like $\rho_r(a) \propto a^{-4}$, photons do get extra heat during various processes in the early evolution. These effects are usually described via a quantity called g_* (or g factor), which reflects the change (decrease) of relativistic species over time. It amounts to calculating the thermal history exactly, i.e. the photon temperature T as a function of a during such periods. As in Paper I, we will again take into account the most notable of these changes, namely the time of electron-positron annihilation that occurs around 0.5 MeV. This effect will be reflected in our solutions as a little dip in the density fraction of radiation at that time. Finally, we assume a cosmological constant, $\rho_\Lambda \simeq$ const., whose present-day density fraction is given by $\Omega_\Lambda = 1 - \Omega_m - \Omega_r$.

D. "Putting it together": homogeneous ΛSFDM universe

In this section we couple the evolution of all cosmic components to obtain the expansion history of the homogeneous ΛSFDM universe. We will also introduce several cosmological observables, which we later use to constrain the ΛSFDM model. Inserting Eq. (14) and the relations mentioned in §III C into the post-reheating Friedmann equation (7) yields

$$\begin{aligned} H^2(a) &= H_0^2 \left(\frac{\Omega_r(a)}{a^4} + \frac{\Omega_b}{a^3} + \Omega_\Lambda \right) + H^2(a)\Omega_{\rm GW}(a) + \frac{8\pi G}{3c^2}\rho_{\rm SFDM} \\ &= H_0^2 \left(\frac{\Omega_r(a)}{a^4} + \frac{\Omega_b}{a^3} + \Omega_\Lambda \right) + H^2(a)\Omega_{\rm GW}(a) \\ &\quad + \frac{8\pi G}{3c^2} \left[\frac{\hbar^2}{2mc^2} \left(\frac{({\rm d}|\psi|^2/{\rm d}t)^2}{4|\psi|^2} + \frac{(\rho_{\rm SFDM,0}/\hbar)^2}{a^6|\psi|^2} \right) + \frac{1}{2}mc^2|\psi|^2 + \frac{1}{2}\lambda|\psi|^4 \right], \end{aligned} \tag{68}$$

where Ω_b and Ω_Λ are given in Table I, the parameter $\Omega_r(a)$ is different before and after the electron-

positron annihilation[9], and $\Omega_{\rm GW}(a)$ is evaluated by Eqs. (65) – (67). Unlike the standard ΛCDM universe in which the Friedmann equation can be solved separately from the equations of motion for each component, it is necessary in the case of SFDM, to solve Eq. (68) fully coupled to the Klein-Gordon equation (24), the equation of motion for the SFDM. Therefore, a numerical integration is required, which we will describe in §III D 1.

To start the description of the evolution of the homogeneous universe, we first remind the reader that, ΛSFDM is embedded in the standard inflationary paradigm in a way similar to ΛCDM, that a ΛSFDM universe commences in a period of cosmic inflation which ends in reheating, as explained in §I D. In the single-field slow-roll inflation picture, the energy scale of inflation, or equivalently, the Hubble constant during inflation, $H_{\rm inf}$, can be determined by the value of the tensor-to-scalar ratio r,

$$H_{\rm inf} = \frac{\pi M_{\rm pl}}{\hbar}\sqrt{rA_s}, \tag{69}$$

where $M_{\rm pl}$ is the reduced Planck mass, $M_{\rm pl} \equiv \sqrt{\frac{\hbar c}{8\pi G}}$.

When inflation ends, the inflaton oscillates and decays, which results in particle production and reheating ($w = 0$). The end of reheating is considered as the emergence of SFDM as well as the SM particles, produced during reheating. Unlike in ΛCDM, in our ΛSFDM model reheating dumps most of the energy of the inflaton into SFDM, which quickly forms a Bose-Einstein condensate, as argued in §I B. Meanwhile, a subdominant amount of energy is dumped into the SM particles, which was a radiation component at $T = T_{\rm reheat}$. In ΛSFDM, this is the moment when the cosmic expansion history starts to be distinguishable from ΛCDM.

While the Hubble constant when inflation ends is fixed in ΛSFDM by Eq. (69), the value of H when reheating ends is set by the value of $a = a_{\rm reheat}$ when $T = T_{\rm reheat}$, which cannot be determined on its own without solving the holistic evolution that follows to match the observed universe at present in the presence of SFDM. This will be apparent if we preview the generic behavior of the expansion history in the full solutions we will calculate later in this section. Fig. 1 (based upon the calculation detailed later) shows a plot of the Hubble parameter for several ΛSFDM models with different parameters, as a function of scale factor, in which the varying EOS of the background universe is reflected in different slopes. Following the end of inflation at $a = a_{\rm inf}$, $H \propto a^{-3/2}$ during reheating until $a = a_{\rm reheat}$. At this point, the ΛSFDM universe is dominated by stiff SFDM, rather than radiation. We have described the relativistic nature of SFDM at early times in §III A, that BEC SFDM starts as stiff matter ($w = 1$), and then transitions into a radiationlike ($w = 1/3$) component, before a final transition into dustlike CDM ($w = 0$). Therefore, we expect to see that, as the energy density of the dominant stiff SFDM decreases as $\rho_{\rm SFDM} \propto a^{-6}$ (faster than radiation), the initially stiff-SFDM-dominated universe ($H \propto a^{-3}$) will later experience a transition in its EOS to radiation-dominated, when SFDM and other relativistic species combine to make the critical energy density of the universe $\rho_{\rm crit} \propto a^{-4}$, so $H \propto a^{-2}$, until the SFDM transitions to CDM-like and once again dominates $\rho_{\rm crit}$, then $H \propto a^{-3/2}$.

It can be inferred from above that, during the stiff and radiationlike phase of SFDM, the expansion rate of the background ΛSFDM universe in its early stage is increased, compared to that in ΛCDM (see Fig. 1). Hence, in the ΛSFDM model, SFDM will contribute to the effective number of relativistic species, also known as effective number of neutrino species, $N_{\rm eff}$. In ΛCDM, where there are only three SM neutrinos, $N_{\rm eff} = N_{\rm eff,standard} = 3.046$. In ΛSFDM, an increased expansion rate can be translated into an increased $N_{\rm eff}$, or vice versa. Thus, measurements of the value of $N_{\rm eff}$ at a certain time will constrain the expansion rate of the ΛSFDM universe at that time.

In fact, BBN is such an epoch during which the value of $N_{\rm eff}$ can be measured, by determining primordial light element (He, D, etc.) abundances from observations. Standard BBN proceeds in a period between the freeze-out of the neutron-proton ratio when the photon temperature $T \simeq T_{\rm n/p} \equiv 1.293$ MeV (the difference between the neutron and the proton mass) and the epoch of nuclei production when $T \simeq T_{\rm nuc} \approx 0.07$ MeV. We denote the respective scale factors as $a_{\rm n/p}$ and $a_{\rm nuc}$. A detailed analysis on how the value of $N_{\rm eff}$ during BBN constrains the expansion rate of ΛSFDM, and thereby the SFDM particle parameters, will be carried out in §IV B.

Later in the expansion history of ΛSFDM, the universe undergoes another transition from radiation-dominated (RD) to matter-dominated (MD). The division of these two eras is described by the epoch

[9] After the e^-e^+ annihilation, $\Omega_r(a)$ is equal to the present-day radiation energy density fraction given in Table I. It is slightly smaller before the e^-e^+ annihilation because photons get heated as e^-e^+ pairs annihilate into photons in thermal equilibrium. We take this into account in our evolution of the thermal history of the universe.

of matter-radiation equality, the redshift at which is denoted as $z_{\rm eq}$. Note that in ΛSFDM, matter-radiation equality refers to the equality between the energy density of the matter component (SFDM plus baryons) and the radiation component (including GWs). After $z_{\rm eq}$, the overdensities in the matter-dominated universe start to grow in proportion to the scale factor, which become seeds for forming cosmic structures. Since we consider SFDM as a variant of CDM, which retains the cosmic structure on large enough scales as predicted by standard CDM (see §I A), we should expect that the expansion history of the background ΛSFDM universe be nearly identical to that in ΛCDM, after the same $z_{\rm eq}$. Besides LSS, $z_{\rm eq}$ is a cosmological observable well determined by CMB anisotropy measurements independently. Therefore, ΛSFDM must respect the value of $z_{\rm eq}$ measured by CMB. In other words, $z_{\rm eq}$ puts constraints on ΛSFDM, too, which we will discuss in §IV A.

The combination of these constraints will allow us to determine allowed ranges of SFDM particle parameters. Allowed regions will correspond to those SFDM models which comply to all the current measurements of the background evolution. The results will be summarized in §IV C.

1. Numerical method

In Paper I, we presented many details of how the evolution of SFDM is numerically calculated, so we refer the reader to that paper for more technical details. We emphasize that, as in Paper I, there are basically two different calculational regimes, as follows. When $\omega/H \gg 1$, the fast-oscillation approximation applies, as described in §III A 1. As long as the oscillation is much faster than the rate at which the scale factor changes, the exact SFDM energy density and pressure should be well approximated by the corresponding time-averaged quantities, and we confirmed in Paper I that this is indeed the case.

At earlier times, ω/H decreases and the fast-oscillation approximation becomes invalid. Then, we have to work in the slow-oscillation regime as described in §III A 2, and the evolution of SFDM has to be calculated exactly, with no reference to an averaging procedure.

The presence of $\rho_{\rm GW}$, which is dependent on the expansion history and, in turn, affects that history, requires us to generalize the method of Paper I. In addition, we have improved the accuracy of our numerical solutions.

(1) Nondimensionalized equations

We have rewritten the coupled Klein-Gordon and Friedmann equations in a nondimensionalized form which takes advantage of the characteristic scales of the dimensional quantities expected during the early, slow-oscillation regime, to improve the accuracy of our numerical solutions.

In the early-time slow-oscillation regime, we solve the Klein-Gordon equation (24) directly in terms of the field amplitude square $|\psi|^2$ as the dependent variable, coupled with the Friedmann equation (68). The hydrodynamical variables $\rho_{\rm SFDM}$ and $p_{\rm SFDM}$ are then related to $|\psi|^2$ by Eqs. (14) and (15).

In particular, we have nondimensionalized this set of ordinary differential equations (ODEs) by expressing variables in terms of their values at the matching point at $a = a_M$, between the slow-oscillation regime and the late-time fast-oscillation regime. We define the dimensionless dependent variable for our numerical integration as follows:

$$y \equiv \frac{|\psi|^2}{|\psi_M|^2}, \tag{70}$$

where ψ_M is the value of the scalar field at the matching point. The independent variable, cosmic time t is nondimensionalized as:

$$x \equiv \omega_M t, \tag{71}$$

where ω_M is the oscillation frequency of the scalar field at the matching point. Likewise the dimensionless Hubble parameter is defined as:

$$\mathscr{H} \equiv H/\omega_M. \tag{72}$$

We note that according to the definition of the Hubble parameter,

$$\dot{a} = \mathscr{H} a, \tag{73}$$

where the upper dot denotes the derivative with respect to the dimensionless time variable x, *throughout this subsection.*

Given these variables, the dimensionless equivalent of the Klein-Gordon equation (24) can be written as

$$\ddot{y} = -3\mathscr{H}\dot{y} + \frac{\dot{y}^2}{2y} + \frac{2F_1}{a^6 y} - 2F_2 y - 4F_3 y^2, \tag{74}$$

in which dimensionless constants F_1, F_2 and F_3 are defined as

$$F_1 \equiv \frac{(\rho_{\rm SFDM,0}/\hbar)^2}{\omega_M^2 |\psi_M|^4}, \tag{75}$$

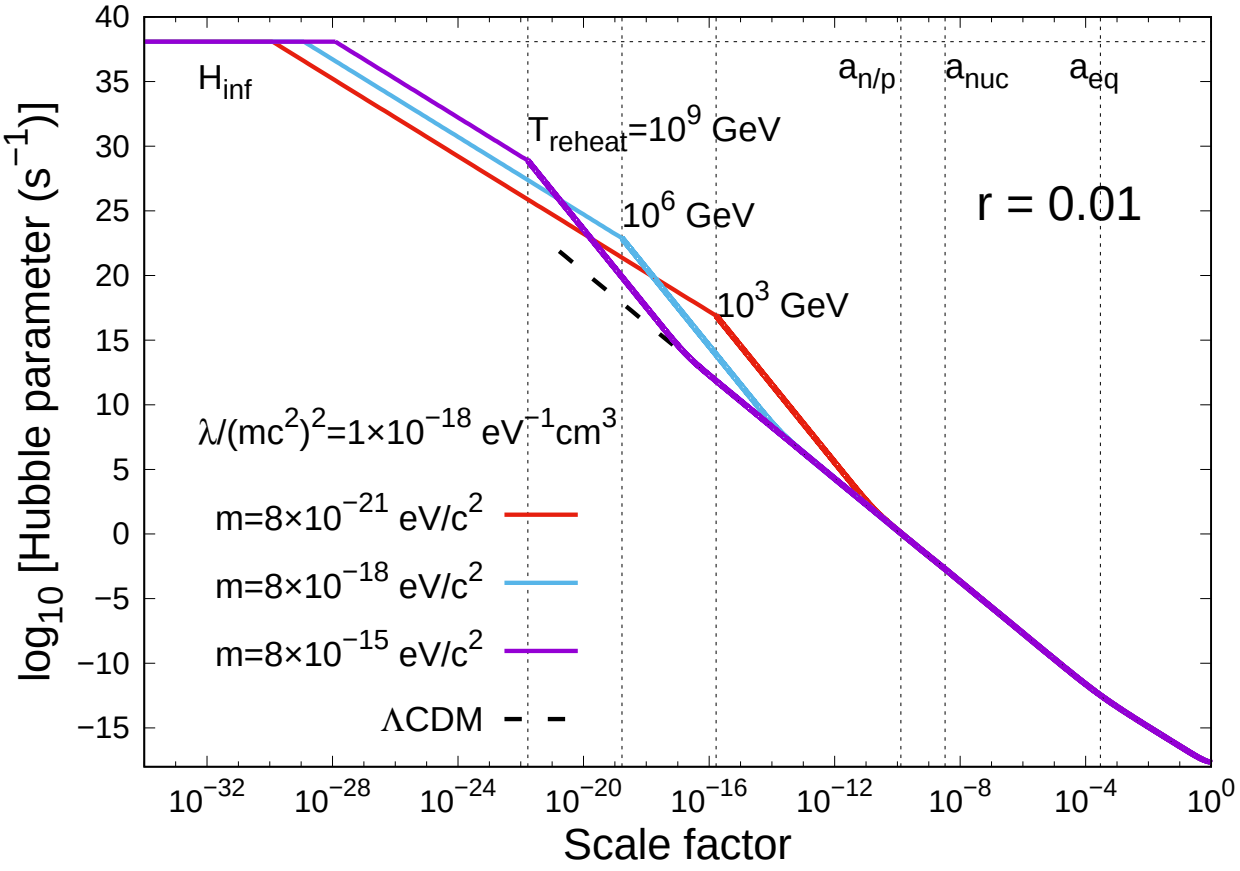


FIG. 1: Expansion history of 3 example ΛSFDM models in the standard inflation paradigm including $w = 0$ reheating.

$$F_2 \equiv \frac{(mc^2)^2}{(\hbar\omega_M)^2} \tag{76}$$

$$F_3 \equiv \frac{\lambda mc^2|\psi_M|^2}{(\hbar\omega_M)^2}. \tag{77}$$

For the dimensionless version of the Friedmann equation, combining Eq. (68) with the expressions of the dimensionless variables and constants above yields

$$\mathscr{H}^2 = \mathscr{H}_0^2\left(\frac{\Omega_r(a)}{a^4} + \frac{\Omega_b}{a^3} + \Omega_\Lambda\right) + \mathscr{H}^2\Omega_{GW}(a) + \frac{\dot{y}^2}{24y} + \frac{F_1}{6a^6y} + \frac{F_2 y}{6} + \frac{F_3 y^2}{6}, \tag{78}$$

where $\mathscr{H}_0 = H_0/\omega_P$ apparently.

The ODEs (73), (74) and (78) will be coupled to solve the holistic evolution of ΛSFDM, provided we are able to evaluate $\Omega_{\rm GW}(a)$ at any scale factor self-consistently.

(2) Integration and iteration scheme

We use a publicly-available ODE solver, *DVODE* [88], which can solve stiff systems in double precision, for all our numerical integrations. In Paper I, we integrated the evolution backward in time, using cosmological parameters at the present as the initial condition, given by the Planck 2013 results [86] . This was necessary in Paper I because otherwise we would have needed to know the initial value of the scalar field and its time derivative, in the early universe, as well as the (conserved) comoving charge density Q, in order to integrate forward in time, but only Q is known in advance (see Eq. [17]).

However, it is difficult for the backward calculation to take into account the SGWB produced by inflation self-consistently. Therefore, in this paper, we must evolve the ODEs forward in time, and iterate. We use a backward integration to make a first guess for the starting values to use in the next forward integra-

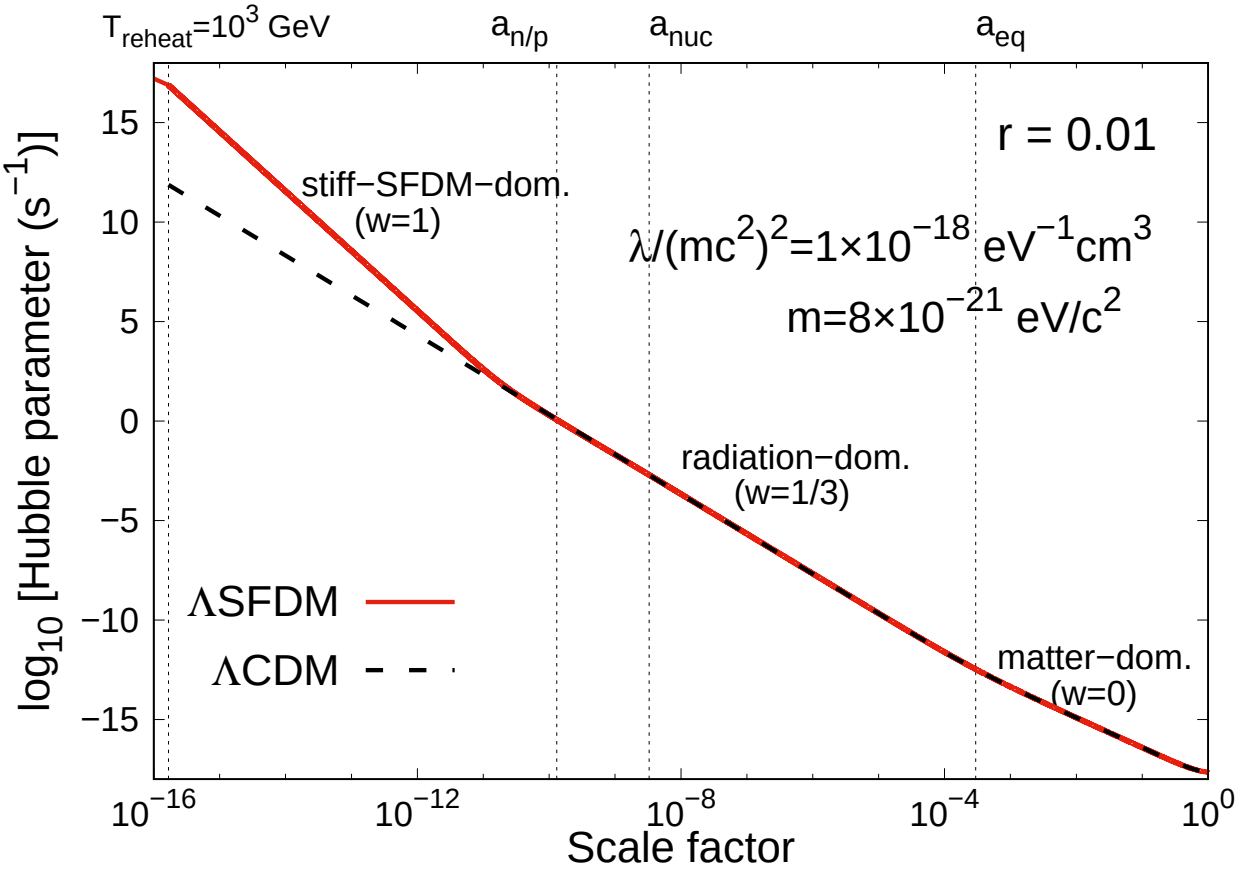


FIG. 2: Expansion history of a ΛSFDM model, of which the particle parameters are $\lambda/(mc^2)^2 = 1\times10^{-18}$ eV^{-1} cm^3 and $m = 8\times10^{-21}$ eV/c^2. This is one of the example models in Fig. 1.

tion, and subsequently iterate by a sequence of backward-forward integrations designed to converge. Convergence in this case means that the end result of a *forward* integration reaches the values of the present-day cosmological parameters in Table I at $a = 1$ with sufficient accuracy, as described below.

For each forward integration, we need to guess the starting values to use for the scalar field and its time derivative at $a = a_{\rm reheat}$. For this, we depend upon a backward integration from the known values of the cosmological parameters at $a = 1$. Unfortunately, the contribution to the total energy density from $\rho_{\rm GW}$ depends upon the accumulation of tensor modes over time as they reenter the horizon, which can only be determined self-consistently by a *forward* integration. Hence, backward integrations, too, must incorporate some guess, for the evolution of $\rho_{\rm GW}(a)$.

For the very first iteration, we integrate backward, neglecting $\rho_{\rm GW}$. A forward integration is then performed from $a = a_{\rm reheat}$ to $a = 1$ and the outcome compared with the cosmological parameters in Table I used to start the backward integration. In particular, we see how close the ending of $\rho_{\rm SFDM}$ is from $\rho_{\rm SFDM,0}$. For $\Delta \equiv \rho_{\rm SFDM}/\rho_{\rm SFDM,0} - 1$, if $\Delta \leq 0.001$, the iteration is deemed to have converged. If, however, $\Delta > 0.001$, then we guess the evolution of $\rho_{\rm GW}(a)$ based upon that first forward integration and insert it in a new backward integration, to find better starting values for the next forward integration. There is a simplification that makes a good $\rho_{\rm GW}(a)$ guess possible, based upon the generic behavior of solutions that are cosmologically allowed. While $\rho_{\rm GW}(a)$ increases over time during reheating and the stiff-SFDM-dominated era, as more and more modes reenter the horizon, this increase peaks when the stiff era ends. Thereafter, for most cases of interest, with a substantial stiff era, $\rho_{\rm GW}(a)$ evolves like radiation,

i.e., $\rho_{\rm GW}(a) \simeq \rho_{\rm GW}(a=1)/a^4$. As a result, we can use this assumed behavior, along with the final value of $\rho_{\rm GW}$ at $a = 1$ from the last forward integration. This can be extrapolated safely back to $a_{\rm reheat}$ in the following backward integration, since $\rho_{\rm GW}$ does not affect the expansion history at earlier times when the energy density of the universe is dominated by the SFDM in the stiff phase. In cases in which the stiff era is too limited in duration to boost $\rho_{\rm GW}$ significantly above the value in ΛCDM, $\rho_{\rm GW}$ is so small that there is no back-reaction on the expansion rate, so this radiationlike extrapolation from $a = 1$ backward in time is fine, as well, since it makes no difference.

In general, each new forward integration in this iteration scheme yields a new, improved $\rho_{\rm GW}(a)$ guess to use in the next backward integration. These iterations are continued until the threshold for convergence is achieved ($\Delta \leq 0.001$) for a forward integration. For example, in the case in which successive iterations cause an increase in Δ, we discard the current iteration and examine carefully the last iteration, to improve the $\rho_{\rm GW}(a)$ guess for the next iteration, by a bisection of the guesses in two previous iterations. There are details for safely converging, which we leave aside.

For the backward integration, we follow the same numerical method as in Paper I. We apply the *fast-oscillation approximation* from the present up to the matching point at $a = a_M$, where that approximation is still valid. We refer to the solution obtained in this regime as the "late-time solution". Then, starting from the matching point, we calculate the *exact* evolution (without any approximation), all the way back to the point at $a_{\rm reheat}$, i.e. the point at which SFDM comes into existence. We refer to this part as the "early-time solution".

When we integrate forward in time, starting from $a_{\rm reheat}$ with the initial condition provided by the backward integration, we obtain the early-time solution first. We have to solve the coupled ODEs (73), (74) and (78) exactly, since we are in the slow-oscillation regime. This recipe is carried out up to the matching point, after which we can apply the fast-oscillation approximation again. Then we combine Eqs. (68), (23) and (33) to calculate the late-time solution.

The contribution from the SGWB is accounted for *self-consistently* in the forward integration, by the following treatment of $\Omega_{\rm GW}(a)$ which appears in the dimensionless Friedmann equation (78). As shown in Eq. (65), $\Omega_{\rm GW}(a)$ is integrated over all wavenumbers k. At each time step, we add to the integral the contribution from the mode that reenters the horizon at the current time step. In fact, using Eqs. (65) – (67),

$$\begin{aligned}\Omega_{\rm GW}(a) &= \left(\int_{k_{\rm reheat}}^{k_{\rm inf}} \Omega_{\rm GW}(k,a)\mathrm{d}\ln k + \int_{k_{\rm hor}+\Delta k}^{k_{\rm reheat}} \Omega_{\rm GW}(k,a)\mathrm{d}\ln k + \Omega_{\rm GW}(k,a)\Delta\ln k\right) + \int_0^{k_{\rm hor}} \Omega_{\rm GW}(k,a)\mathrm{d}\ln k \\ &= \frac{rA_s}{24(2-n_t)}\frac{a_{\rm inf}^4 H_{\rm inf}^2}{a^4H^2}\left(\frac{a_{\rm reheat}}{a_{\rm inf}}\left(\frac{k_{\rm reheat}}{k_*}\right)^{n_t} - \left(\frac{k_{\rm inf}}{k_*}\right)^{n_t}\right) + \frac{rA_s}{12a^2H^2}\int_{k_{\rm hor}+\Delta k}^{k_{\rm reheat}} a_k^2 H_k^2 T_h(k,a)\left(\frac{k}{k_*}\right)^{n_t}\mathrm{d}\ln k \\ &\quad + \frac{rA_s}{12}T_h(k_{\rm hor},a)\left(\frac{k_{\rm hor}}{k_*}\right)^{n_t}\Delta\ln k + \frac{rA_s}{24(2+n_t)}\left(\frac{k_{\rm hor}}{k_*}\right)^{n_t}, \end{aligned} \tag{79}$$

where $k_{\rm hor} = aH/c$ is the wavenumber of the mode that fills the horizon at the current time step and Δk is the difference between such a wavenumber at the current time step and the previous one, $\Delta\ln k \equiv \Delta k/k$. The equation above demonstrates how we account for $\Omega_{\rm GW}(a)$ in the coupled ODEs, for both the early-time and late-time solution.

The tensor transfer function $T_h(k,a)$ that we use in Eq. (79) is the one in Eq. (52) in which α_k is evaluated with the corresponding $w(a_k) = p(a_k)/\rho(a_k)$ of the background universe, multiplied by a factor A^2 mentioned at the end of §III B 2, which accounts for the damping of tensor modes from free-streaming neutrinos, which is nontrivial during the radiation-dominated era. It was first pointed out by [82] that, since a free-

streaming relativistic component contributes an anisotropic stress-energy tensor π_{ij} on the right-hand side of the tensor wave equation (27), the growth of h_k will be damped, once it reenters the horizon, compared with the solution without anisotropic inertia (see §III B 2). This effect amounts to a multiplicative factor A as a function of the fraction of the free streaming species, calculated by [83]. In cosmology, the only important case is the free streaming neutrinos during the radiation-dominated era, when their fraction $\Omega_\nu(a)$ is not negligible. Therefore, $A = A(\Omega_\nu(a))$ should be applied to modes which reenter the horizon during the radiation-dominated era. In this paper, we will only quote the result of $A(\Omega_\nu(a))$ from [83], and incorporate it into Eq. (79), which yields

$$\begin{aligned}\Omega_{\rm GW}(a) = &\frac{rA_s}{24(2-n_t)}\frac{a_{\rm inf}^4 H_{\rm inf}^2}{a^4H^2}\left(\frac{a_{\rm reheat}}{a_{\rm inf}}\left(\frac{k_{\rm reheat}}{k_*}\right)^{n_t} - \left(\frac{k_{\rm inf}}{k_*}\right)^{n_t}\right)\\ &+ \frac{rA_s}{12a^2H^2}\int_{k_{\rm hor}+\Delta k}^{k_{\rm reheat}} a_k^2 H_k^2 T_h(k,a)\left(\frac{k}{k_*}\right)^{n_t} A^2(\Omega_\nu(a))\mathrm{d}\ln k\\ &+ \frac{rA_s}{12}T_h(k_{\rm hor},a)\left(\frac{k_{\rm hor}}{k_*}\right)^{n_t} A^2(\Omega_\nu(a))\Delta\ln k + \frac{rA_s}{24(2+n_t)}\left(\frac{k_{\rm hor}}{k_*}\right)^{n_t}. \end{aligned} \quad (80)$$

This equation (80) is the final version of $\Omega_{\rm GW}(a)$ which we insert into the dimensionless Friedmann equation (78) for our numerical calculation. We are hereby able to treat the back reaction of GWs unto the expansion history of the background ΛSFDM universe, an effect that has not been self-consistently taken into account in previous literature. In this paper, we provide the first example of a holistic numerical evolution of the homogenous universe, which correctly accounts for the back reaction from GWs.

2. *Results: example ΛSFDM models*

We will now show the evolutionary aspects of ΛSFDM by presenting results for some example models obtained from our numerical calculation in detail.[10] As we sill see in §IV, these models are chosen to fulfill the constraints from the observables described there and in §III D, while still being in the range of parameters of interest for solving the small-scale structure problems of CDM.

Again, we refer the reader to Fig. 1, the evolution of the Hubble parameter of several example ΛSFDM models with different parameters, as a function of scale factor. As in Paper I, we find it convenient to work with the ratio $\lambda/(mc^2)^2$, rather than λ, because many observables constrain the former, rather than the latter. For all these example models, the value of $\lambda/(mc^2)^2$ is chosen to be

$$\lambda/(mc^2)^2 = 1\times10^{-18}\ \mathrm{eV}^{-1}\ \mathrm{cm}^3. \quad (81)$$

The value of $\lambda/(mc^2)^2$ corresponds, for example, to the minimum size of a virialized halo in SFDM models with significant self-interaction, in the Thomas-Fermi regime (see §I C), i.e. choosing a fixed value for $\lambda/(mc^2)^2$ amounts to fixing the minimum clustering scale below which structure formation is suppressed. Since observations suggest a scale of order kpc, we adopt the above value, corresponding to a scale of 0.8 kpc (which is smaller than that of the fiducial model in Paper I).

Also, the value of the tensor-to-scalar ratio is fixed, $r = 0.01$, for all three models in Fig 1. It satisfies the latest upper bound given in Table I, $r < 0.07$, from CMB polarization experiments. The other input parameters, the SFDM particle mass m and the reheat temperature $T_{\rm reheat}$, are varied among the three models, as illustrated by the plot labels. We have chosen three values for the reheat temperature, $T_{\rm reheat} = 10^3,\ 10^6$ and 10^9 GeV, which span a wide range of possible $T_{\rm reheat}$ in ΛSFDM (the energy density at $T_{\rm reheat}$ should not exceed the inflationary energy scale). We vary the SFDM particle mass m accordingly with these choices of $T_{\rm reheat}$, so as to satisfy the constraints described in §IV.

As shown in Fig 1, the Hubble parameter of the universe drops from the initial plateau, $H_{\rm inf}$, when

[10] The fiducial model in Paper I was $m = 3\times10^{-21}$ eV/c^2, $\lambda/(mc^2)^2 = 2\times10^{-18}$ eV^{-1}cm^3, see Fig. 1,2,3 in [23].

inflation ends, at different scale factors $a_{\rm inf}$ for different example models. The duration of the prolonged $w = 0$ reheating, in which $H(a) \propto a^{-3/2}$, is also different among these models. In accordance with the definition of $T_{\rm reheat}$, the higher it is, the shorter the duration of reheating. The end of reheating marks the emergence of BEC SFDM and all the SM particles. To describe the homogeneous evolution of the ΛSFDM universe hereafter, we will focus on one of the example models, in which $T_{\rm reheat} = 10^3$ GeV, and

$$m = 8 \times 10^{-21}\ {\rm eV/c^2}. \tag{82}$$

For this model, the evolution of the Hubble parameter as a function of scale factor is plotted in Fig. 2, and the evolution of the energy density fractions of all its components can be found in the left-hand plot of Fig 3. We can see that SFDM dominates in the universe twice: first, from the time of the onset of the stiff phase —which follows the epoch of reheating at $a_{\rm reheat}$, to shortly before the time of neutron-proton freeze-out $a_{n/p}$, and then after the time of matter-radiation equality at $a_{\rm eq}$ to shortly before the present, which is Λ-dominated. At present, Ω_i of all the components, as well as the Hubble constant H_0, match the cosmological parameters measured by Planck in Table I.

The intermediate radiation-dominated era of ΛSFDM also has a different expansion history from that of ΛCDM. There are two extra radiation components besides the standard radiation (photons plus neutrinos), namely radiationlike SFDM and primordial GWs amplified by the stiff era. As shown in the left-hand plot of Fig. 3, $\Omega_{\rm SFDM}$ is constant during its radiationlike phase, as a "plateau" (see Paper I for a more detailed description). In the same era, this model allows for another plateau contributed by the energy density fraction of the SGWB from inflation, $\Omega_{\rm GW}$. As predicted in §III B 3, it is possible that $\rho_{\rm GW}$ can emerge as a significant contribution to the total energy density of the universe during the RD era (indicated by the plateau of $\Omega_{\rm GW}$ in the left-hand plot of Fig. 3), resulting from the amplification of subhorizon GWs during the stiff-SFDM-dominated era. For all the example models shown here, the boost effect is significant, due to the considerable number of e-foldings during the stiff era. For tensor modes that reenter the horizon after the stiff-SFDM-domination ends, of lower frequencies than those that reentered before, their energy density is not boosted relative to that of the background universe, so they add little to the total energy density of the SGWB, or its fraction $\Omega_{\rm GW}(a)$ given by Eq. (65), throughout their subhorizon evolution. Hence, for ΛSFDM models like these, $\Omega_{\rm GW}(a)$ will always be dominated by modes which have reentered the horizon by the end of the stiff-SFDM-dominated era. From that moment on, the relative contributions to the total $\rho_{\rm GW}(a)$ are fixed for all modes that contribute significantly, and, as subhorizon modes, they evolve thereafter like radiation, $\mathrm{d}\rho_{\rm GW}/\mathrm{d}\ln k \propto a^{-4}$, thus, so must $\rho_{\rm GW}(a) \propto a^{-4}$ approximately. Therefore, $\Omega_{\rm GW}(a)$, only beginning to emerge at the end of the stiff-SFDM-dominated era, soon stops growing and becomes a plateau when the stiff-to-radiation transition finishes.

The evolution of the SFDM, itself, is shown in Fig. 4, from our numerical calculation. The respective phases of stiff, radiationlike, and CDM-like evolution are indicated in the left-hand plot. They follow the behavior derived heuristically in §III A. The right-hand plot shows the evolution of the EOS parameter of the SFDM $w = p_{\rm SFDM}/\rho_{\rm SFDM}$, respectively. The wiggles in this figure reflect the oscillatory nature of the scalar field ψ, which generally appear in exact solutions of all types of DM modeled by a scalar field (see, e.g., [89]). This oscillation feature stops at $a = a_M$ when we change the calculational method, between the slow- and the fast-oscillation regime (see and §III A and §III D 1). Note that there are no wiggles in the left-hand plot of Fig 4, indicating that the oscillations are not manifest in $\rho_{\rm SFDM}$, only in $p_{\rm SFDM}$. This guarantees that the expansion history of the background universe, which only depends on the mean energy density of SFDM, is not affected by these oscillations.

For fixed r and $T_{\rm reheat}$, the transition of the SFDM EOS between the radiationlike ($w = 1/3$) and CDM-like (matter-like, $w = 0$) phase is determined solely by the parameter $\lambda/(mc^2)^2$. The larger $\lambda/(mc^2)^2$ is, the later the transition. In contrast, the transition between the stiff ($w = 1$) and radiationlike phase is determined by both SFDM particle parameters, m and $\lambda/(mc^2)^2$. In other words, while the beginning of the stiff phase is set by $T_{\rm reheat}$, its end is determined by both m and $\lambda/(mc^2)^2$. For fixed $\lambda/(mc^2)^2$, the larger the mass m, the earlier the stiff phase ends. For fixed m, the larger $\lambda/(mc^2)^2$ is, the earlier the stiff phase ends, as well. In the limit of small $\lambda/(mc^2)^2$, the end of the stiff phase is determined primarily by m alone. Hence, the duration of each phase can be tuned by SFDM particle parameters. It was also shown in Paper I how changing these parameters affects the evolution of SFDM.

We highlight again that SFDM in its early stiff phase dominates the energy density of the background universe, which gives rise to several interesting implications on cosmological observables as mentioned above in §III D. For example, both SFDM and GWs contribute to $N_{\rm eff}$ during BBN (from $a_{\rm n/p}$

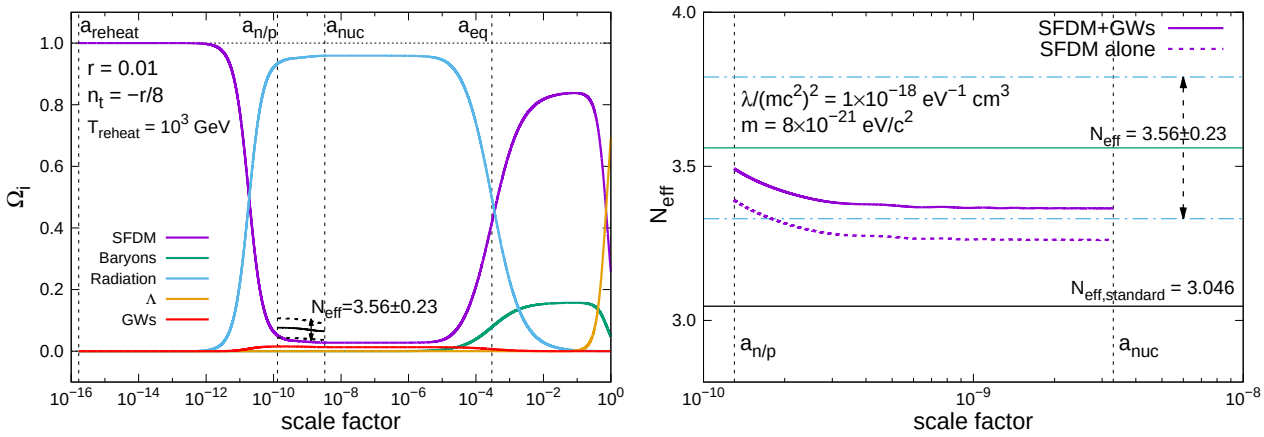


FIG. 3: *left-hand plot:* Post-inflationary evolution of energy density fractions of all cosmic components, Ω_i *vs.* a, for an example ΛSFDM model. *right-hand plot:* Evolution of $N_{\rm eff,BBN}$ *vs.* a, for the same model during BBN. The solid purple curve accounts for all contributions to $N_{\rm eff,BBN}$, including SFDM and the SGWB from inflation.

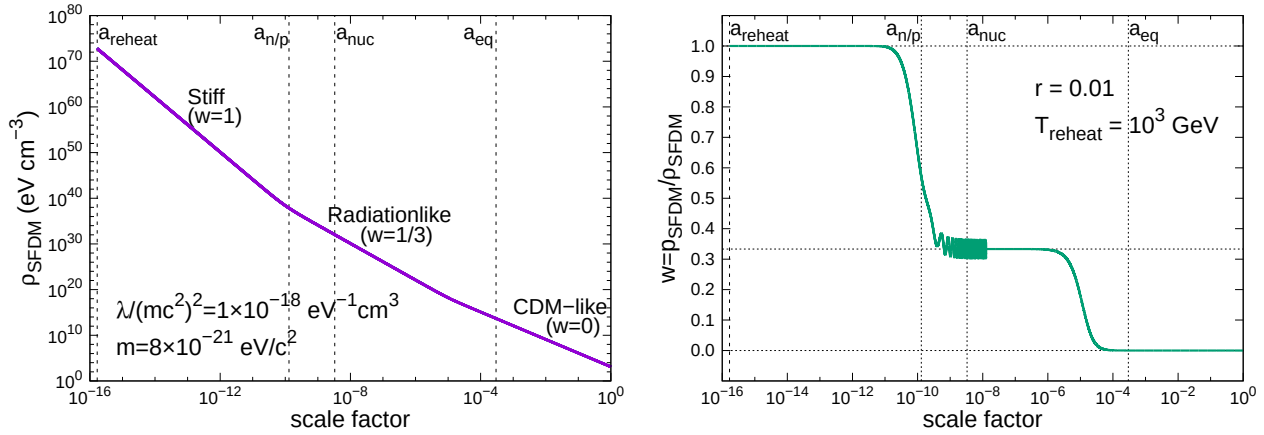


FIG. 4: *left-hand plot:* Evolution of the energy density of SFDM. *right-hand plot:* Evolution of equation of state of SFDM. Oscillations are shown explicitly for $a < a_M$, which are manifest in the EOS plot, but only the smooth average is plotted for $a > a_M$.

to $a_{\rm nuc}$), increasing the expansion rate of the background universe. The evolution of $N_{\rm eff}$ during BBN is illustrated in the right-hand plot of Fig 3. For the example model, the contribution from the SGWB from inflation is noticeable. When SFDM transitions from radiationlike to CDM-like, it will no longer contribute to $N_{\rm eff}$. However, the SGWB contribution will always remain, which could affect other cosmological observables at later times, such as $z_{\rm eq}$. Therefore, such observables will be capable of constraining ΛSFDM parameters, via the relic SGWB from inflation. We will carry out the analyses and show results from these constraints in the next section.

IV. RESULTS: NEW CONSTRAINTS ON SFDM PARTICLE PARAMETERS FROM COSMOLOGICAL OBSERVABLES

A. Constraint from matter-radiation equality $z_{\rm eq}$

As briefly mentioned in §III D, a ΛSFDM model has to preserve the redshift of matter-radiation equality, $z_{\rm eq}$, according to the measurement from CMB. The constraint on the value of $z_{\rm eq}$ from the Planck 2015 results reads

$$z_{\rm eq} = 3365 \pm 44, \quad (68\% \text{ confidence limit}). \quad (83)$$

This requires that SFDM should be well into its CDM-like phase (i.e. be fully non-relativistic) at

$z_{\rm eq}$. As a result, it sets a constraint on the transition point between the radiation-like and CDM-like phases of SFDM, which is a function of $\lambda/(mc^2)^2$, as described in §III D 2 and in Paper I. As long as SFDM has completed this transition well before $z_{\rm eq}$, one can derive from the definition of $z_{\rm eq}$ that

$$1 + z_{\rm eq} \equiv \frac{1}{a_{\rm eq}} = \frac{\Omega_b h^2 + \Omega_c h^2}{\Omega_r h^2 + \Omega_{\rm GW} h^2}, \tag{84}$$

where $a_{\rm eq}$ is the scale factor at matter-radiation equality, and $\Omega_i h^2$ $(i = b, c, r)$ is given in Table I. In particular, $\rho_{\rm SFDM}$ after the transition evolves as matter all along until today and matches the present-day value determined by $\Omega_c h^2$. We first ignore the term $\Omega_{\rm GW} h^2$ in Eq. (84) for a moment, as in Paper I. Then the value of $z_{\rm eq}$ calculated by Eq. (84) must exactly agree with the constraint in Eq. (83). Therefore, without GWs, the only aspect through which SFDM is constrained is its radiation-to CDM-like transition point, governed by $\lambda/(mc^2)^2$. We have shown this constraint on $\lambda/(mc^2)^2$ in Paper I. Here we update it with the latest constraint on $z_{\rm eq}$ in Eq. (83), but use the same threshold value of $w = p/\rho = 0.001$ (neglecting the subscript SFDM here), a tiny deviation from zero, to indicate the point after which SFDM can be considered as fully non-relativistic (i.e., $w < 0.001$ for $a > a_{w=0.001}$). The requirement of $a_{w=0.001} \leq a_{\rm eq}$ can be translated into the following constraint on $\lambda/(mc^2)^2$:

$$\frac{\lambda}{(mc^2)^2} \leq 4.3 \times 10^{-17}\ {\rm eV}^{-1}\ {\rm cm}^3. \tag{85}$$

The choice of this threshold $w = 0.001$ is artificial. If we relaxed it to higher values of w, the corresponding constraint on $\lambda/(mc^2)^2$ would become less tight, allowing a broader range of values. A more precise threshold would require a recalculation of the CMB power spectrum for different SFDM particle parameters, to solve for the best-fitting ΛSFDM parameters, which is well-beyond the scope of this paper.

Now we add the contribution from the amplified inflationary SGWB. From Eq. (84), we see that not only should SFDM be fully non-relativistic by $z_{\rm eq}$, but the amount of $\Omega_{\rm GW}$, amplified by the stiff era, is also subject to the constraint. Since for fixed r and $T_{\rm reheat}$, $\Omega_{\rm GW}(a)$ is determined by SFDM particle parameters, m and $\lambda/(mc^2)^2$, *both* these parameters will be constrained further. By matter-radiation equality, $\Omega_{\rm GW}(a)$ has already evolved through the "plateau" described in §III D 2, the height of which is determined by the duration of the stiff-SFDM-dominated era. The later the stiff era ends, the more modes get amplified and thus the higher the plateau of $\Omega_{\rm GW}(a)$ is, which will result in a later $z_{\rm eq}$ as inferred from Eq. (84). Therefore, to keep it in agreement with the measured value of $z_{\rm eq}$, it is required that the stiff phase of SFDM ends early enough. We adopt the -1σ confidence limit in Eq. (83) as the minimum allowed value for $z_{\rm eq}$. Thus, for fixed r and $T_{\rm reheat}$, there will be a lower limit on the mass m for each allowed value of $\lambda/(mc^2)^2$. With the inclusion of GWs, the allowed range of $(\lambda/(mc^2)^2,\ m)$ due to the $z_{\rm eq}$ constraint will be more stringent than the half-plane given by Eq. (85) for the case without GWs. This is illustrated in the SFDM particle parameter space, shown in Figs. 5 and 6. A detailed description of the allowed ranges from the $z_{\rm eq}$ constraint, parametrized by r and $T_{\rm reheat}$, will be given in §IV C.

B. Constraint from $N_{\rm eff}$ during Big Bang nucleosynthesis

The effective number of neutrino species, $N_{\rm eff}$, is introduced in §III D as a measure of relativistic degrees of freedom of the universe. It affects the expansion rate in the early universe, at all times before the matter-dominated era, which encompasses the important epoch of Big Bang nucleosynthesis. The abundances of primordial light elements produced by BBN are very sensitive to the expansion rate then. As a result, measurements of these abundances through astronomical observations of metal-poor systems set a constraint on $N_{\rm eff,BBN}$ during BBN [90–92]. BBN is not an instantaneous event; it undergoes two important stages which we explained in §III D, first, neutron-to-proton freeze-out occurs at $a_{\rm n/p}$ and then, light nuclei production occurs at $a_{\rm nuc}$ [93], where $a_{\rm nuc}/a_{\rm n/p} \simeq T_{\rm n/p}/T_{\rm nuc} \approx 20$. Therefore, BBN actually cares about the evolution of $N_{\rm eff,BBN}(a)$ throughout this window $(a_{\rm n/p},\ a_{\rm nuc})$. Nevertheless, it is often the case that only a single value of $N_{\rm eff,BBN}$ is reported from observations, in which the expansion history is modeled by a constant $N_{\rm eff,BBN}$ at all times, since it is the simplest model to fit. In this paper, we use the following measurement result [91] to constrain the SFDM model,

$$N_{\rm eff,BBN} = 3.56 \pm 0.23, \quad (68\%\ \text{confidence limit}). \tag{86}$$

We comment that this value is not required to be consistent with the $N_{\rm eff,CMB}$ measured by CMB anisotropies, because $N_{\rm eff}(a)$ can in principle evolve over time as in our ΛSFDM model (see Fig. 3), and $N_{\rm eff,CMB}$ is only affected by its values later at around recombination. In other words, $N_{\rm eff,BBN}$ and $N_{\rm eff,CMB}$ indicate relativistic degrees of freedom at

different epochs of the expansion history. As a matter of fact, current measurements mildly suggest that $N_{\rm eff,BBN}$ be greater than $N_{\rm eff,CMB}$ by $\sim 1\sigma$ [1, 90–92].

In ΛCDM, where there are only three SM neutrino species all the time, $N_{\rm eff,BBN}(a) = N_{\rm eff,standard} = 3.046$. In contrast, in ΛSFDM, SFDM has an EOS which evolves over time, affecting the expansion rate during BBN if SFDM is relativistic then, and will hence contribute to $N_{\rm eff,BBN}(a) \equiv N_{\rm eff,standard} + \Delta N_{\rm eff,BBN}(a)$ as an extra relativistic component, as we pointed out in §III D and in Paper I. In addition, the inflationary SGWB which we have included self-consistently, amplified by the earlier stiff-SFDM-dominated era, also adds to $\Delta N_{\rm eff,BBN}(a)$, so it must be taken into account as well. In fact, in a ΛSFDM model with the SGWB, we infer $N_{\rm eff,BBN}(a)$ between $a_{\rm n/p}$ and $a_{\rm nuc}$, from the energy density fractions of relativistic SFDM, $\Omega_{\rm SFDM}$, and the GWs, $\Omega_{\rm GW}$. Both are sources to $\Delta N_{\rm eff,BBN}(a)$,

$$\frac{\Delta N_{\rm eff,BBN}(a)}{N_{\rm eff,standard}} = \frac{\Omega_{\rm SFDM}(a) + \Omega_{\rm GW}(a)}{\Omega_\nu(a)}, \qquad (87)$$

where $\Omega_\nu(a)$ denotes the energy density fraction of the SM neutrinos. The evolution of $N_{\rm eff,BBN}(a)$ for one example ΛSFDM model has been shown in the right-hand plot of Fig. 3.

We compare the $N_{\rm eff,BBN}(a)$ obtained this way to the measured value given by Eq. (86), and impose on it a conservative threshold that throughout BBN (from $a_{\rm n/p}$ to $a_{\rm nuc}$), it shall be within the 1σ confidence interval of the measured value. In Eq. (87), both values of $\Omega_{\rm SFDM}(a)$ and $\Omega_{\rm GW}(a)$ are controlled by the properties of SFDM, i.e., its particle parameters m and $\lambda/(mc^2)^2$, once the values of r and $T_{\rm reheat}$ are fixed, as described in §III D 2. Therefore, the constraint on $N_{\rm eff,BBN}(a)$ will again translate as a constraint on the SFDM particle parameter pair $(\lambda/(mc^2)^2,\ m)$.

Eq. (87) shows that, for fixed r and $T_{\rm reheat}$, if the stiff phase of SFDM ends too late into the BBN epoch, the considerable amount of $\Omega_{\rm SFDM}(a)$ can lead to too large an $N_{\rm eff,BBN}(a)$ which violates its measured value given by Eq. (86). In addition, the later the stiff-to-radiationlike transition of SFDM is, the larger the amplified $\Omega_{\rm GW}(a)$ is, increasing the value of $N_{\rm eff,BBN}(a)$ as well. Therefore, any change in the stiff-to-radiationlike transition point affects both $\Omega_{\rm SFDM}(a)$ and $\Omega_{\rm GW}(a)$ in the same direction. In order for this transition to finish early enough that the sum of $\Omega_{\rm SFDM}(a)$ and $\Omega_{\rm GW}(a)$ should observe the $+1\sigma$ confidence limit of $N_{\rm eff,BBN}$, there must be a lower bound on m, for any allowed value of $\lambda/(mc^2)^2$.

The radiationlike "plateau" of SFDM (see §III D), as well as its stiff-to-radiationlike transition, is subject to the BBN constraint. If the plateau overlaps BBN, i.e., SFDM is well into its radiationlike phase by $a_{\rm nuc}$, then $\Omega_{\rm SFDM}$(plateau) during the plateau, as a function of $\lambda/(mc^2)^2$, must comply with the constraint on $N_{\rm eff,BBN}(a)$ according to Eq. (87). In particular, for large enough m, the stiff phase of SFDM ends so early that not only the radiationlike phase of SFDM would enclose BBN, but also the amplification of the inflationary SGWB be insignificant, which leads to $\Omega_{\rm GW}(a) \simeq 0$. In this limit, the constraint from BBN amounts to a constraint on the value of $\Omega_{\rm SFDM}$(plateau), and hence on $\lambda/(mc^2)^2$ alone. The BBN constraint can thereby be analyzed the same way as in Paper I, for the case without GWs. We will not repeat that analysis here but just write down the result as follows:

$$2.3{\times}10^{-18}\,{\rm eV}^{-1}\,{\rm cm}^3 \le \frac{\lambda}{({\rm mc}^2)^2} \le 4.1{\times}10^{-17}\,{\rm eV}^{-1}\,{\rm cm}^3, \qquad (88)$$

for ΛSFDM models in which the SGWB from inflation is negligible, and the radiationlike phase of SFDM overlaps BBN. The lower and upper bounds on $\lambda/(mc^2)^2$ in the equation above correspond to the -1σ and $+1\sigma$ confidence limits of the measured value of $N_{\rm eff,BBN}$ given by Eq. (86), respectively. The difference between Eq. (88) and the equivalent bounds in Paper I only reflects our update on the measured value of $N_{\rm eff,BBN}$.

If $\lambda/(mc^2)^2$ is less than the lower bound in Eq. (88), the SFDM plateau alone cannot make up a $\Delta N_{\rm eff,BBN}(a)$ which meets the -1σ confidence limit of its measured value. Therefore, for any of these smaller values of $\lambda/(mc^2)^2$, there must be an upper bound on m, which sets a constraint on how early the stiff phase can end, so that the sum of $\Omega_{\rm SFDM}(a)$ and $\Omega_{\rm GW}(a)$ can be substantial enough to reach the -1σ limit of $N_{\rm eff,BBN}$.

These constraints from $N_{\rm eff,BBN}$ on the allowed ranges of $(\lambda/(mc^2)^2,\ m)$ can also be illustrated in the SFDM particle parameter space plots, Figs. 5 and 6, for a wide range of r and $T_{\rm reheat}$. In the upper plot of Fig. 5, we show the result for case without GWs (i.e., setting $\Omega_{\rm GW}(a) = 0$ in Eq. [87]), which can be compared to our previous result on the corresponding allowed region in Paper I. The bounds given by Eq. (88) are also reflected in Figs. 5 and 6, as described in §IV C. There we will discuss in more details the allowed region due to the $N_{\rm eff,BBN}$ constraint in the SFDM particle parameter space and its dependence on the values of r and $T_{\rm reheat}$.

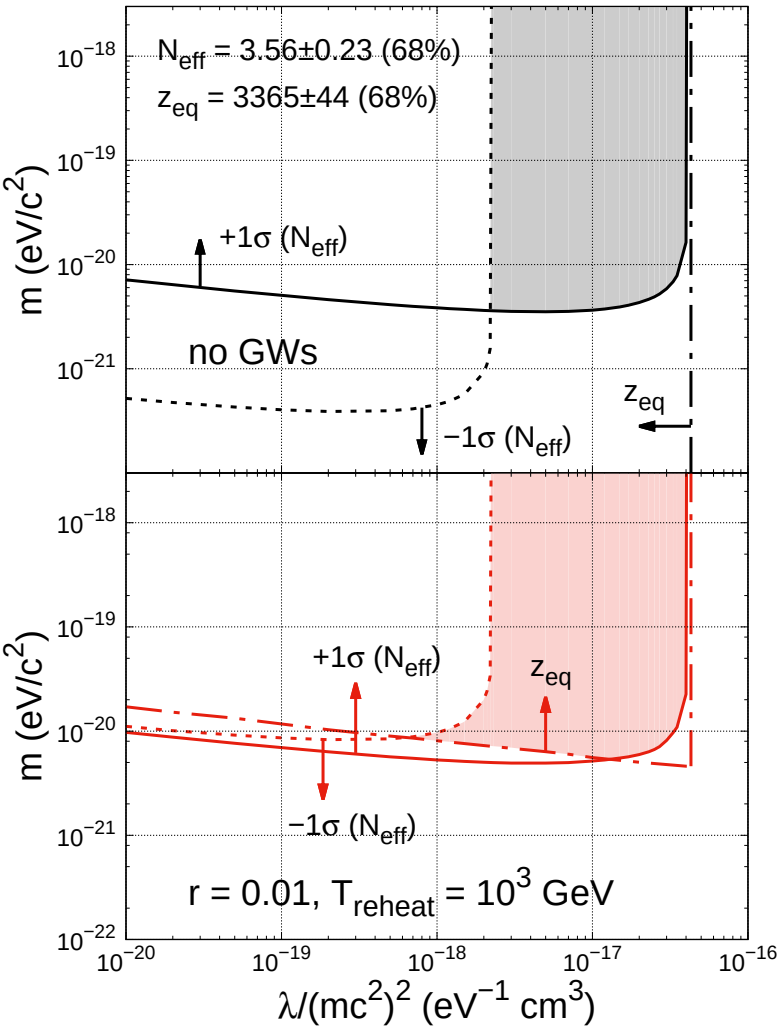


FIG. 5: Cosmological constraints expressed in the SFDM parameter space for values $(\lambda/(mc^2)^2, m)$. *Upper plot:* for the case which does not include GWs, as in Paper I. *Lower plot:* for the case which self-consistently includes GWs, in which $r = 0.01$ and $T_{\rm reheat} = 10^3$ GeV. In both plots, the solid curve corresponds to the constraint from the $+1\sigma$ confidence limit of $N_{\rm eff,BBN}$ at $a_{\rm n/p}$, the dashed curve corresponds to the constraint from the -1σ confidence limit of $N_{\rm eff,BBN}$ at $a_{\rm nuc}$, and the dash-dotted curve indicates the constraint from $z_{\rm eq}$. The arrows indicate the directions in which the SFDM particle parameters satisfy the respective cosmological constraints. In each plot, the shaded region denotes the overall allowed range of the SFDM particle parameters, for the respective case.

C. Results: allowed SFDM particle parameter space

Combining the constraints from the two cosmological observables described above, we can confine the allowed values of the SFDM particle parameters, $(\lambda/(mc^2)^2, m)$, in the two-dimensional parameter space, for various choices of r and $T_{\rm reheat}$ (see Figs. 5 and 6 for the parameter space plots).

In both figures, the constraints from $z_{\rm eq}$ and $N_{\rm eff,BBN}$ are expressed by curves of critical parameter values that marginally satisfy the respective constraints. Specifically, in each plot, the constraint from $z_{\rm eq}$ is indicated by the dash-dotted curve, and the region above this curve is allowed by the -1σ confidence limit of the measured value of $z_{\rm eq}$, given by Eq. (83). The solid curve refers to the constraint from the $+1\sigma$ confidence limit of $N_{\rm eff,BBN}$ at $a_{\rm n/p}$, and the dashed curve to the constraint from the -1σ confidence limit of $N_{\rm eff,BBN}$ at $a_{\rm nuc}$, given by BBN measurements (see Eq. [86]). The region below the solid curve and above the dashed curve is consistent with the 1σ confidence interval of the measured value of $N_{\rm eff,BBN}$ throughout BBN (see the right-

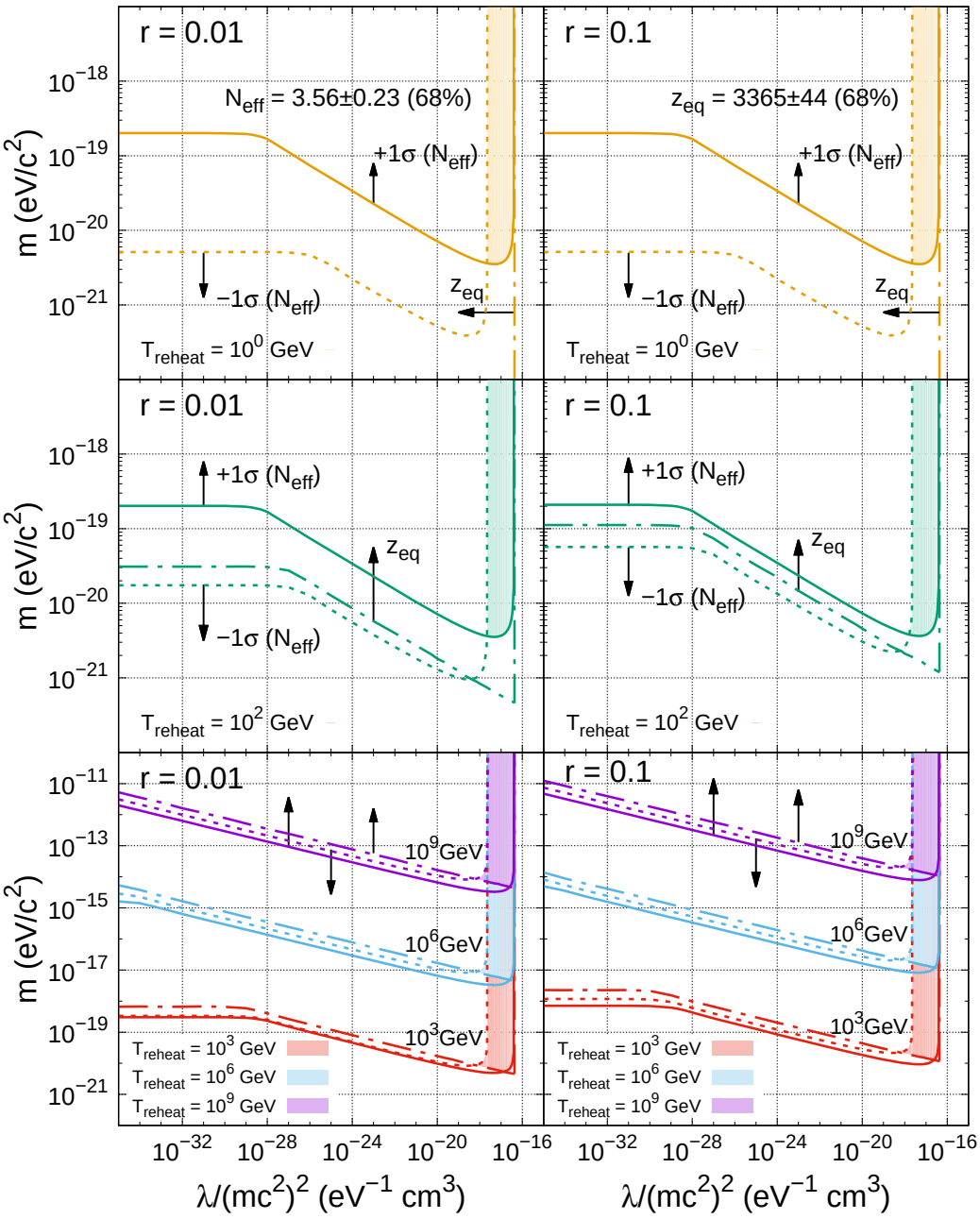


FIG. 6: Cosmological constraints expressed in the SFDM parameter space for values $(\lambda/(mc^2)^2, m)$, for multiple choices of $T_{\rm reheat}$ and r. In each panel, the shaded region indicates the values of the SFDM particle parameters which are allowed by the cosmological constraints, and the arrows indicate the directions of these constraints, the same as in Fig. 5. In the bottom two panels, the allowed regions of the SFDM particle parameters, for multiple choices of $T_{\rm reheat}$, are plotted together; all of them actually extend and overlap in the direction of larger-mass, exceeding the plot range, same as in the upper and middle panels.

hand plot of Fig. 3 for reference). The arrows in each plot indicate the directions in which the values of the SFDM particle parameters can satisfy the respective constraints, which result in the shaded region that denotes the overall allowed range of the SFDM particle parameters, satisfying all cosmological constraints.

Fig. 5 is a blow-up of Fig. 6. It shows the compar-

ison between the case which does not include GWs in the evolution of ΛSFDM (the upper plot) so the values of r and $T_{\rm reheat}$ are not important, as studied in Paper I, and the case in which the SGWB from inflation is self-consistently included (the lower plot), which we study in this paper. In the upper plot, the constraint from $z_{\rm eq}$ is given by the upper bound on $\lambda/(mc^2)^2$ in Eq. (85), indicated by the vertical dash-dotted line: the half-plane on its left side is allowed. In the lower plot, the corresponding critical curve takes the same vertical line but pivots at a minimum value of m and provides a lower bound on m for every value of $\lambda/(mc^2)^2$ below its upper bound. This change is due to the inclusion of the inflationary SGWB, which contributes a radiation component at $z_{\rm eq}$, as explained in §IV A. In both the upper and lower plots of Fig. 5, it is easily seen that for large enough m, the parameter values $(\lambda/(mc^2)^2,\ m)$ allowed by the $N_{\rm eff,BBN}$ constraint indeed correspond to models in which the radiation-like phase of SFDM overlaps BBN and the effect from the SGWB is negligible, so that the value of $\lambda/(mc^2)^2$ must be bounded between the asymptotic vertical solid and dashed lines given by Eq. (88), as explained in §IV B. In this limit, the allowed region in the lower plot becomes indistinguishable from the one in the upper plot, since the SGWB makes no difference to the background evolution of the universe.

Multiple cases are plotted in Fig. 6, with different choices for r and $T_{\rm reheat}$. In every panel, the overall allowed region for the SFDM particle parameters is given by combining all the cosmological constraints, leaving the shaded area. In the above and middle panels, i.e., the four cases with $r = 0.01$ or either 0.1, and $T_{\rm reheat} = 1$ GeV or either 100 GeV, the shaded regions are nearly indistinguishable from one case to another. This reflects the fact that if the reheat temperature is too low, the stiff era is then too short to boost the inflationary SGWB to a considerable degree. In this situation, the allowed range of SFDM particle parameters simply reduces to that in the "no GWs" case as shown in Fig. 5. Reheat temperatures $T_{\rm reheat} \gtrsim 10^3$ GeV start to make differences to the allowed regions, as shown in the bottom two panels of Fig. 6, where the allowed regions for $T_{\rm reheat} = 10^3,\ 10^6$ and 10^9 GeV are plotted together and overlap. In these cases, they are significantly affected by the SGWB from inflation. The larger the energy density of the SGWB amplified by the stiff era, resulting from an increase in either the value of r or $T_{\rm reheat}$, the more stringent the constraints on the SFDM particle parameters, as one should expect. In fact, for fixed $T_{\rm reheat}$, the allowed region contracts slightly when the value of r increases from $r = 0.01$ to 0.1. Its dependence on the value of r is found to be relatively weak. On the other hand, however, for fixed r, the allowed region shrinks significantly every time $T_{\rm reheat}$ increases by a factor of 1000. We find that, for given values of r, for $T_{\rm reheat} \gtrsim 10^3$ GeV, the minimum value of the SFDM particle mass, $m_{\rm min}$, among the models which satisfy all the cosmological constraints, is proportional to $T_{\rm reheat}$. For $r \gtrsim 0.01$, the dependence of $m_{\rm min}$ on both r and $T_{\rm reheat}$ can be empirically expressed as

$$m_{\rm min} \simeq (5\times10^{-21}\ {\rm eV}/c^2)\times \begin{cases} \dfrac{T_{\rm reheat}}{10^3\ {\rm GeV}}\sqrt{\dfrac{r}{0.01}}, & T_{\rm reheat} \gtrsim 10^3\ {\rm GeV}, \quad (89) \\ 1, & T_{\rm reheat} < 10^3\ {\rm GeV}. \quad (90) \end{cases}$$

V. RESULTS: PRESENT-DAY SGWB ENERGY DENSITY SPECTRUM AND ITS DETECTABILITY BY LIGO

In the ΛSFDM model, the integrated inflationary SGWB energy density predicted in §III contributes only a small fraction of the total energy density today, $\Omega_{\rm GW}(a=1) \sim 10^{-8} - 10^{-7}$. As such, its effect on the universe today is negligible. Remarkably enough, however, in its spectrum at high frequencies where amplification by the stiff-SFDM-dominated era was greatest, which can overlap the range of GW laser interferometer experiments, the amplitude can be significant enough to be detectable. We demonstrate this here, in light of the SGWB energy density spectrum predicted in §III and the cosmological constraints on the SFDM particle parameters derived in §IV, by analyzing the detectability of the amplified inflationary SGWB at the present by current and future laser interferometer experiments, as a unique signature of the ΛSFDM model.

The expansion history of the ΛSFDM universe described in §III D is imprinted in the present-day energy density spectrum of the SGWB from inflation,

$\Omega_{\rm GW}(f)$, defined as follows:

$$\Omega_{\rm GW}(f) \equiv \Omega_{\rm GW}(k = 2\pi f/c, a = 1). \quad (91)$$

For each mode whose (comoving) frequency is f, there corresponds an epoch of horizon reentry at $a_f \equiv a_{k=2\pi f/c}$, which determines the outcome of the cosmic evolution of its $\Omega_{\rm GW}(f)$ to the present-day, as described in §III B. For different SFDM model parameters and values of $T_{\rm reheat}$ and r, there is a different mapping between f and a_f. This is illustrated in Fig. 7. In general, as long as the horizon increases with time, as it does from the end of inflation to the end of matter-domination when the cosmological constant begins to dominate afterward, a_f increases as f decreases. For $a_f > a_{\rm eq}$, the dependence of a_f on f is universal, since the expansion history of ΛSFDM is the same as that of ΛCDM. The maximum a_f in all example models corresponds to the moment when modes begin to exit, instead of reentering the horizon, once $w = -1/3$ for the EOS of the background universe. From this moment on, all modes that are still outside the horizon will never reenter the horizon, as the cosmological-constant-dominated era begins. On the other hand, toward the high-frequency end, manifest distinctions arise for a_f earlier than the end of the stiff-SFDM-dominated era, among the three example ΛSFDM models. We note that, since the dependence of f on a_f is different in ΛSFDM from its dependence in ΛCDM, for $a_f < a_{\rm eq}$, so will the dependence of f on the CMB photon temperature $T(a)$ at $a = a_f$ be different. For ΛCDM, we can write $f \approx 10^{-4}{\rm Hz}\frac{{\rm T}({\rm a_f})}{10^3{\rm GeV}}$, for $a_{\rm eq} < a < a_{\rm reheat}$ [72], while this is not true for ΛSFDM. For example, as seen in Fig. 7, for the example model in which $T_{\rm reheat} = 10^4$ GeV, $f \approx 20$Hz at $T(a_f) = T_{\rm reheat}$.

We begin by presenting the present-day SGWB energy density spectra, $\Omega_{\rm GW}(f)$, for three example ΛSFDM models, to guide our discussion. In §V A below, we will use these models to explain the generic features of the inflationary SGWB spectra in relation to that in ΛCDM and in relation to the current and future GW detection experiments. In §V B, we will revisit these illustrative models as we quantify the detectability of the SGWB in ΛSFDM as a function of the SFDM particle parameters, for given values of r and $T_{\rm reheat}$. In the upper plots of Figs. 8 – 10, we show the present-day SGWB energy density spectra of the same example ΛSFDM models shown in Fig. 7. For all three models shown in this section, the values of $\lambda/(mc^2)^2$ are fixed according to Eq. (81) such that the corresponding core size of an SFDM halo is ~ 0.8 kpc due to the repulsive self-interaction of SFDM. We also hold the value of $r = 0.01$ fixed for all these models, for the purpose of comparison. For $T_{\rm reheat}$, in contrast to the choices in §III D, we here choose $T_{\rm reheat} = 10^3,\ 10^4$, and 10^6 GeV, such that the span of corresponding $f_{\rm reheat}$, the frequency of the mode that reenters the horizon at the end of reheating at $a_{\rm reheat}$, is nearly centered on the LIGO sensitive frequency band $(10 - 50$ Hz) [71]. The SFDM particle mass m is different for each value of $T_{\rm reheat}$, as labeled. The particular choice of m values will be described below in §V B; all ΛSFDM models shown in Figs. 8 – 10 satisfy all cosmological constraints. We will first describe the shape of $\Omega_{\rm GW}(f)$ from the example models and the respective detectabilities of these SGWBs, with special emphasis on the Advanced LIGO/Virgo experiment.

A. Generic features of the present-day energy density spectrum $\Omega_{\rm GW}(f)$ of the inflationary SGWB and its detectability

As derived in §III B 3, the generic energy density spectrum $\Omega_{\rm GW}(f)$ of the primordial SGWB from inflation, predicted by ΛSFDM models, must be approximately piece-wise power laws, the power indices of which are determined by the EOS parameters $w = p/\rho$ of the universe throughout all eras in the expansion history. In particular, if we neglect the primordial tensor index n_t, then $\Omega_{\rm GW}(f) \propto f^{-2}$ for modes which reenter the horizon during the matter-dominated era, after $z_{\rm eq}$. For modes which reenter the horizon earlier than $z_{\rm eq}$, during the radiation-dominated era, $\Omega_{\rm GW}(f) \propto f^0$. These two power laws actually apply to the $\Omega_{\rm GW}(f)$ predicted by ΛCDM, indicated by the green curve in the upper plot of, e.g., Fig. 8. There, $\Omega_{\rm GW}(f)$ exhibits a long plateau ($\propto f^0$) over a frequency range which covers the bands of most GW experiments at the present, e.g., aLIGO/Virgo and the Evolved LISA mission (shortened as "eLISA"). The amplitude of this plateau depends on the value of r alone, independent of f (see, e.g., [94]). For $r = 0.01$ shown here, this amplitude is $\sim 10^{-16}$, more than six orders of magnitude below the sensitivities of current GW detectors, which is the main reason why the SGWB from inflation (in ΛCDM) was not expected to be detectable by current major GW detection experiments listed in §I D.

However, we will now show that the SGWB from inflation, predicted by the ΛSFDM model, has the potential to be detectable by current GW experiments like aLIGO/Virgo, i.e., can reach their detection sensitivities for a wide range of model parameters, due to the amplification of the SGWB during the stiff-SFDM-dominated era. Its present-day energy density spectra $\Omega_{\rm GW}(f)$ are indicated

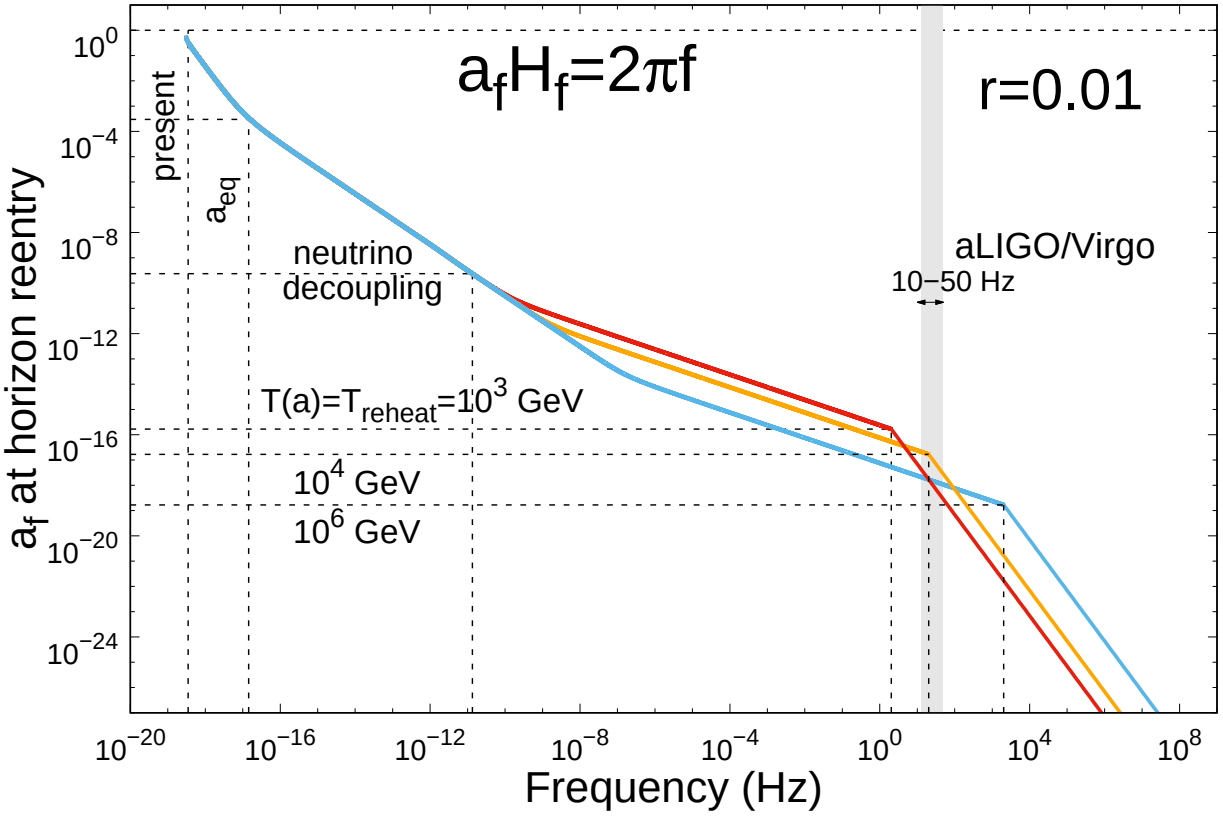


FIG. 7: Scale factor a_f at the horizon reentry ($a_f H_f = 2\pi f$) vs. the comoving frequency f for each mode, plotted for three example ΛSFDM models with different $T_{\rm reheat}$. $T(a)$ refers to the CMB photon temperature at this scale factor.

by purple curves in Figs. 8 – 10. They show yet another frequency dependence; $\Omega_{\rm GW}(f) \propto f^1$ for modes reentering the horizon during the stiff-SFDM-dominated era. Therefore, $\Omega_{\rm GW}(f)$ in ΛSFDM models, amplified by the stiff era, has a triangle-shaped part peaked at $f_{\rm reheat}$.[11] The baseline of this triangle sits on the plateau which corresponds to modes that reenter during RD. It almost lies on top of the ΛCDM's plateau mentioned above.

In Figs. 8 – 10, we display a comprehensive collection of latest constraints on cosmological SGWB, from various types of observations. Specifically, ranging from lowest to highest frequencies, they are from the BICEP2/Keck Array CMB polarization experiment[66], pulsar timing array (PTA) experiments (NANOGrav[73], PPTA[74], EPTA[75]), and the (initial, pre-2015) LIGO experiment[95, 96]. All three example models shown here satisfy all these constraints on SGWB. In fact, these constraints are weaker than the ones from $z_{\rm eq}$ and BBN discussed in §IV. Therefore, we do not utilize them to constrain the SFDM particle parameters. However, the frontier laser interferometer experiments, aLIGO/Virgo[71], and eLISA[72] (currently in its Pathfinder stage) will put much better and useful constraints on the inflationary SGWB, or, the other way, *detect the SGWB*. For eLISA, we also display in Figs. 8 – 10 the expected strain noise function provided in [97], labeled by "eLISA". If $\Omega_{\rm GW}(f)$ is higher than (i.e., intersects) this noise sensitivity curve, it is possible for eLISA to detect this SGWB.

In this paper, we concentrate mostly on the detectability of the SGWB from inflation by the ongoing aLIGO/Virgo experiment, whose O1 run has detected several GW signals from binary black hole merger events. aLIGO/Virgo has also the potential to detect a stochastic background, which is in fact one of the major interests of this experiment [71].

[11] In Figs. 8 – 10, the discontinuity in $\Omega_{\rm GW}(f)$ at $f_{\rm reheat}$ is due to the fact that we assume an instantaneous change of the EOS at the end of reheating, from $w = 0$ to $w = 1$, in our ΛSFDM model. We will adopt a more realistic model for reheating in the future, in which w changes smoothly.

Although the present-day SGWB, were it detected by aLIGO/Virgo, could have multiple sources other than the primordial SGWB from inflation, such as unresolved black hole mergers [71], we will only consider the inflationary SGWB in this paper, which has a unique spectral shape in $\Omega_{\rm GW}(f)$ as predicted by ΛSFDM, and probe its detectablity characterized by the SNR.

As shown by [98], the SNR of any fixed SGWB today, for a certain laser interferometer experiment, is proportional to the square root of the accumulated observation time. Therefore, we can in principle enhance the detectability of a reasonably-motivated SGWB to a required level of significance, provided enough observation time. The solid and dashed curves in the upper plots of Figs. 8 – 10, labeled by "aLIGO/Virgo", indicate the "integrated 1σ sensitivity curves", for the O1 and O5 observing runs, respectively. These curves are a useful tool developed by [99] to visualize the sensitivity of GW detectors. Their physical interpretation is that, if the predicted $\Omega_{\rm GW}(f)$ for some SGWB touches the curve for the O1(O5) run at any f, this SGWB will reach a 1σ significance of detection (SNR = 1) by the end of the O1(O5) run. The dashed curve (O5) is much lower than the solid curve (O1), which mainly results from the fact that O5 has a much longer accumulated observation time than O1. Thus, the $\Omega_{\rm GW}(f)$ of a given SGWB obviously has a better chance to intersect the sensitivity curve for O5 than for O1, so that by the end of the final observing run O5, this SGWB will reach a higher SNR. These curves are calculated by integrating $\Omega_{\rm GW}(f)$ over frequency, convolved with the LIGO strain sensitivity, which is concentrated in the $10-50$ Hz band. Thus, they are model-dependent, i.e., dependent on the form of $\Omega_{\rm GW}(f)$. Their equivalents in the left panel of Fig. 1 in [71] are calculated for $\Omega_{\rm GW}(f)$ from unresolved binary black hole mergers, which is basically a power law across the $10-50$ Hz band (that is why they are called "power-law integrated sensitivity curves" there). [12]

For the SGWB from standard inflation, which is enhanced in ΛSFDM, its predicted $\Omega_{\rm GW}(f)$ has a triangle-shaped part as described above, by which $\Omega_{\rm GW}(f)$ can possibly reach the aLIGO/Virgo sensitivity curves, an impossible task for the same SGWB in ΛCDM (see Figs. 8 – 10 and [94]). To see this in more details, there are three cases for our predicted $\Omega_{\rm GW}(f)$, with regard to the relative position of the peak of the triangle in $\Omega_{\rm GW}(f)$, at $f_{\rm reheat}$, to the narrow sensitive window, $10-50$ Hz, of aLIGO/Virgo. These cases can be expressed as:

1. $f_{\rm reheat} < 10$ Hz,
2. 10 Hz $< f_{\rm reheat} <$ 50 Hz,
3. $f_{\rm reheat} > 50$ Hz.

We choose on purpose the values of $T_{\rm reheat} = 10^3,\ 10^4,\ 10^6$ GeV in the three example models shown here, such that each of them fits one of the above three cases, respectively. Intuitively, one should expect that among these three models of which $\Omega_{\rm GW}(f)$ have relatively equal peak amplitude $\Omega_{\rm GW}(f_{\rm reheat})$, the maximally detectable model, i.e., the one with the highest SNR for a given observation time, must be the one with $T_{\rm reheat} = 10^4$ GeV that fits Case 2, where $f_{\rm reheat}$ lies inside the sensitive window of LIGO. Indeed, this is shown to be true by the lower plots of Figs. 8 – 10, for the evolution of the expected SNR from the SGWB predicted in ΛSFDM, vs. the accumulated observation time of aLIGO/Virgo. These plots can be compared to the right panel of Fig. 1 in [71]. From Fig. 9 we see that if $T_{\rm reheat} = 10^4$ GeV and $r = 0.01$, the expected SNR can achieve a value as high as ~ 10, even by the end of the recent O1 run, for such SFDM parameter choice $(\lambda/(mc^2)^2,\ m) = (10^{-18}$ eV^{-1}cm^3, 8×10^{-20} eV$/c^2)$. Consequently, a non-detection of SGWB from aLIGO O1 would rule out this example model. On the other hand, take the model in Fig. 10 for instance, where the values of r and $\lambda/(mc^2)^2$ are the same but $T_{\rm reheat} = 10^6$ GeV and $m = 8\times10^{-18}$ eV$/c^2$. While its expected SNR, less than 1 for O1, satisfies all current upper bounds on SGWB from null detections by initial LIGO/Virgo[95, 96], even this case will reach an SNR > 30 by the end of O5 in 2022. This suggests that a wider range of SFDM parameters and reheat temperatures, to which aLIGO O1 is not sensitive, will be accessible to the aLIGO/Virgo O5 run, in terms of their expected SNR of SGWB by then (see §V B for a more detailed analysis). **Hence, we have shown that the SFDM model is promising to be detectable via its predicted SGWB from inflation, or otherwise seriously constrained/excluded with regard to its particle parameters, over the course of the ongoing aLIGO/Virgo.** In the next subsection, we refine this argument from the perspective of ΛSFDM models which marginally satisfy all the constraints derived in §IV.

[12] We note that the "power-law integrated sensitivity curves" developed by [99] are applicable to any power-law spectra for $\Omega_{\rm GW}(f)$. However, in ΛSFDM, $\Omega_{\rm GW}(f)$ is *not* a single power-law. Hence, we had to produce our own equivalent sensitivity curves (for which we are grateful to Joseph Romano for letting us modify his code.)

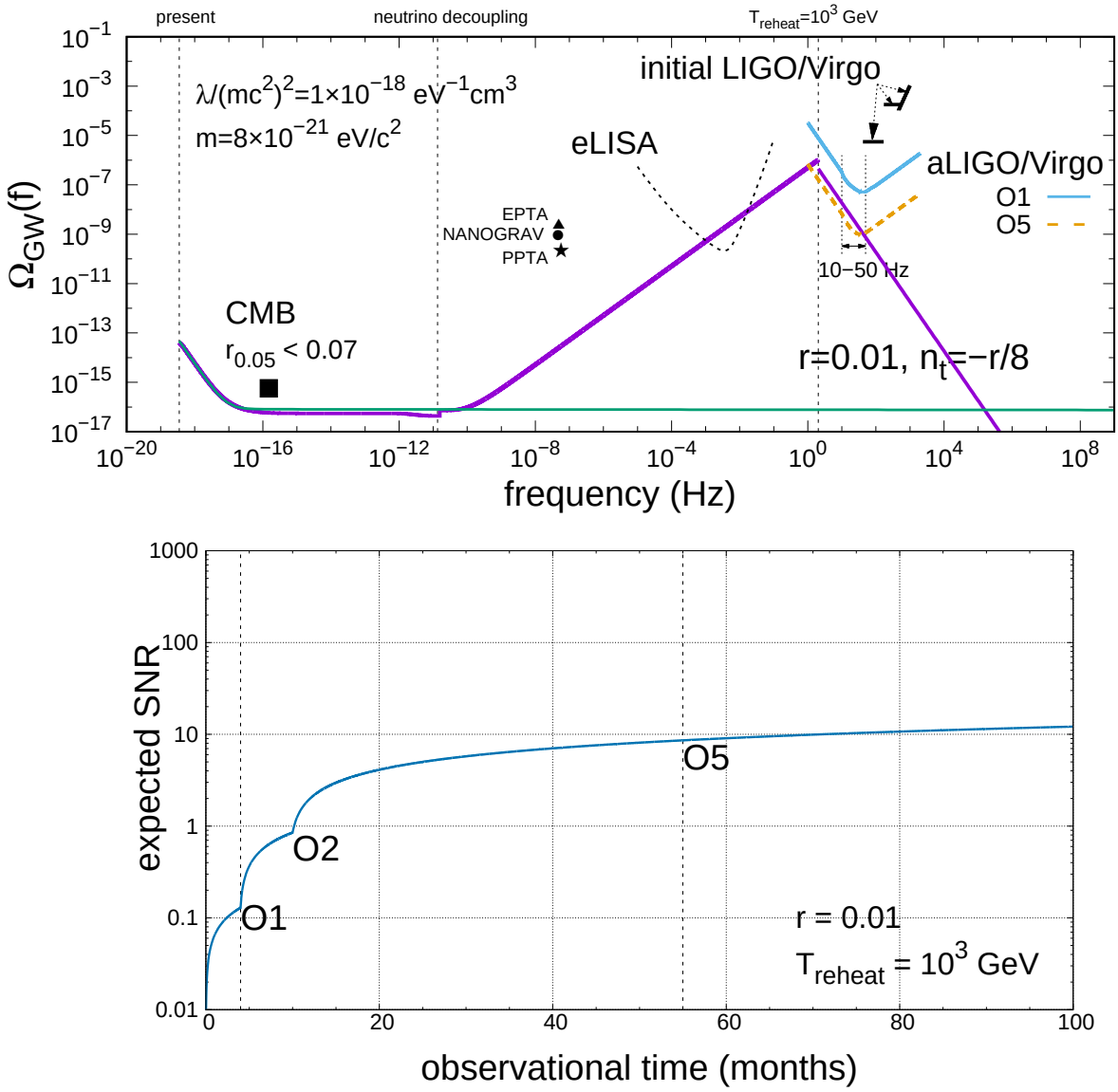


FIG. 8: *Upper plot:* Present-day energy density spectrum of the SGWB from inflation. The purple curve shows the prediction from one example ΛSFDM model in which reheating ends at $T_{\rm reheat} = 10^3$ GeV. The green curve shows the prediction of the standard model. $r = 0.01$ for both cases. The blue solid curve and the yellow dashed curve indicate the 1σ-sensitivity curves of aLIGO/Virgo by the end of O1 and O5 (for 2 years), respectively, integrated for the inflationary SGWB energy density spectra in ΛSFDM. Current upper limits from various experiments are shown, including the joint CMB analysis, PTA experiments and the (initial) LIGO/Virgo, all at 95% confidence level. The predicted eLISA sensitivity curve at design level is also plotted. *Lower plot:* The expected SNR of the inflationary SGWB predicted by the same ΛSFDM model *vs.* the accumulative observation time of aLIGO/Virgo. The dashed vertical lines indicate the observation time by the end of O1 and O5 run, respectively.

B. Implications from ΛSFDM models marginally satisfying cosmological constraints

The total $\Omega_{\rm GW}(a = 1)$ at the present, integrated over all frequencies, is equal to the total area underneath the spectrum curve $\Omega_{\rm GW}(f)$. As we confirm, this total area is dominated by the area of the triangle for a wide range of ΛSFDM model parameters, including all three example models shown here. For

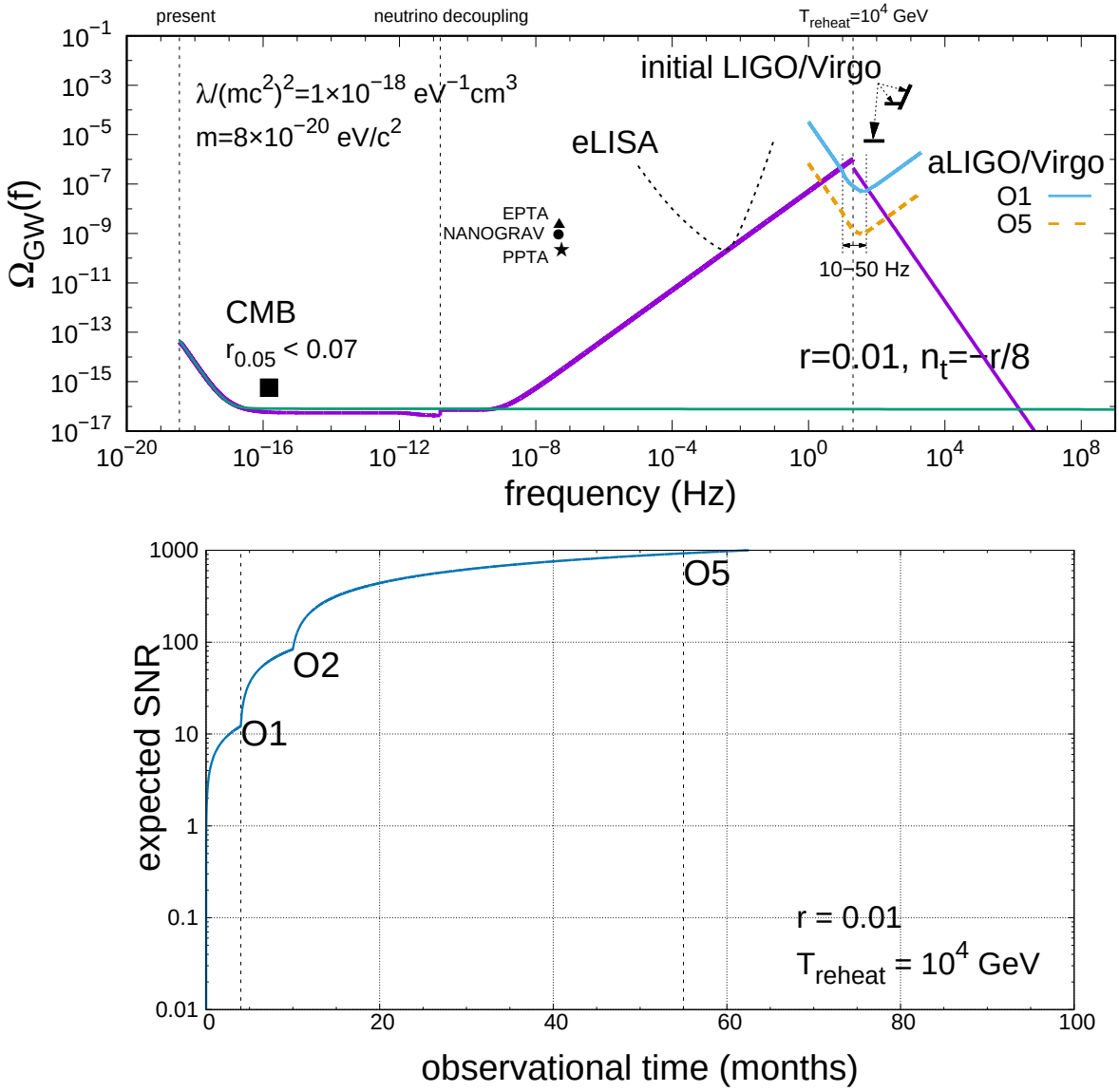


FIG. 9: *Upper plot:* Present-day energy density spectrum of the SGWB from inflation. The purple curve shows the prediction from one example ΛSFDM model in which reheating ends at $T_{\rm reheat} = 10^4$ GeV. The green curve shows the prediction of the standard model. $r = 0.01$ for both cases. The blue solid curve and the yellow dashed curve indicate the 1σ-sensitivity curves of aLIGO/Virgo by the end of O1 and O5 (for 2 years), respectively, integrated for the inflationary SGWB energy density spectra in ΛSFDM. Current upper limits from various experiments are shown, including the joint CMB analysis, PTA experiments and the (initial) LIGO/Virgo, all at 95% confidence level. The predicted eLISA sensitivity curve at design level is also plotted. *Lower plot:* The expected SNR of the inflationary SGWB predicted by the same ΛSFDM model *vs.* the accumulative observation time of aLIGO/Virgo. The dashed vertical lines indicate the observation time by the end of O1 and O5 run, respectively.

these models, r and $\lambda/(mc^2)^2$ are fixed as described at the beginning of §V, but $T_{\rm reheat}$ is different in each model, and for each $T_{\rm reheat}$, the SFDM particle mass m is adjusted to be the marginal value such that all the example models satisfy the current cosmological constraints derived in §IV. For other given values of r and $\lambda/(mc^2)^2$, the marginally allowed ΛSFDM models can be defined similarly, among which m varies

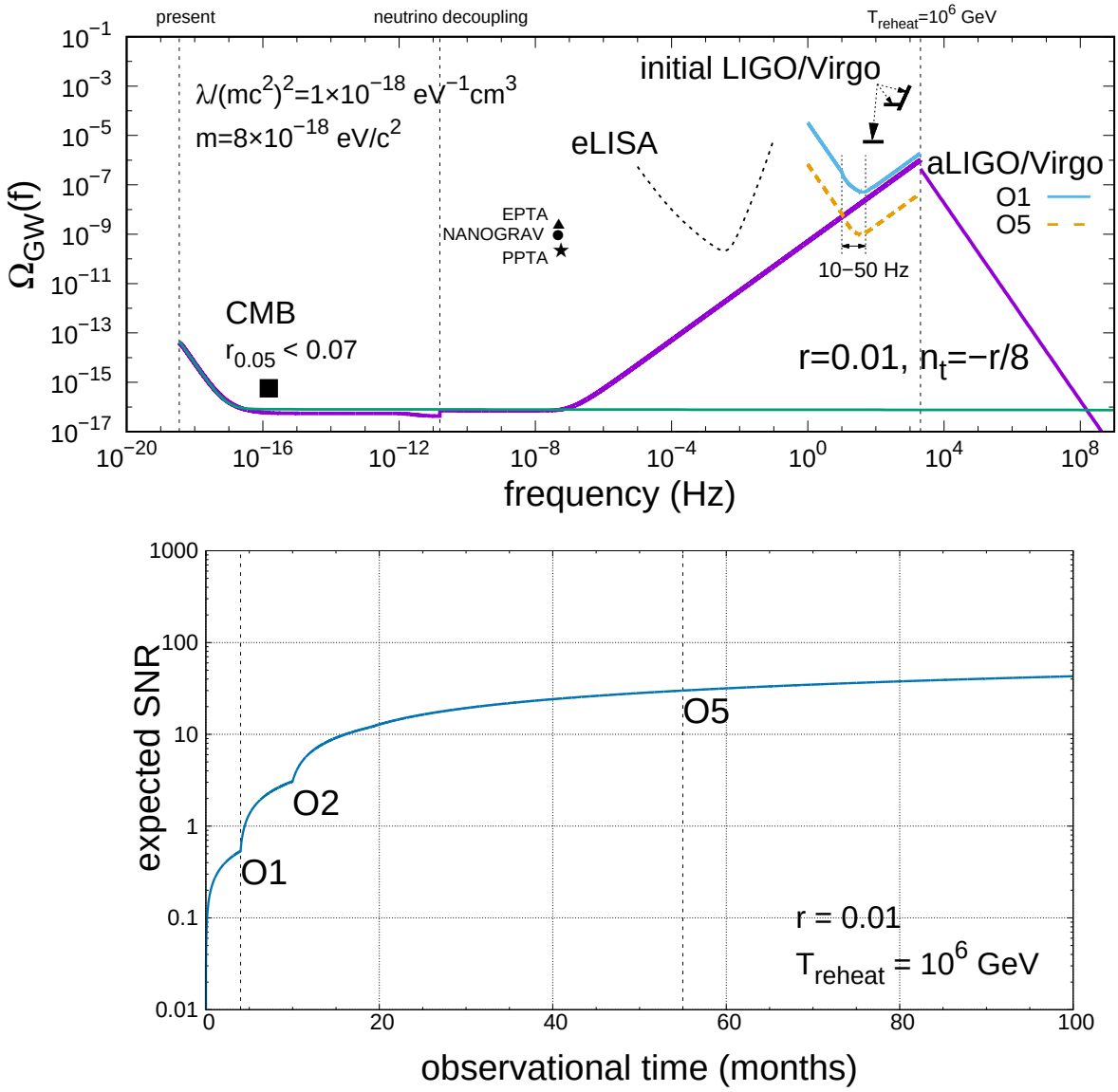


FIG. 10: *Upper plot:* Present-day energy density spectrum of the SGWB from inflation. The purple curve shows the prediction from one example ΛSFDM model in which reheating ends at $T_{\rm reheat} = 10^6$ GeV. The green curve shows the prediction of the standard model. $r = 0.01$ for both cases. The blue solid curve and the yellow dashed curve indicate the 1σ-sensitivity curves of aLIGO/Virgo by the end of O1 and O5 (for 2 years), respectively, integrated for the inflationary SGWB energy density spectra in ΛSFDM. Current upper limits from various experiments are shown, including the joint CMB analysis, PTA experiments and the (initial) LIGO/Virgo, all at 95% confidence level. The predicted eLISA sensitivity curve at design level is also plotted. *Lower plot:* The expected SNR of the inflationary SGWB predicted by the same ΛSFDM model *vs.* the accumulative observation time of aLIGO/Virgo. The dashed vertical lines indicate the observation time by the end of O1 and O5 run, respectively.

according to different values of $T_{\rm reheat}$. As a matter of fact, for a given $T_{\rm reheat}$ in each marginally allowed model, m is given by its respective lower bound, when r and $\lambda/(mc^2)^2$ are fixed (see Fig. 6). In this subsection, we will study the implications from these marginal ΛSFDM models.

First, among all ΛSFDM models which satisfy the cosmological constraints, the marginal ones have the

highest detectability. This can be shown by decreasing m but fixing all other parameters in an allowed model, until m reaches its lower bound. During this procedure, SFDM ends its stiff phase later, while the beginning of the stiff phase does not change for fixed $T_{\rm reheat}$, so the duration of the stiff-SFDM-dominated era becomes prolonged. As a result, the SGWB experiences more boost, and $\Omega_{\rm GW}(f)$ has higher amplitudes in the triangle, i.e., for modes which reenter the horizon by the end of the stiff era. This leads to a larger SNR of $\Omega_{\rm GW}(f)$ measured by aLIGO/Virgo. Therefore, the marginally allowed ΛSFDM models, among which are the three example models here, are to the interest of maximizing the detectability of the predicted SGWB today.

In the upper plots of Figs. 8 – 10 for these models, as $T_{\rm reheat}$ changes from 10^3 GeV to 10^6 GeV, the peak frequency of the spectrum at $f_{\rm reheat}$ shifts from low to high, passing the $10-50$ Hz sensitive band of aLIGO/Virgo, whereas the peak amplitude $\Omega_{\rm GW}(f_{\rm reheat})$, and thus the area of the triangle in $\Omega_{\rm GW}(f)$, remains almost the same. This is not surprising, because for these marginally allowed models with the same values of r and $\lambda/(mc^2)^2$, they must produce approximately the same amount of $\rho_{\rm GW}$ of the SGWB, at epochs which correspond to the cosmological constraints. Therefore, the corresponding total $\Omega_{\rm GW}$ at the present is nearly the same for all marginal models, dominated by the area of the triangle in $\Omega_{\rm GW}(f)$, as mentioned above. Interestingly, we find that $f_{\rm reheat}$ is nearly proportional to $T_{\rm reheat}$ among these marginally allowed models. We provide an analytical explanation for this relation in Appendix C.

Although the total present-day $\Omega_{\rm GW}$ is almost constant for all marginal models, the detectability of their predicted SGWB, by aLIGO/Virgo, is highly distinguishable from one model to another (see lower plots of Figs. 8 – 10). As we discussed in §V A, this is apparently due to the narrowness of the LIGO sensitive frequency band and the strong dependence on $f_{\rm reheat}$ of the overlap between this band and the peak of the SGWB spectrum. The maximally detectable case, with the largest expected SNR, is when $f_{\rm reheat}$ lies inside this window. Therefore, among the marginally allowed ΛSFDM models with fixed r and $\lambda/(mc^2)^2$, there is further a choice of $T_{\rm reheat}$ and a corresponding m which can maximize the SNR of the predicted SGWB. Among the three example models, the model with the most detectability is the one with $T_{\rm reheat}=10^4$ GeV. We can plot the distribution of the expected SNR for a given series of marginal ΛSFDM models with constant r and $\lambda/(mc^2)^2$, *vs.* varying $T_{\rm reheat}$, and find the maximally detectable model; see Fig. 11 for $r=0.01$ and $\lambda/(mc^2)^2=1\times10^{-18}$ eV^{-1}cm^3.

As seen in Fig. 11, for both the aLIGO/Virgo O1 and O5 run, the expected SNR has a peak between $T_{\rm reheat}=10^4$ GeV and 10^5 GeV, which corresponds to the most sensitive (lowest strain noise) frequency range of the experiment. For $r=0.01$, which is still 7 times below the current upper bound from CMB polarization measurements, the maximally detectable ΛSFDM model has an expected SNR >10 even for the past O1 run. For the O5 run, the same model can reach an SNR greater than 1000. Therefore, if the O1 run had a null detection of the SGWB with 95% confidence, for example, it would suggest that the above maximally detectable model be excluded, along with the marginally allowed ΛSFDM models for which $r=0.01$ and $T_{\rm reheat}$ ranges between about 4×10^3 and 3×10^5 GeV, as shown in Fig. 11. This would then provide a new kind of cosmological constraint on the ΛSFDM model. On the other hand, as aLIGO/Virgo improves its sensitivity and accumulates more data from O1 to O5, the expected SNR of the SGWB predicted by any given ΛSFDM model will also increase over time. As a result, by the end of the final observing run O5, ΛSFDM models with a wider range of parameters, which are not expected to be detectable for O1, will become accessible. In particular, the marginally allowed models with $r=0.01$ and $\lambda/(mc^2)^2=1\times10^{-18}$ eV^{-1}cm^3 predict an inflationary SGWB signal with an SNR >3, by the end of O5, for those in which $T_{\rm reheat}$ lies approximately inside (6×10^2 GeV, 10^7 GeV), and the corresponding SFDM mass range is about (5×10^{-21} eV/c^2, 8×10^{-17} eV/c^2), as shown in Fig. 11. Table II summarizes the results of the accessible ranges of $T_{\rm reheat}$ and m for these marginally allowed ΛSFDM models, to an aLIGO/Virgo detection at 2σ or 3σ confidence level by the end of its O1 and O5 runs, respectively. In conclusion, the ΛSFDM model shows a great prospect of detectability by the Advanced LIGO/Virgo experiment, thanks to its unique prediction of the present-day energy density spectrum of the primordial SGWB from inflation.

VI. DISCUSSION

A. What happens to ΛSFDM if $N_{\rm eff,BBN}\approx N_{\rm eff,standard}$?

In §IV, we apply the cosmological observables, $z_{\rm eq}$ and $N_{\rm eff,BBN}$, to constrain the SFDM particle parameters, through constraining the background expansion history of the ΛSFDM universe. These constraints result in the allowed range of the parameters $(\lambda/(mc^2)^2, m)$, expressed as shaded region in

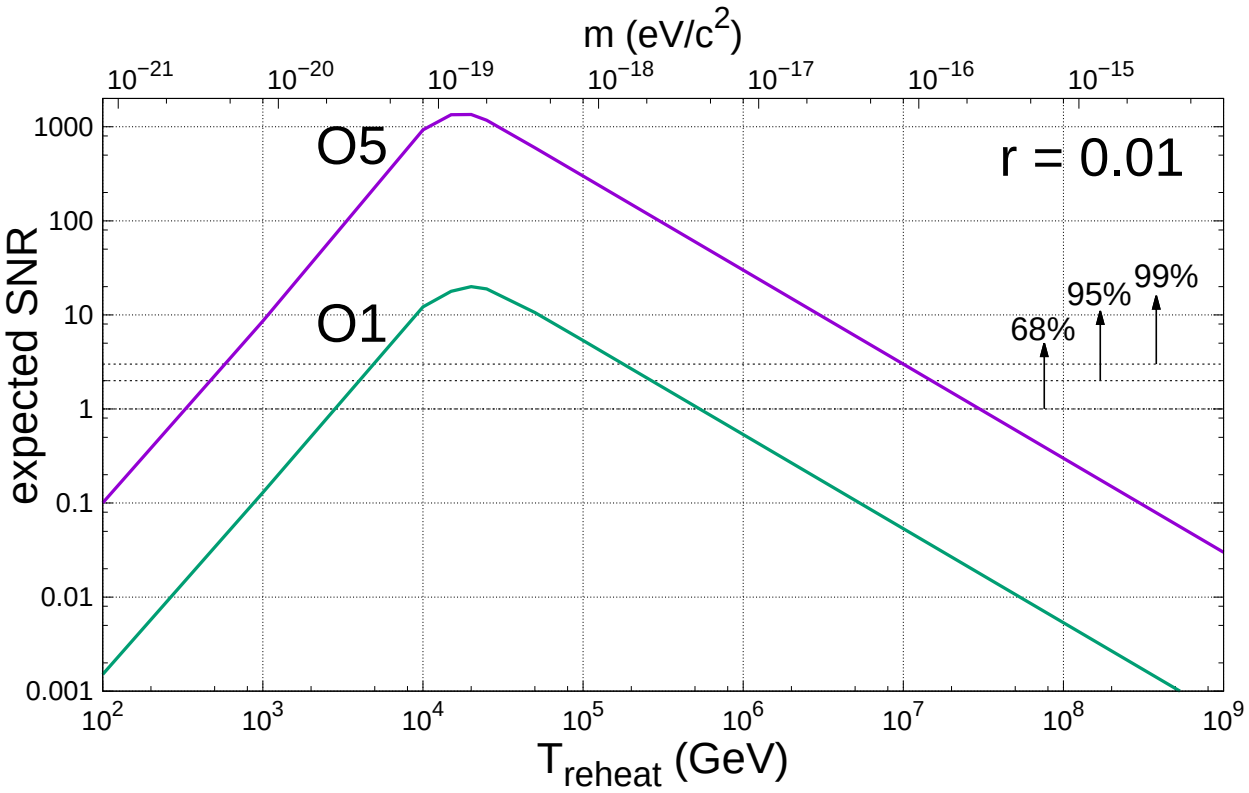


FIG. 11: Distribution of the expected SNR *vs.* $T_{\rm reheat}$, for the inflationary SGWB measured by aLIGO/Virgo by the end of the O1 and O5 run, respectively. Both curves are predicted by ΛSFDM models which marginally satisfy current cosmological constraints, in which $r = 0.01$ and $\lambda/(mc^2)^2 = 1 \times 10^{-18}$ eV^{-1}cm^3 are fixed, but m is tuned according to $T_{\rm reheat}$. The maximal detectable model corresponds to a value of $T_{\rm reheat}$ between 10^4 and 10^5 GeV.

LIGO run	Epoch	$T_{\rm reheat}$/GeV (SNR > 2)	$m/({\rm eV/c^2})$ (SNR > 2)	$T_{\rm reheat}$/GeV (SNR > 3)	$m/({\rm eV/c^2})$ (SNR > 3)
O1	2015-2016	$(4 \times 10^3,\ 3 \times 10^5)$	$(3 \times 10^{-20},\ 2 \times 10^{-18})$	$(5 \times 10^3,\ 2 \times 10^5)$	$(4 \times 10^{-20},\ 1.5 \times 10^{-18})$
O5	2020-2022	$(5 \times 10^2,\ 1.5 \times 10^7)$	$(4 \times 10^{-21},\ 10^{-16})$	$(6 \times 10^2,\ 10^7)$	$(5 \times 10^{-21},\ 8 \times 10^{-17})$

TABLE II: Accessible parameter ranges of $T_{\rm reheat}$ and m for ΛSFDM models that marginally satisfy the cosmological constraints, in which $r = 0.01$ and $\lambda/(mc^2)^2 = 1 \times 10^{-18}$ eV^{-1}cm^3, by the end of the O1 and O5 observing runs of aLIGO/Virgo, respectively. The accessible ranges corresponding to either a 2σ or 3σ detection are given.

the two-dimensional parameter space, as a function of the tensor-to-scalar ratio r and the reheat temperature $T_{\rm reheat}$, (see Figs. 5 and 6). We adopt conservative thresholds, the 1σ confidence intervals from measurements, for both the $z_{\rm eq}$ and $N_{\rm eff,BBN}$ constraints. These thresholds lead to the shapes of the allowed regions as thin stripes, for all cases. In particular, since the -1σ confidence limit of the measured value of $N_{\rm eff,BBN}$ in Eq. (86) is greater than the standard value, $N_{\rm eff,standard} = 3.046$, all of the allowed ΛSFDM models can explain a higher value of $N_{\rm eff}$ at BBN than at recombination, as mildly suggested by current measurements, mentioned in §IV B.

However, if we adopt a more relaxed threshold, e.g., the 2σ confidence interval, particularly for the $N_{\rm eff,BBN}$ constraint, we will allow a much broader range of ΛSFDM models which satisfy these cosmological constraints. In fact, the 2σ confidence interval of the measured value of $N_{\rm eff,BBN}$ contains the standard value $N_{\rm eff,standard}$, as shown by Eq. (86). Therefore, there would be then no lower bound from the BBN constraint on the value of $\Delta N_{\rm eff,BBN}$ predicted by the ΛSFDM model. Only an upper bound on $\Delta N_{\rm eff,BBN}$ would be left, translated to a lower bound on m for any allowed value

of $\lambda/(mc^2)^2$. As a result, the allowed ranges of $(\lambda/(mc^2)^2, m)$ illustrated in Figs. 5 and 6 would amount to the whole "quadrants" above the solid and dashed-dotted curves (for the $z_{\rm eq}$ constraint), free from the dashed curves. The quadrant regions, as opposed to the stripe-shaped shaded regions in Figs. 5 and 6, allow the $\lambda \to 0$ limit, in which SFDM is (nearly) non-self-interacting. This implies that while the non-self-interacting SFDM model is mildly disfavored by the 1σ confidence interval from current measurements of $N_{\rm eff,BBN}$, it is consistent with the 2σ limits.

Furthermore, should the measured value of $N_{\rm eff,BBN}$ decrease in the future to the extent of strongly favoring $N_{\rm eff,standard}$, the allowed ranges of SFDM particle parameters can be adjusted accordingly. In that case, the allowed regions in the parameter space would be like the quadrants described above.

B. SGWB from inflation versus that from unresolved binary black hole mergers?

Since LIGO has a narrow sensitive frequency band ($10 - 50$ Hz), for any potential SGWB signal, it is conventional to assume a power law for its present-day energy density spectrum, $\Omega_{\rm GW}(f)$, inside this band, and convolve this power-law spectrum with observational data to test this potential signal or to put an upper bound on it. This assumption is applicable to the SGWB from unresolved binary black hole mergers, since theoretical modeling suggests a power-law spectrum for such a signal, $\Omega_{\rm GW}(f) \propto f^{2/3}$, within the LIGO band [71]. However, the $\Omega_{\rm GW}(f)$ of the inflationary SGWB predicted by the ΛSFDM model has a unique triangle-like spectral shape as described in §V, for which the power-law based detection analysis may be invalid. In addition, by tuning the model parameters (see Figs. 8 – 10), the inflationary SGWB in ΛSFDM can achieve a comparable or much greater amplitude, within the LIGO band, than that from astrophysical sources. For example, currently the SNR of the SGWB from unresolved binary black hole mergers is predicted to be less than 10 at 90% confidence level by the end of O5 (in 2022) [71], while in ΛSFDM, the expected SNR of the inflationary SGWB ranges from 3 to over 1000 by then, for $6 \times 10^2 < T_{\rm reheat}\ ({\rm GeV}) < 10^7$ (see Fig. 11 and Table II). Therefore, it is important for aLIGO/Virgo and future GW detection experiments to consider the SGWB from inflation predicted by the ΛSFDM model, and to develop means to distinguish this potential SGWB signal from that sourced by binary black hole mergers, e.g., via their different spectral shapes.

C. Future detectability of the SGWB from inflation in ΛSFDM with eLISA?

We have briefly mentioned the prospective constraints on the present-day SGWB from the space laser interferometer mission eLISA, currently in its Pathfinder stage, in §V A. eLISA can potentially probe SGWB signals from various cosmological and astrophysical sources, in the milli-Hertz frequency range. According to our examples in Figs 8 – 10, the SGWB from inflation in the ΛSFDM model is predicted to lie above the eLISA design sensitivity curve (for our two lower values of $T_{\rm reheat}$). Therefore, the synergy between eLISA and LIGO will prospectively provide crucial information about the spectral shape of $\Omega_{\rm GW}(f)$ over frequencies which span the bands of these two experiments, and thus the strongest constraint on the inflationary SGWB predicted by ΛSFDM, in terms of its triangle-shaped $\Omega_{\rm GW}(f)$ at high frequencies. In other words, if this signal is detected by both experiments and consistent with a ΛSFDM model, it will be a smoking-gun evidence for SFDM and determines its particle parameters as well as $T_{\rm reheat}$ to a good accuracy. Otherwise, if both experiments suggest null detection of any SGWB signal, it would place stringent constraints on the SFDM particle parameters and $T_{\rm reheat}$, in the context of the ΛSFDM model.

VII. SUMMARY AND CONCLUSION

We extended our analysis in Paper I of the cosmological evolution of a universe in which dark matter is comprised of ultralight self-interacting bosonic particles, which form a Bose-Einstein condensate, described by a classical complex scalar field (SFDM). Unlike standard CDM, which is always non-relativistic once it decouples from the background, SFDM has an evolving equation of state (EOS). As we had shown previously, there are four eras in the evolution of a homogeneous ΛSFDM universe: the familiar radiation-dominated, matter-dominated and Λ-dominated eras common to standard ΛCDM as well, but also an earlier era dominated by SFDM with a stiff equation of state. In this paper, we embedded this model self-consistently into the standard inflationary paradigm by postulating that inflation is followed by an extended epoch of reheating (with matter-like EOS), from which SFDM emerges, as well as the particles of the Standard Model. We assumed that most of the energy density of the inflaton goes into the creation of the DM bosons, which quickly condense into their ground state, thereafter giving rise to SFDM in its stiff phase. The subdominant energy density of standard model particles constitutes the radiation com-

ponent. We adopted an instant transition, where the end of reheating at $T = T_{\rm reheat}$ is followed by the stiff-SFDM-dominated era of ΛSFDM.

Standard inflation predicts a stochastic background of gravitational waves (SGWB), which is mainly encoded in a finite value of the tensor-to-scalar ratio r, which is related to the energy scale of inflation. We showed that this SGWB is amplified during the stiff-SFDM-dominated epoch, compared to what it would be in a ΛCDM universe. SFDM in its relativistic phase (stiff plus radiation-like EOS) and this amplified SGWB from inflation, both, add to the number of relativistic degrees of freedom, $N_{\rm eff}$, in the early universe before and around Big Bang nucleosynthesis (BBN), and possibly up to the time of matter-radiation equality at $z_{\rm eq}$. In order to preserve those observables, we were able to place new and modified constraints on the SFDM particle parameters, boson mass m and boson two-particle self-interaction $\lambda > 0$. Indeed, many cosmological observables are dependent upon the ratio $\lambda/(mc^2)^2$, rather than λ, so we express our results of the constraints on SFDM in terms of the parameter pair $(\lambda/(mc^2)^2,\ m)$. It is necessary to ensure that the stiff-SFDM-dominated era is ending when BBN begins. Moreover, since SFDM should be nonrelativistic by the time of $z_{\rm eq}$, we could place further constraints from the requirement that the combined energy density of SFDM plus the amplified SGWB do preserve $z_{\rm eq}$ from CMB measurements.

We considered two values for r, $r = 0.01$ and $r = 0.1$, focusing on the former in particular, which is still seven times below current upper bounds from CMB measurements. We chose several values of the reheat temperatures, spanning a wide range from 10 to 10^9 GeV, to probe the range of impacts of SFDM on the inflationary SGWB. To this end, we solved the fully-coupled Klein-Gordon and Einstein field equations for the time-dependence of different ΛSFDM models, which self-consistently account for their amplification of the SGWB from inflation. We studied the back-reaction of the energy density of the enhanced SGWB on the expansion history of the universe, which in turn affected the SGWB, requiring us to develop an elaborate numerical methodology. We incorporated important additional effects, like the effect of electron-positron annihilation on the thermal history, as well as the damping of tensor modes due to the free streaming of neutrinos.

The amplification of the SGWB from inflation in ΛSFDM makes possible the prospective detection of the latter, using current and upcoming gravitational wave observatories. In fact, we calculated the present-day gravitational wave energy spectra, as a function of frequency, and found that the detection of the SGWB at high frequencies is within reach of the Advanced LIGO/Virgo experiment and possibly eLISA in the future. We showed that, for SFDM particle parameters that satisfy the above cosmological constraints, the amplified SGWB is currently detectable by aLIGO for a broad range of reheat temperature, for values of the tensor-to-scalar ratio currently allowed by CMB polarization measurements. A non-detection by aLIGO by the end of the observing run O1 would provide a new kind of cosmological constraint on SFDM, while a wider range of SFDM parameters and reheat temperatures will be accessible to the aLIGO O5 run, potentially detecting this unique signature of the SFDM model.

• Cosmological constraints on SFDM particle parameters

In §IV, we described in detail how observational constraints on $N_{\rm eff,BBN}$ and $z_{\rm eq}$ constrain the allowed range of SFDM particle parameters $(\lambda/(mc^2)^2,\ m)$ for given values of r and $T_{\rm reheat}$. Details aside, a rough summary of those results can be described as follows. For $\lambda/(mc^2)^2$, we found

$$10^{-18}\ {\rm eV}^{-1}\ {\rm cm}^3 \lesssim \frac{\lambda}{({\rm mc}^2)^2} \lesssim 4\times 10^{-17}\ {\rm eV}^{-1}\ {\rm cm}^3, \tag{92}$$

For m, we found

$$m \gtrsim 5\times 10^{-21}\times \frac{T_{\rm reheat}}{10^3\ {\rm GeV}}\sqrt{\frac{r}{0.01}}\ {\rm eV}/c^2, \tag{93}$$

for $r \gtrsim 0.01$ and $T_{\rm reheat} \gtrsim 10^3$ GeV, and $m \gtrsim 5\times 10^{-21}$ eV$/c^2$ for for $r \gtrsim 0.01$ and $T_{\rm reheat} < 10^3$ GeV. As discussed in §VI A, if we relax the $N_{\rm eff,BBN}$ constraint, such that $\Delta N_{\rm eff,BBN} = 0$ is allowed, then the lower limit in Eq. (92) goes away, and even $\lambda \to 0$ is allowed.

• Detectability of the SGWB from inflation in ΛSFDM

As described in §V, the detectability of the SGWB $\Omega_{\rm GW}(f)$ amplified in ΛSFDM depends upon the SFDM particle parameters, $T_{\rm reheat}$, and r. For fixed r and $T_{\rm reheat}$, the maximum predicted signal corresponds to the pairs of $(\lambda/(mc^2)^2,\ m)$ which marginally satisfy the cosmological constraints and maximize the duration of the stiff era. For LIGO, the overall maximum predicted signal (at fixed r) corresponds to this maximum when $T_{\rm reheat}$ is chosen so that $f_{\rm reheat}$ lies inside the LIGO sensitive frequency band. For $r = 0.01$, this corresponds to $T_{\rm reheat} \simeq 10^4$ GeV, for which we predict and SNR ~ 10 for the recent aLIGO/Virgo O1 run. If no detection is reported at this level, then we might conclude that these parameters are excluded.

A wider range of parameters will be accessible to aLIGO/Virgo as time goes on. For $r = 0.01$ and $\lambda/(mc^2)^2 = 10^{-18}$ eV^{-1} cm^3, for example, a 3σ detection is predicted for the O1 run if $5 \times 10^3 \lesssim T_{\rm reheat}$ (GeV) $\lesssim 2 \times 10^5$, while for the O5 run, this becomes $6 \times 10^2 \lesssim T_{\rm reheat}$ (GeV) $\lesssim 10^7$. For these $T_{\rm reheat}$ ranges, the ranges of particle masses in the marginally allowed models correspond to $4 \times 10^{-20} \lesssim m$ (eV/c^2) $\lesssim 1.5 \times 10^{-18}$ (O1) and $5 \times 10^{-21} \lesssim m$ (eV/c^2) $\lesssim 8 \times 10^{-17}$ (O5).

For parameters in these ranges, our predicted SNR for aLIGO/Virgo for the SGWB from inflation in ΛSFDM can exceed current predictions of the background from unresolved binary black hole mergers in [71]. It will be important, therefore, to consider this inflationary SGWB in ΛSFDM in interpreting the current and future GW detection results.

We have also shown here that, for a range of values of $T_{\rm reheat}$ and allowed values of r, the inflationary SGWB in ΛSFDM may also be detectable by eLISA. In that case, the difference in spectral shape between the primordial and black-hole merger GW backgrounds may allow them to be distinguished.

ACKNOWLEDGMENTS

During the work on this paper, we benefitted from discussions with many people to whom we express our gratitude: Joel Meyers, Dustin Lorshbough, Aditya Aravind, Thomas Crawford, Can Kilic, Raphael Flauger, Takeshi Kobayashi, and Eiichiro Komatsu. We thank Paul Lasky especially for sharing his code for plotting current experimental constraints on the present-day SGWB background. We are grateful to members of the LIGO Scientific Collaboration for helpful discussion, including Tania Regimbau and David Reitze. We give special thanks to Joseph Romano for sharing his code for computing aLIGO/Virgo sensitivity and signal-to-noise ratios for a stochastic background of GWs with a power-law spectrum, from unresolved sources like binary black hole mergers. We modified this code to compute these for the non-power-law spectrum of the SGWB from inflation in our ΛSFDM model.

This work was supported in part by U.S. NSF grant AST-1009799, NASA grant NNX11AE09G, NASA/JPL grant RSA Nos.1492788 and 1515294, and supercomputer resources from NSF XSEDE grant TG-AST090005 and the Texas Advanced Computing Center (TACC) at the University of Texas at Austin. TRD was supported by the U.S. Department of Energy under grants DE-FG02-95ER40899 and de-sc0007859. TRD acknowledges the support by the Austrian Science Fund FWF through a Lise Meitner fellowship (M2008-N36).

Appendix A: Gravitational Waves in a FLRW universe

1. Effective stress-energy tensor of gravitational waves

It is instructive to show how it is that tensor perturbations associated with gravitational waves also contribute an effective mean stress-energy to the background curvature of the universe, which is spatially homogeneous on large scales.

For a FLRW universe of which the metric is defined in Eq. (2), only allowing tensor perturbations, let us evaluate the left-hand side of the Einstein field equations (4),

$$R^{\mu}_{\ \nu} - \frac{1}{2}R = \left(R^{\mu}_{\ \nu}{}^{(0)} - \frac{1}{2}R^{(0)} \right) + \left(R^{\mu}_{\ \nu}{}^{(2)} - \frac{1}{2}R^{(2)} \right), \tag{A1}$$

where we have expanded the left-hand side in perturbations h_{ij}, up to the second order. On the right-hand side of the expansion above, the zeroth-order term contributed by the unperturbed FLRW metric $\bar{g}_{\mu\nu}$ is familiar, of which the nonzero components are

$$R^{0}_{\ 0}{}^{(0)} - \frac{1}{2}R^{(0)} = \frac{3\dot{a}^2}{c^2 a^2}, \tag{A2}$$

$$R^{i}_{\ i}{}^{(0)} - \frac{1}{2}R^{(0)} = \frac{-a\ddot{a} + \dot{a}^2}{c^2 a^2}. \tag{A3}$$

The first-order term in the expansion vanishes. The second-order term (of the order $O(h^2)$) due to tensor perturbations, can be moved to the right-hand side of the Einstein field equations (4), and hence viewed as an effective contribution to the total stress-energy tensor $T^{\mu}_{\ \nu}$. That is to say, $T_{\mu\nu,\ \rm GW}$ purely results from the spatial metric perturbations, rather than the stress-energy tensor of an intrinsic cosmic component.

The stress-energy carried by GWs can not be localized within a wavelength [80]. Instead, it is only meaningful to interpret the effective $T_{\mu\nu,\ \rm GW}$ as a macroscopic average over several wavelengths. With this understanding, we see that the stress-energy of GWs indeed contributes to the curvature of the homogeneous background universe. In other words, it back-reacts to the zeroth-order term in Eq. (A1) once moved to the right-hand side. Let us, for simplicity, focus on subhorizon modes. We can then explicitly write down the stress-energy tensor of GWs,

$$\begin{aligned} T_{\mu\nu,\ \rm GW} &\equiv -\frac{c^4}{8\pi G}\left(\langle R^{(2)}_{\mu\nu} \rangle - \frac{1}{2}\bar{g}_{\mu\nu}\langle R^{(2)} \rangle \right) \\ &= \frac{c^4}{32\pi G}\langle (a^2 h_{ij})_{;\mu} (\frac{1}{a^2}h^{ij})_{;\nu} \rangle, \end{aligned} \tag{A4}$$

where the brackets $\langle\cdot\rangle$ denote the spatial average over several wavelengths, and the semicolon denotes the covariant derivative with respect to the background metric $\bar{g}_{\mu\nu}$. This was first derived by Isaacson in [100, 101]. Therefore, $T_{\mu\nu,\ \mathrm{GW}}$ is also known as the Isaacson tensor.

Particularly, the time-time component of $T_{\mu\nu,\ \mathrm{GW}}$ defines the energy density of GWs,

$$\rho_{\mathrm{GW}} \equiv T^0_{0,\ \mathrm{GW}} = \frac{c^4}{32\pi G}\langle (a^2 h_{ij})_{;0} (\frac{1}{a^2} h^{ij})^{;0}\rangle = \frac{c^2}{32\pi G}\langle \partial_t h_{ij} \partial_t h^{ij}\rangle. \quad \text{(A5)}$$

Remember that $h^{ij} = h_{ij}$ (see also [72, 98, 102]).

2. Fourier decomposition of h_{ij}

It is customary to move into $\mathbf{k}$-space by Fourier transforming the tensor perturbations,

$$h_{ij}(\mathbf{x}, t) = \sum_P \int \frac{\mathrm{d}^3\mathbf{k}}{(2\pi)^3} h^P_{\mathbf{k}}(t) \mathrm{e}^{i\mathbf{k}\cdot\mathbf{x}} \epsilon^P_{ij}(\mathbf{k}), \quad \text{(A6)}$$

where $\mathbf{k}$ is the comoving wave vector, and $\epsilon^P_{ij}(\mathbf{k})$ are the spin-2 polarization tensors for the "plus" and "cross" polarization states, $P = +$ or $\times$, with respect to the wave vector $\mathbf{k}$. Both $\epsilon^+_{ij}(\mathbf{k})$ and $\epsilon^\times_{ij}(\mathbf{k})$ are symmetric, traceless ($\sum_i \epsilon^P_{ii}(\mathbf{k}) = 0$), and perpendicular to the direction in which the plane wave propagates (transverse), $\epsilon^P_{ij}(\mathbf{k}) \cdot \mathbf{k} = 0$. Also, $\epsilon^P_{ij}(-\mathbf{k}) = \epsilon^P_{ij}(\mathbf{k})$. They follow such normalization convention,

$$\sum_{i,j} \epsilon^P_{ij}(\mathbf{k}) \epsilon^{P'}_{ij}(\mathbf{k}) = 2\delta_{PP'}, \quad \text{(A7)}$$

where $\delta_{PP'}$ is the Kronecker delta. In three-dimensional space with Cartesian coordinates, if $\mathbf{k}$ goes along the z-direction, the explicit form of ϵ^P_{ij} can be written as

$$\epsilon^+_{ij} = \mathbf{e}_x \otimes \mathbf{e}_x - \mathbf{e}_y \otimes \mathbf{e}_y = \begin{pmatrix} 1 & 0 & 0 \\ 0 & -1 & 0 \\ 0 & 0 & 0 \end{pmatrix},$$
$$\epsilon^\times_{ij} = \mathbf{e}_x \otimes \mathbf{e}_y + \mathbf{e}_y \otimes \mathbf{e}_x = \begin{pmatrix} 0 & 1 & 0 \\ 1 & 0 & 0 \\ 0 & 0 & 0 \end{pmatrix}, \quad \text{(A8)}$$

where $\mathbf{e}_x$ and $\mathbf{e}_y$ are unit polarization vectors in the xy plane, both perpendicular to $\mathbf{k}$.

Appendix B: Thin-horizon approximation: analytical solution and asymptotic behavior of tensor modes

In this appendix, we show that the thin-horizon approximation is valid for tensor modes which reenter the horizon during an era with constant w for the EOS of the background universe, the case of most interest to us throughout the ΛSFDM expansion history. For this purpose, we show an example of how well the exact analytical solution matches the asymptotic sub- and superhorizon evolution, in their respective regime of validity (we draw this example from other work in progress, Rindler-Daller, Shapiro, Li, in prep.). Fig. 12 shows plots of the evolution of $h_k(\tau)$ and $\Omega_{\mathrm{GW}}(k, \tau)$ in the case of a matter-like ($w = 0$) EOS of the background universe. We confirm that the range in $k\tau$ around horizon crossing is rather narrow, justifying the thin-horizon approximation in which the horizon crossing is deemed to occur suddenly at $k = aH(a)/c$ for each k.

Appendix C: Marginally allowed ΛSFDM models with given r and $\lambda/(mc^2)^2$: $f_{\mathrm{reheat}} \propto T_{\mathrm{reheat}}$

It can be analytically shown that for ΛSFDM models which marginally satisfy the cosmological constraints, with given values of r and $\lambda/(mc^2)^2$, f_{reheat} is nearly proportional to T_{reheat}.

First, let us express f_{reheat} as follows:

$$f_{\mathrm{reheat}} = \frac{f_{\mathrm{reheat}}}{f_{\mathrm{sr}}} \frac{f_{\mathrm{sr}}}{f_{\mathrm{r,late}}} f_{\mathrm{r,late}}, \quad \text{(C1)}$$

where f_{sr} is the frequency of the mode that reenters the horizon (approximately) at $a_{\mathrm{sr}} = 2\pi f_{\mathrm{sr}}/H_{\mathrm{sr}}$, the transition between the stiff-SFDM-dominated era and the radiation-dominated era, and $f_{\mathrm{r,late}}$ is the frequency of a mode that reenters later in the radiation-dominated era at $a_{\mathrm{r,late}} = 2\pi f_{\mathrm{r,late}}/H_{\mathrm{r,late}}$. Both $f_{\mathrm{r,late}}$ and $a_{\mathrm{r,late}}$ are required to be the same for all models, the feasibility of which is guaranteed by the fact that these marginally allowed ΛSFDM models share a uniform expansion history in the radiation-dominated era, since the values of r and $\lambda/(mc^2)^2$ are fixed.

Since the area of triangle in $\Omega_{\mathrm{GW}}(f)$ is almost constant, the triangle itself must be almost identical for all marginally allowed ΛSFDM models, as the slopes of the two "sides" of the triangle are fixed by the power-law indices. In other words, they can be approximated by the same triangle which slides on a fixed plateau, whose height is determined by the value of r alone. Thus, the ratio $f_{\mathrm{reheat}}/f_{\mathrm{sr}}$ must be the same for all marginally allowed models, since the x-axis in the $\Omega_{\mathrm{GW}}(f)$ plots is logarithmic. This implies that the number of e-foldings between a_{reheat} and a_{sr} must be the same as well, shown by the

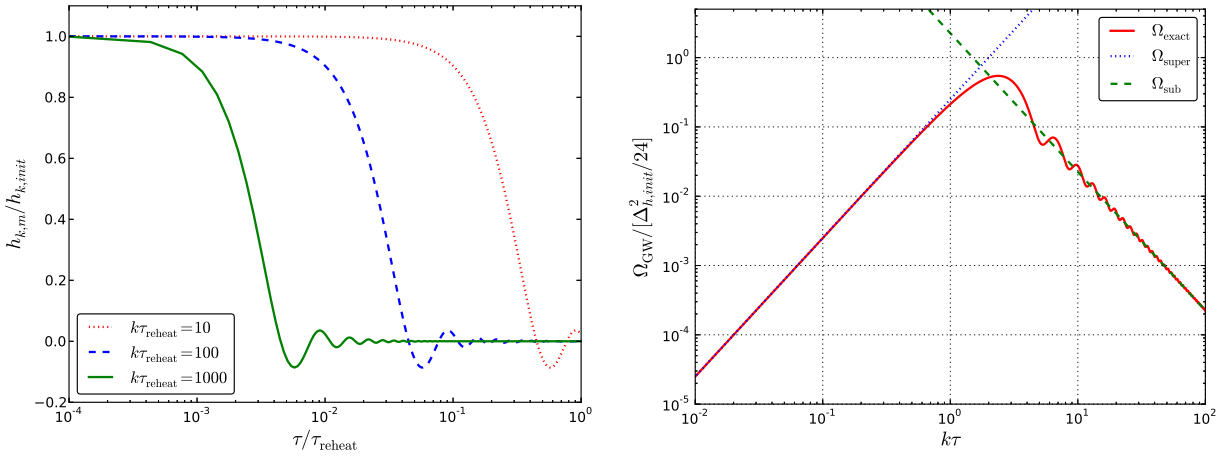


FIG. 12: *Left-hand plot:* Tensor perturbations for different k-modes, as they reenter the horizon during reheating (with $w = 0$) at different times. At $\tau/\tau_{\rm reheat} = 1$, the reheating era gives rise to the stiff era. The tensor modes (strains) are normalized over their initial amplitude $h_{k,\ \rm init}$, for each k. *Right-hand plot:* The exact solution for $\Omega_{\rm GW}(k,\tau)$ as a function of $k\tau$ (solid curve), as well as the respective asymptotic expressions (superhorizon in dot, subhorizon in dash), for a reheating era with $w = 0$. $\Omega_{\rm GW}$ is normalized over $\Delta^2_{h,\ \rm init}/24$.

following equation:

$$\frac{f_{\rm reheat}}{f_{\rm sr}} = \frac{a_{\rm reheat}H_{\rm reheat}}{a_{\rm sr}H_{\rm sr}} = \left(\frac{a_{\rm reheat}}{a_{\rm sr}}\right)\left(\frac{a_{\rm reheat}}{a_{\rm sr}}\right)^{-3} = \left(\frac{a_{\rm reheat}}{a_{\rm sr}}\right)^{-2}. \tag{C2}$$

Also,

$$\frac{f_{\rm sr}}{f_{\rm r,late}} = \frac{a_{\rm sr}H_{\rm sr}}{a_{\rm r,late}H_{\rm r,late}} = \left(\frac{a_{\rm sr}}{a_{\rm r,late}}\right)\left(\frac{a_{\rm sr}}{a_{\rm r,late}}\right)^{-2} = \left(\frac{a_{\rm sr}}{a_{\rm reheat}}\right)^{-1}\left(\frac{a_{\rm reheat}}{a_{\rm r,late}}\right)^{-1}. \tag{C3}$$

Combining the above two equations yields

$$f_{\rm reheat} = f_{\rm r,late}\left(\frac{a_{\rm reheat}}{a_{\rm sr}}\right)^{-2}\left(\frac{a_{\rm sr}}{a_{\rm reheat}}\right)^{-1}\left(\frac{a_{\rm reheat}}{a_{\rm r,late}}\right)^{-1} = f_{\rm r,late}\left(\frac{a_{\rm reheat}}{a_{\rm sr}}\right)^{-1}\left(\frac{a_{\rm reheat}}{a_{\rm r,late}}\right)^{-1} \propto a_{\rm reheat}^{-1}. \tag{C4}$$

Since $T_{\rm reheat} \propto a_{\rm reheat}^{-1}$ to a very good accuracy, ignoring the details in the thermal history of the universe, we conclude that $f_{\rm reheat} \propto T_{\rm reheat}$, for all marginally allowed ΛSFDM models with fixed r and $\lambda/(mc^2)^2$.

[1] Planck Collaboration, P. A. R. Ade, N. Aghanim, M. Arnaud, M. Ashdown, J. Aumont, C. Baccigalupi, A. J. Banday, R. B. Barreiro, J. G. Bartlett, and et al., ArXiv e-prints (2015), arXiv:1502.01589.

[2] É. Aubourg, S. Bailey, J. E. Bautista, F. Beutler, V. Bhardwaj, D. Bizyaev, M. Blanton, M. Blomqvist, A. S. Bolton, J. Bovy, H. Brewington, J. Brinkmann, J. R. Brownstein, A. Burden, N. G. Busca, W. Carithers, C.-H. Chuang, J. Comparat, R. A. C. Croft, A. J. Cuesta, K. S. Dawson, T. Delubac, D. J. Eisenstein, A. Font-Ribera, J. Ge, J.-M. Le Goff, S. G. A. Gontcho, J. R. Gott, J. E. Gunn, H. Guo, J. Guy, J.-C. Hamilton, S. Ho, K. Honscheid, C. Howlett, D. Kirkby, F. S. Kitaura, J.-P. Kneib, K.-G. Lee, D. Long, R. H. Lupton, M. V. Magaña, V. Malanushenko, E. Malanushenko, M. Manera, C. Maraston, D. Margala, C. K. McBride, J. Miralda-Escudé, A. D. Myers, R. C. Nichol, P. Noterdaeme, S. E. Nuza, M. D. Olmstead, D. Oravetz, I. Pâris, N. Padmanabhan, N. Palanque-Delabrouille, K. Pan, M. Pellejero-Ibanez, W. J. Percival, P. Petitjean, M. M. Pieri, F. Prada, B. Reid, J. Rich, N. A. Roe, A. J. Ross, N. P. Ross, G. Rossi, J. A. Rubiño-Martín, A. G. Sánchez, L. Samushia, R. T. G. Santos, C. G. Scóccola, D. J. Schlegel, D. P. Schneider, H.-J. Seo, E. Sheldon, A. Simmons, R. A. Skibba, A. Slosar, M. A. Strauss, D. Thomas, J. L. Tinker, R. Tojeiro, J. A. Vazquez, M. Viel, D. A. Wake, B. A. Weaver, D. H. Weinberg, W. M. Wood-Vasey, C. Yèche,

I. Zehavi, G.-B. Zhao, and BOSS Collaboration, Phys. Rev. D **92**, 123516 (2015), arXiv:1411.1074.

[3] S. Alam, M. Ata, S. Bailey, F. Beutler, D. Bizyaev, J. A. Blazek, A. S. Bolton, J. R. Brownstein, A. Burden, C.-H. Chuang, J. Comparat, A. J. Cuesta, K. S. Dawson, D. J. Eisenstein, S. Escoffier, H. Gil-Marín, J. N. Grieb, N. Hand, S. Ho, K. Kinemuchi, D. Kirkby, F. Kitaura, E. Malanushenko, V. Malanushenko, C. Maraston, C. K. McBride, R. C. Nichol, M. D. Olmstead, D. Oravetz, N. Padmanabhan, N. Palanque-Delabrouille, K. Pan, M. Pellejero-Ibanez, W. J. Percival, P. Petitjean, F. Prada, A. M. Price-Whelan, B. A. Reid, S. A. Rodríguez-Torres, N. A. Roe, A. J. Ross, N. P. Ross, G. Rossi, J. A. Rubiño-Martín, A. G. Sánchez, S. Saito, S. Salazar-Albornoz, L. Samushia, S. Satpathy, C. G. Scóccola, D. J. Schlegel, D. P. Schneider, H.-J. Seo, A. Simmons, A. Slosar, M. A. Strauss, M. E. C. Swanson, D. Thomas, J. L. Tinker, R. Tojeiro, M. Vargas Magaña, J. A. Vazquez, L. Verde, D. A. Wake, Y. Wang, D. H. Weinberg, M. White, W. M. Wood-Vasey, C. Yèche, I. Zehavi, Z. Zhai, and G.-B. Zhao, ArXiv e-prints (2016), arXiv:1607.03155.

[4] A. Vikhlinin, A. V. Kravtsov, R. A. Burenin, H. Ebeling, W. R. Forman, A. Hornstrup, C. Jones, S. S. Murray, D. Nagai, H. Quintana, and A. Voevodkin, Astrophys. J. **692**, 1060 (2009), arXiv:0812.2720.

[5] M. G. Walker, M. Mateo, E. W. Olszewski, J. Peñarrubia, N. Wyn Evans, and G. Gilmore, Astrophys. J. **704**, 1274 (2009), arXiv:0906.0341 [astro-ph.CO].

[6] J. Wolf, G. D. Martinez, J. S. Bullock, M. Kaplinghat, M. Geha, R. R. Muñoz, J. D. Simon, and F. F. Avedo, Mon.Not.Roy.Astron.Soc. **406**, 1220 (2010), arXiv:0908.2995.

[7] A. B. Newman, R. S. Ellis, and T. Treu, Astrophys. J. **814**, 26 (2015), arXiv:1503.05282.

[8] B. Moore, T. Quinn, F. Governato, J. Stadel, and G. Lake, Mon.Not.Roy.Astron.Soc. **310**, 1147 (1999), arXiv:astro-ph/9903164.

[9] W. J. G. de Blok, F. Walter, E. Brinks, C. Trachternach, S.-H. Oh, and R. C. Kennicutt, Jr., Astron.J. **136**, 2648-2719 (2008), arXiv:0810.2100.

[10] N. C. Amorisco and N. W. Evans, Mon.Not.Roy.Astron.Soc. **419**, 184 (2012), arXiv:1106.1062 [astro-ph.CO].

[11] S.-H. Oh, D. A. Hunter, E. Brinks, B. G. Elmegreen, A. Schruba, F. Walter, M. P. Rupen, L. M. Young, C. E. Simpson, M. C. Johnson, K. A. Herrmann, D. Ficut-Vicas, P. Cigan, V. Heesen, T. Ashley, and H.-X. Zhang, Astron.J. **149**, 180 (2015), arXiv:1502.01281.

[12] K. A. Oman, J. F. Navarro, L. V. Sales, A. Fattahi, C. S. Frenk, T. Sawala, M. Schaller, and S. D. M. White, Mon.Not.Roy.Astron.Soc. **460**, 3610 (2016), arXiv:1601.01026.

[13] A. Klypin, A. V. Kravtsov, O. Valenzuela, and F. Prada, Astrophys. J. **522**, 82 (1999), arXiv:astro-ph/9901240.

[14] B. Moore, S. Ghigna, F. Governato, G. Lake, T. Quinn, J. Stadel, and P. Tozzi, Astrophy.J. Letter **524**, L19 (1999), arXiv:astro-ph/9907411.

[15] M. Boylan-Kolchin, J. S. Bullock, and M. Kaplinghat, Mon.Not.Roy.Astron.Soc. **415**, L40 (2011), arXiv:1103.0007 [astro-ph.CO].

[16] M. Boylan-Kolchin, J. S. Bullock, and M. Kaplinghat, Mon.Not.Roy.Astron.Soc. **422**, 1203 (2012), arXiv:1111.2048 [astro-ph.CO].

[17] D. S. Akerib, H. M. Araújo, X. Bai, A. J. Bailey, J. Balajthy, P. Beltrame, E. P. Bernard, A. Bernstein, T. P. Biesiadzinski, E. M. Boulton, A. Bradley, R. Bramante, S. B. Cahn, M. C. Carmona-Benitez, C. Chan, J. J. Chapman, A. A. Chiller, C. Chiller, A. Currie, J. E. Cutter, T. J. R. Davison, L. de Viveiros, A. Dobi, J. E. Y. Dobson, E. Druszkiewicz, B. N. Edwards, C. H. Faham, S. Fiorucci, R. J. Gaitskell, V. M. Gehman, C. Ghag, K. R. Gibson, M. G. D. Gilchriese, C. R. Hall, M. Hanhardt, S. J. Haselschwardt, S. A. Hertel, D. P. Hogan, M. Horn, D. Q. Huang, C. M. Ignarra, M. Ihm, R. G. Jacobsen, W. Ji, K. Kazkaz, D. Khaitan, R. Knoche, N. A. Larsen, C. Lee, B. G. Lenardo, K. T. Lesko, A. Lindote, M. I. Lopes, D. C. Malling, A. Manalaysay, R. L. Mannino, M. F. Marzioni, D. N. McKinsey, D.-M. Mei, J. Mock, M. Moongweluwan, J. A. Morad, A. S. J. Murphy, C. Nehrkorn, H. N. Nelson, F. Neves, K. O'Sullivan, K. C. Oliver-Mallory, R. A. Ott, K. J. Palladino, M. Pangilinan, E. K. Pease, P. Phelps, L. Reichhart, C. Rhyne, S. Shaw, T. A. Shutt, C. Silva, V. N. Solovov, P. Sorensen, S. Stephenson, T. J. Sumner, M. Szydagis, D. J. Taylor, W. Taylor, B. P. Tennyson, P. A. Terman, D. R. Tiedt, W. H. To, M. Tripathi, L. Tvrznikova, S. Uvarov, J. R. Verbus, R. C. Webb, J. T. White, T. J. Whitis, M. S. Witherell, F. L. H. Wolfs, K. Yazdani, S. K. Young, C. Zhang, and LUX Collaboration, Physical Review Letters **116**, 161301 (2016), arXiv:1512.03506.

[18] R. Agnese, A. J. Anderson, T. Aramaki, M. Asai, W. Baker, D. Balakishiyeva, D. Barker, R. Basu Thakur, D. A. Bauer, J. Billard, A. Borgland, M. A. Bowles, P. L. Brink, R. Bunker, B. Cabrera, D. O. Caldwell, R. Calkins, D. G. Cerdeno, H. Chagani, Y. Chen, J. Cooley, B. Cornell, P. Cushman, M. Daal, P. C. F. Di Stefano, T. Doughty, L. Esteban, S. Fallows, E. Figueroa-Feliciano, M. Ghaith, G. L. Godfrey, S. R. Golwala, J. Hall, H. R. Harris, T. Hofer, D. Holmgren, L. Hsu, M. E. Huber, D. Jardin, A. Jastram, O. Kamaev, B. Kara, M. H. Kelsey, A. Kennedy, A. Leder, B. Loer, E. Lopez Asamar, P. Lukens, R. Mahapatra, V. Mandic, N. Mast, N. Mirabolfathi, R. A. Moffatt, J. D. Morales Mendoza, S. M. Oser, K. Page, W. A. Page, R. Partridge, M. Pepin, A. Phipps, K. Prasad, M. Pyle, H. Qiu, W. Rau, P. Redl, A. Reisetter, Y. Ricci, A. Roberts, H. E. Rogers,

T. Saab, B. Sadoulet, J. Sander, K. Schneck, R. W. Schnee, S. Scorza, B. Serfass, B. Shank, D. Speller, D. Toback, R. Underwood, S. Upadhyayula, A. N. Villano, B. Welliver, J. S. Wilson, D. H. Wright, S. Yellin, J. J. Yen, B. A. Young, J. Zhang, and SuperCDMS Collaboration, Physical Review Letters **116**, 071301 (2016).

[19] M. Ackermann, A. Albert, B. Anderson, W. B. Atwood, L. Baldini, G. Barbiellini, D. Bastieri, K. Bechtol, R. Bellazzini, E. Bissaldi, R. D. Blandford, E. D. Bloom, R. Bonino, E. Bottacini, T. J. Brandt, J. Bregeon, P. Bruel, R. Buehler, G. A. Caliandro, R. A. Cameron, R. Caputo, M. Caragiulo, P. A. Caraveo, C. Cecchi, E. Charles, A. Chekhtman, J. Chiang, G. Chiaro, S. Ciprini, R. Claus, J. Cohen-Tanugi, J. Conrad, A. Cuoco, S. Cutini, F. D'Ammando, A. de Angelis, F. de Palma, R. Desiante, S. W. Digel, L. Di Venere, P. S. Drell, A. Drlica-Wagner, R. Essig, C. Favuzzi, S. J. Fegan, E. C. Ferrara, W. B. Focke, A. Franckowiak, Y. Fukazawa, S. Funk, P. Fusco, F. Gargano, D. Gasparrini, N. Giglietto, F. Giordano, M. Giroletti, T. Glanzman, G. Godfrey, G. A. Gomez-Vargas, I. A. Grenier, S. Guiriec, M. Gustafsson, E. Hays, J. W. Hewitt, D. Horan, T. Jogler, G. Jóhannesson, M. Kuss, S. Larsson, L. Latronico, J. Li, L. Li, M. Llena Garde, F. Longo, F. Loparco, P. Lubrano, D. Malyshev, M. Mayer, M. N. Mazziotta, J. E. McEnery, M. Meyer, P. F. Michelson, T. Mizuno, A. A. Moiseev, M. E. Monzani, A. Morselli, S. Murgia, E. Nuss, T. Ohsugi, M. Orienti, E. Orlando, J. F. Ormes, D. Paneque, J. S. Perkins, M. Pesce-Rollins, F. Piron, G. Pivato, T. A. Porter, S. Rainò, R. Rando, M. Razzano, A. Reimer, O. Reimer, S. Ritz, M. Sánchez-Conde, A. Schulz, N. Sehgal, C. Sgrò, E. J. Siskind, F. Spada, G. Spandre, P. Spinelli, L. Strigari, H. Tajima, H. Takahashi, J. B. Thayer, L. Tibaldo, D. F. Torres, E. Troja, G. Vianello, M. Werner, B. L. Winer, K. S. Wood, M. Wood, G. Zaharijas, S. Zimmer, and Fermi-LAT Collaboration, Physical Review Letters **115**, 231301 (2015), arXiv:1503.02641 [astro-ph.HE].

[20] A. Drlica-Wagner, A. Albert, K. Bechtol, M. Wood, L. Strigari, M. Sánchez-Conde, L. Baldini, R. Essig, J. Cohen-Tanugi, B. Anderson, R. Bellazzini, E. D. Bloom, R. Caputo, C. Cecchi, E. Charles, J. Chiang, A. de Angelis, S. Funk, P. Fusco, F. Gargano, N. Giglietto, F. Giordano, S. Guiriec, M. Gustafsson, M. Kuss, F. Loparco, P. Lubrano, N. Mirabal, T. Mizuno, A. Morselli, T. Ohsugi, E. Orlando, M. Persic, S. Rainò, N. Sehgal, F. Spada, D. J. Suson, G. Zaharijas, S. Zimmer, Fermi-LAT Collaboration, T. Abbott, S. Allam, E. Balbinot, A. H. Bauer, A. Benoit-Lévy, R. A. Bernstein, G. M. Bernstein, E. Bertin, D. Brooks, E. Buckley-Geer, D. L. Burke, A. Carnero Rosell, F. J. Castander, R. Covarrubias, C. B. D'Andrea, L. N. da Costa, D. L. DePoy, S. Desai, H. T. Diehl, C. E. Cunha, T. F. Eifler, J. Estrada, A. E. Evrard, A. Fausti Neto, E. Fernandez, D. A. Finley, B. Flaugher, J. Frieman, E. Gaztanaga, D. Gerdes, D. Gruen, R. A. Gruendl, G. Gutierrez, K. Honscheid, B. Jain, D. James, T. Jeltema, S. Kent, R. Kron, K. Kuehn, N. Kuropatkin, O. Lahav, T. S. Li, E. Luque, M. A. G. Maia, M. Makler, M. March, J. Marshall, P. Martini, K. W. Merritt, C. Miller, R. Miquel, J. Mohr, E. Neilsen, B. Nord, R. Ogando, J. Peoples, D. Petravick, A. Pieres, A. A. Plazas, A. Queiroz, A. K. Romer, A. Roodman, E. S. Rykoff, M. Sako, E. Sanchez, B. Santiago, V. Scarpine, M. Schubnell, I. Sevilla, R. C. Smith, M. Soares-Santos, F. Sobreira, E. Suchyta, M. E. C. Swanson, G. Tarle, J. Thaler, D. Thomas, D. Tucker, A. R. Walker, R. H. Wechsler, W. Wester, P. Williams, B. Yanny, J. Zuntz, and The DES Collaboration, Astrophy.J. Letter **809**, L4 (2015), arXiv:1503.02632 [astro-ph.HE].

[21] T. Rindler-Daller and P. R. Shapiro, Mon.Not.Roy.Astron.Soc. **422**, 135 (2012), arXiv:1106.1256.

[22] T. Rindler-Daller and P. R. Shapiro, in *Accelerated Cosmic Expansion*, Astrophysics and Space Science Proceedings, Vol. 38, edited by C. Moreno González, J. E. Madriz Aguilar, and L. M. Reyes Barrera (2014) p. 163, arXiv:1209.1835.

[23] B. Li, T. Rindler-Daller, and P. R. Shapiro, Phys. Rev. D **89**, 083536 (2014), arXiv:1310.6061.

[24] B. Li, P. R. Shapiro, and T. Rindler-Daller, in *Proceedings of the Frank N. Bash Symposium 2015 (BASH2015). 18-20 October. The University of Texas at Austin, USA.* (2015) p. 28.

[25] D. J. E. Marsh, Phys. Rev. D **91**, 123520 (2015), arXiv:1504.00308.

[26] S.-J. Sin, Phys. Rev. D **50**, 3650 (1994), hep-ph/9205208.

[27] P. J. E. Peebles and A. Vilenkin, Phys. Rev. D **60**, 103506 (1999), astro-ph/9904396.

[28] W. Hu, R. Barkana, and A. Gruzinov, Physical Review Letters **85**, 1158 (2000), astro-ph/0003365.

[29] T.-P. Woo and T. Chiueh, Astrophys. J. **697**, 850 (2009), arXiv:0806.0232.

[30] L. Hui, J. P. Ostriker, S. Tremaine, and E. Witten, ArXiv e-prints (2016), arXiv:1610.08297.

[31] H.-Y. Schive, T. Chiueh, and T. Broadhurst, Nature Physics **10**, 496 (2014), arXiv:1406.6586.

[32] D. J. E. Marsh, E. Macaulay, M. Trebitsch, and P. G. Ferreira, Phys. Rev. D **85**, 103514 (2012), arXiv:1110.0502 [astro-ph.CO].

[33] R. Hlozek, D. Grin, D. J. E. Marsh, and P. G. Ferreira, Phys. Rev. D **91**, 103512 (2015), arXiv:1410.2896.

[34] A. Suárez and T. Matos, Mon.Not.Roy.Astron.Soc. **416**, 87 (2011), arXiv:1101.4039 [gr-qc].

[35] J. Magaña, T. Matos, A. Suárez, and F. J. Sánchez-Salcedo, J.Cosm.Astropart.Phys. **10**, 003 (2012), arXiv:1204.5255.

[36] E. Calabrese and D. N. Spergel, Mon.Not.Roy.Astron.Soc. **460**, 4397 (2016),

arXiv:1603.07321.
[37] P. J. E. Peebles, Astrophy.J. Letter **534**, L127 (2000), astro-ph/0002495.
[38] J. Goodman, New Astronomy **5**, 103 (2000), astro-ph/0003018.
[39] Z. Slepian and J. Goodman, Mon.Not.Roy.Astron.Soc. **427**, 839 (2012), arXiv:1109.3844.
[40] T. Matos, F. S. Guzmán, and D. Núñez, Phys. Rev. D **62**, 061301 (2000), astro-ph/0003398.
[41] T. Matos and L. Arturo Ureña-López, Phys. Rev. D **63**, 063506 (2001), arXiv:astro-ph/0006024.
[42] C. G. Böhmer and T. Harko, J.Cosm.Astropart.Phys. **6**, 025 (2007), arXiv:0705.4158.
[43] T. Harko, Phys. Rev. D **83**, 123515 (2011), arXiv:1105.5189 [gr-qc].
[44] P. H. Chavanis, Astron.& Aastrophys. **537**, A127 (2012), arXiv:1103.2698.
[45] B. Kain and H. Y. Ling, Phys. Rev. D **85**, 023527 (2012), arXiv:1112.4169 [hep-ph].
[46] D. N. Spergel and P. J. Steinhardt, Physical Review Letters **84**, 3760 (2000), astro-ph/9909386.
[47] K. Ahn and P. R. Shapiro, Mon.Not.Roy.Astron.Soc. **363**, 1092 (2005), astro-ph/0412169.
[48] J. Koda and P. R. Shapiro, Mon.Not.Roy.Astron.Soc. **415**, 1125 (2011), arXiv:1101.3097.
[49] P. Sikivie and Q. Yang, Physical Review Letters **103**, 111301 (2009), arXiv:0901.1106 [hep-ph].
[50] O. Erken, P. Sikivie, H. Tam, and Q. Yang, Phys. Rev. D **85**, 063520 (2012), arXiv:1111.1157 [astro-ph.CO].
[51] S. Davidson and M. Elmer, J.Cosm.Astropart.Phys. **12**, 034 (2013), arXiv:1307.8024 [hep-ph].
[52] A. H. Guth, M. P. Hertzberg, and C. Prescod-Weinstein, Phys. Rev. D **92**, 103513 (2015), arXiv:1412.5930.
[53] H. E. Haber and H. A. Weldon, Phys. Rev. D **25**, 502 (1982).
[54] J. I. Kapusta, Phys. Rev. D **24**, 426 (1981).
[55] G. Mangano, G. Miele, S. Pastor, and M. Peloso, Phys. Rev. D **64**, 123509 (2001), hep-ph/0102080.
[56] A. Arbey, J. Lesgourgues, and P. Salati, Phys. Rev. D **65**, 083514 (2002), astro-ph/0112324.
[57] F. Briscese, Physics Letters B **696**, 315 (2011), arXiv:1101.0028 [astro-ph.CO].
[58] L. A. Boyle, R. R. Caldwell, and M. Kamionkowski, Physics Letters B **545**, 17 (2002), astro-ph/0105318.
[59] M. Colpi, S. L. Shapiro, and I. Wasserman, Physical Review Letters **57**, 2485 (1986).
[60] M. Joyce, Phys. Rev. D **55**, 1875 (1997), arXiv:hep-ph/9606223.
[61] P. G. Ferreira and M. Joyce, Phys. Rev. D **58**, 023503 (1998), astro-ph/9711102.
[62] S. Dutta and R. J. Scherrer, Phys. Rev. D **82**, 083501 (2010), arXiv:1006.4166 [astro-ph.CO].
[63] V. A. Belinsky, L. P. Grishchuk, I. M. Khalatnikov, and Y. B. Zeldovich, Physics Letters B **155**, 232 (1985).
[64] G. Mangano, G. Miele, S. Pastor, T. Pinto, O. Pisanti, and P. D. Serpico, Nuclear Physics B **729**, 221 (2005), arXiv:hep-ph/0506164.
[65] Planck Collaboration, P. A. R. Ade, N. Aghanim, M. Arnaud, F. Arroja, M. Ashdown, J. Aumont, C. Baccigalupi, M. Ballardini, A. J. Banday, and et al., ArXiv e-prints (2015), arXiv:1502.02114.
[66] BICEP2 Collaboration, Keck Array Collaboration, P. A. R. Ade, Z. Ahmed, R. W. Aikin, K. D. Alexander, D. Barkats, S. J. Benton, C. A. Bischoff, J. J. Bock, R. Bowens-Rubin, J. A. Brevik, I. Buder, E. Bullock, V. Buza, J. Connors, B. P. Crill, L. Duband, C. Dvorkin, J. P. Filippini, S. Fliescher, J. Grayson, M. Halpern, S. Harrison, G. C. Hilton, H. Hui, K. D. Irwin, K. S. Karkare, E. Karpel, J. P. Kaufman, B. G. Keating, S. Kefeli, S. A. Kernasovskiy, J. M. Kovac, C. L. Kuo, E. M. Leitch, M. Lueker, K. G. Megerian, C. B. Netterfield, H. T. Nguyen, R. O'Brient, R. W. Ogburn, A. Orlando, C. Pryke, S. Richter, R. Schwarz, C. D. Sheehy, Z. K. Staniszewski, B. Steinbach, R. V. Sudiwala, G. P. Teply, K. L. Thompson, J. E. Tolan, C. Tucker, A. D. Turner, A. G. Vieregg, A. C. Weber, D. V. Wiebe, J. Willmert, C. L. Wong, W. L. K. Wu, and K. W. Yoon, Physical Review Letters **116**, 031302 (2016), arXiv:1510.09217.
[67] U. Seljak and M. Zaldarriaga, Physical Review Letters **78**, 2054 (1997), astro-ph/9609169.
[68] M. A. Amin, M. P. Hertzberg, D. I. Kaiser, and J. Karouby, International Journal of Modern Physics D **24**, 1530003 (2015), arXiv:1410.3808 [hep-ph].
[69] L. P. Grishchuk, Zhurnal Eksperimentalnoi i Teoreticheskoi Fiziki **67**, 825 (1974).
[70] V. F. Mukhanov, H. A. Feldman, and R. H. Brandenberger, Physics Reports **215**, 203 (1992).
[71] B. P. Abbott, R. Abbott, T. D. Abbott, M. R. Abernathy, F. Acernese, K. Ackley, C. Adams, T. Adams, P. Addesso, R. X. Adhikari, and et al., Physical Review Letters **116**, 131102 (2016), arXiv:1602.03847 [gr-qc].
[72] P. Binétruy, A. Bohé, C. Caprini, and J.-F. Dufaux, J.Cosm.Astropart.Phys. **6**, 027 (2012), arXiv:1201.0983 [gr-qc].
[73] Z. Arzoumanian, A. Brazier, S. Burke-Spolaor, S. J. Chamberlin, S. Chatterjee, B. Christy, J. M. Cordes, N. J. Cornish, K. Crowter, P. B. Demorest, X. Deng, T. Dolch, J. A. Ellis, R. D. Ferdman, E. Fonseca, N. Garver-Daniels, M. E. Gonzalez, F. Jenet, G. Jones, M. L. Jones, V. M. Kaspi, M. Koop, M. T. Lam, T. J. W. Lazio, L. Levin, A. N. Lommen, D. R. Lorimer, J. Luo, R. S. Lynch, D. R. Madison, M. A. McLaughlin, S. T. McWilliams, C. M. F. Mingarelli, D. J. Nice, N. Palliyaguru, T. T. Pennucci, S. M. Ransom, L. Sampson, S. A. Sanidas, A. Sesana, X. Siemens,

J. Simon, I. H. Stairs, D. R. Stinebring, K. Stovall, J. Swiggum, S. R. Taylor, M. Vallisneri, R. van Haasteren, Y. Wang, W. W. Zhu, and The NANOGrav Collaboration, Astrophys. J. **821**, 13 (2016), arXiv:1508.03024.

[74] R. M. Shannon, V. Ravi, L. T. Lentati, P. D. Lasky, G. Hobbs, M. Kerr, R. N. Manchester, W. A. Coles, Y. Levin, M. Bailes, N. D. R. Bhat, S. Burke-Spolaor, S. Dai, M. J. Keith, S. Osłowski, D. J. Reardon, W. van Straten, L. Toomey, J.-B. Wang, L. Wen, J. S. B. Wyithe, and X.-J. Zhu, Science **349**, 1522 (2015), arXiv:1509.07320.

[75] L. Lentati, S. R. Taylor, C. M. F. Mingarelli, A. Sesana, S. A. Sanidas, A. Vecchio, R. N. Caballero, K. J. Lee, R. van Haasteren, S. Babak, C. G. Bassa, P. Brem, M. Burgay, D. J. Champion, I. Cognard, G. Desvignes, J. R. Gair, L. Guillemot, J. W. T. Hessels, G. H. Janssen, R. Karuppusamy, M. Kramer, A. Lassus, P. Lazarus, K. Liu, S. Osłowski, D. Perrodin, A. Petiteau, A. Possenti, M. B. Purver, P. A. Rosado, R. Smits, B. Stappers, G. Theureau, C. Tiburzi, and J. P. W. Verbiest, Mon.Not.Roy.Astron.Soc. **453**, 2576 (2015), arXiv:1504.03692.

[76] L. A. Boyle and A. Buonanno, Phys. Rev. D **78**, 043531 (2008), arXiv:0708.2279.

[77] L. A. Boyle and P. J. Steinhardt, Phys. Rev. D **77**, 063504 (2008), astro-ph/0512014.

[78] M. Giovannini, Phys. Rev. D **58**, 083504 (1998), hep-ph/9806329.

[79] V. Mukhanov, *Physical Foundations of Cosmology, by Viatcheslav Mukhanov, pp. 442. Cambridge University Press, November 2005. ISBN-10: 0521563984. ISBN-13: 9780521563987. LCCN: QB981 .M89 2005* (2005) p. 442.

[80] C. W. Misner, K. S. Thorne, and J. A. Wheeler, *San Francisco: W.H. Freeman and Co., 1973* (1973).

[81] S. Weinberg, *Cosmology, by Steven Weinberg. ISBN 978-0-19-852682-7. Published by Oxford University Press, Oxford, UK, 2008.* (Oxford University Press, 2008).

[82] S. Weinberg, Phys. Rev. D **69**, 023503 (2004), astro-ph/0306304.

[83] D. A. Dicus and W. W. Repko, Phys. Rev. D **72**, 088302 (2005), astro-ph/0509096.

[84] B. P. Abbott, R. Abbott, T. D. Abbott, M. R. Abernathy, F. Acernese, K. Ackley, C. Adams, T. Adams, P. Addesso, R. X. Adhikari, and et al., Physical Review Letters **116**, 061102 (2016), arXiv:1602.03837 [gr-qc].

[85] É. É. Flanagan and S. A. Hughes, New Journal of Physics **7**, 204 (2005), gr-qc/0501041.

[86] Planck Collaboration, P. A. R. Ade, N. Aghanim, C. Armitage-Caplan, M. Arnaud, M. Ashdown, F. Atrio-Barandela, J. Aumont, C. Baccigalupi, A. J. Banday, and et al., ArXiv e-prints (2013), arXiv:1303.5076 [astro-ph.CO].

[87] M. S. Turner, Phys. Rev. D **28**, 1243 (1983).

[88] P. N. Brown, G. D. Byrne, and A. C. Hindmarsh, SIAM Journal on Scientific and Statistical Computing **10**, 1038 (1989).

[89] A. Suárez, V. H. Robles, and T. Matos, in *Accelerated Cosmic Expansion*, Astrophysics and Space Science Proceedings, Vol. 38, edited by C. Moreno González, J. E. Madriz Aguilar, and L. M. Reyes Barrera (2014) p. 107, arXiv:1302.0903 [astro-ph.CO].

[90] Y. I. Izotov, T. X. Thuan, and N. G. Guseva, Mon.Not.Roy.Astron.Soc. **445**, 778 (2014), arXiv:1408.6953.

[91] K. M. Nollett and G. Steigman, Phys. Rev. D **91**, 083505 (2015), arXiv:1411.6005.

[92] R. J. Cooke, M. Pettini, K. M. Nollett, and R. Jorgenson, Astrophys. J. **830**, 148 (2016), arXiv:1607.03900.

[93] S. Dodelson, *Modern cosmology / Scott Dodelson. Amsterdam (Netherlands): Academic Press. ISBN 0-12-219141-2, 2003, XIII + 440 p.* (Academic Press, 2003).

[94] P. D. Lasky, C. M. F. Mingarelli, T. L. Smith, J. T. Giblin, E. Thrane, D. J. Reardon, R. Caldwell, M. Bailes, N. D. R. Bhat, S. Burke-Spolaor, S. Dai, J. Dempsey, G. Hobbs, M. Kerr, Y. Levin, R. N. Manchester, S. Osłowski, V. Ravi, P. A. Rosado, R. M. Shannon, R. Spiewak, W. van Straten, L. Toomey, J. Wang, L. Wen, X. You, and X. Zhu, Physical Review X **6**, 011035 (2016), arXiv:1511.05994.

[95] J. Aasi, B. P. Abbott, R. Abbott, T. Abbott, M. R. Abernathy, T. Accadia, F. Acernese, K. Ackley, C. Adams, T. Adams, and et al., Physical Review Letters **113**, 231101 (2014), arXiv:1406.4556 [gr-qc].

[96] J. Aasi, J. Abadie, B. P. Abbott, R. Abbott, T. Abbott, M. R. Abernathy, T. Accadia, F. Acernese, C. Adams, T. Adams, and et al., Phys. Rev. D **91**, 022003 (2015), arXiv:1410.6211 [gr-qc].

[97] P. Amaro-Seoane, S. Aoudia, S. Babak, P. Binétruy, E. Berti, A. Bohé, C. Caprini, M. Colpi, N. J. Cornish, K. Danzmann, J.-F. Dufaux, J. Gair, O. Jennrich, P. Jetzer, A. Klein, R. N. Lang, A. Lobo, T. Littenberg, S. T. McWilliams, G. Nelemans, A. Petiteau, E. K. Porter, B. F. Schutz, A. Sesana, R. Stebbins, T. Sumner, M. Vallisneri, S. Vitale, M. Volonteri, and H. Ward, Classical and Quantum Gravity **29**, 124016 (2012), arXiv:1202.0839 [gr-qc].

[98] B. Allen and J. D. Romano, Phys. Rev. D **59**, 102001 (1999), gr-qc/9710117.

[99] E. Thrane and J. D. Romano, Phys. Rev. D **88**, 124032 (2013), arXiv:1310.5300 [astro-ph.IM].

[100] R. A. Isaacson, Physical Review **166**, 1263 (1968).

[101] R. A. Isaacson, Physical Review **166**, 1272 (1968).

[102] Y. Watanabe and E. Komatsu, Phys. Rev. D **73**, 123515 (2006), astro-ph/0604176.